Theoretical Studies of Heterogeneous Catalysis by Molybdates

Thesis by

Janet Noel Allison

In Partial Fulfillment of the Requirements

For the Degree of Doctor of Philosophy

California Institute of Technology

Pasadena, California

1985

(Submitted November 28, 1984)

"The same thrill, the same awe and mystery, come again and again when we look at any problem deeply enough. With more knowledge comes deeper, more wonderful mystery, luring one on to penetrate deeper still. Never concerned that the answer may prove disappointing, but with pleasure and confidence, we turn over each new stone to find unimagined strangeness leading on to more wonderful questions and mysteries—certainly a grand adventure!"

RICHARD P. FEYNMAN

Winner of the Nobel Prize in Physics,

Richard Chace Tolman Professor of

Theoretical Physics,

at the California Institute of Technology

To Jerry

Acknowledgment

ABSTRACT

Chapter 1: We use thermochemical results from *ab initio* quantum chemical calculations (generalized valence bond) to examine the reaction mechanism for

$$H_3COH + \tfrac{1}{2}O_2 \longrightarrow H_2CO + H_2O$$
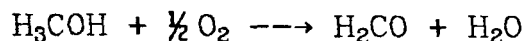
as catalyzed by MoO_3. We find that surface dioxo sites
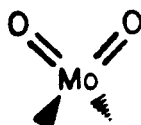
are critical to activating the methanol, but we find that the Trifiro proposal of a single site-single step process
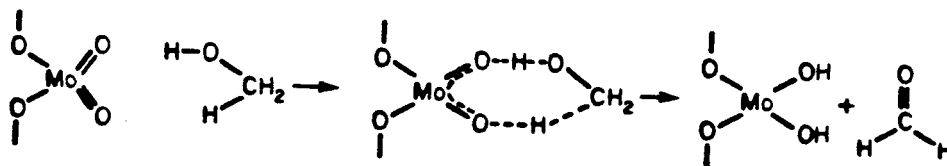
is not favorable ($\Delta H \simeq +31.5$ kcal). Our conclusion is that the catalytic site involves two adjacent surface *dioxo units* (the *dual dioxo site*), with each dioxo site extracting one H in a sequence of steps. The required dual dioxo site exists on the (010) surface of MoO_3 but does not exist on the other low index surfaces. This mechanism is supported by atmospheric pressure experimental studies which indicate that MoO_3 (010) is selective for CH_2O products. A detailed sequence of reaction steps and the associated thermochemistry is proposed.

Chapter 2: Molybdates involving various metal additives play a dominant role in such industrially important catalytic processes as selective oxidation (propene to acrolein) and ammoxidation (propene to acrylonitrile); however, the details of the reaction mechanism and of the surface sites responsible are yet quite uncertain. In order to establish the thermochemistry and detailed mechanistic steps involved with such reactions, we have performed *ab initio* quantum chemical calculations [generalized valence bond (GVB) and configuration interaction (CI)]. These studies indicate a special importance of multiple surface dioxo Mo sites (possessing two Mo-O double bonds and hence spectator oxo groups) arranged together so as to provide the means for promoting the sequence of transformations.

Chapter 3: Extensive *ab initio* calculations have been carried out on molybdenum (VI, V and IV) complexes containing oxygen and nitrogen. A detailed description of the bonding of oxo, nitrido and imido terminally attached ligands to molybdenum is presented. These results are used to explain the preferred geometries of complexes as well as the periodic trends as ligands to molybdenum are varied from O, N, NH.

Chapter 4: We find that the ground state of MoN ($^4\Sigma^-$) has a covalent triple bond where the σ bond is dz^2-like on the Mo, leading to a quartet state with unpaired electrons in the Mo 5s, Mo $4d\delta_{xy}$, and Mo $4d\delta_{x^2-y^2}$ orbitals. The first excited state ($^4\Pi$) corresponds to the $5p_\pi \leftarrow 5s$ excitation. The calculated properties of $R_e = 1.60$ Å, $\omega_e = 1100$ cm^{-1}, $D_e = 4.07$ eV, and ΔE ($^4\Pi - {}^4\Sigma^-$) = 2.128 eV are in good agreement with recent experimental results ($R_e = 1.63$ Å and $\Delta E = 2.011$ eV). Particularly interesting is a dramatic nonmonotonic change of dipole moment with distance ($\mu = $

-3.123 D at R_e = 1.60 Å, -5.982 D at R = 2.60 Å and μ = -0.176 D at R = 5.0 Å. This effect is explained.

.

PREFACE

In order to understand catalytic reactions, it is necessary to have some knowledge of the chemical mechanism which converts reactants into products. This also necessitates understanding the role of the catalyst itself in the reaction. Once we have an idea of the reaction mechanism, which includes the role that the catalyst plays, we can predict what type of chemistry may occur on the many specific catalytic surfaces. We are then in a position to design more efficient catalysts.

We believe this thesis demonstrates that theoretical techniques are useful in predicting likely catalytic mechanisms. In a quantitative way, we are able to look at intermediate species that may be impossible to isolate experimentally and to interpret the results both structurally and energetically. In a qualitative way, theory is useful in determining which of the reaction pathways may be energetically feasible -- processes for which no experimental data may be available.

Consistent with the above ideas, in Chapter 1 we show a reaction mechanism for the conversion of methanol to formaldehyde over molybdenum trioxide. The detailed relationship between the mechanism and surface specificity is examined and compared with the experimental results. In Chapter 2 an analogous study is made of the selective oxidation of propene to acrolein over bismuth molybdate. Specific surface properties are correlated with the chemical properties of the catalyst. Chapters 3 and 4 describe in detail the bonding of imido, oxo and nitrido ligands to molybdenum complexes.

Table of Contents

CHAPTER 1

OXIDATIVE DEHYDROGENATION OF

METHANOL TO FORMALDEHYDE

INTRODUCTION

The mild catalytic oxidation of aliphatic alcohols ($C_nH_{2n+1}OH$) over simple metal oxides usually leads to the formation of carbonyl compounds $C_2H_{2n}O$. Thus, primary alcohols are selectively oxidized to aldehydes

$$HOCH_2R \longrightarrow O{=}C\begin{smallmatrix} R \\ \\ H \end{smallmatrix} \qquad (1)$$
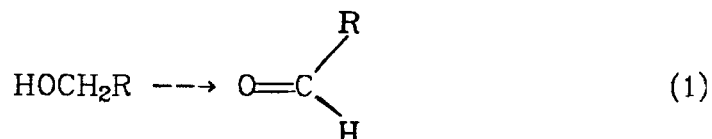
A classic example of this is the oxidative dehydrogenation of methanol to formaldehyde over the molybdenum trioxide catalyst, MoO_3

$$CH_3OH + \tfrac{1}{2}O_2 \longrightarrow CH_2O + H_2O \qquad (2)$$
$$MoO_3$$
$$(200-300)°C$$
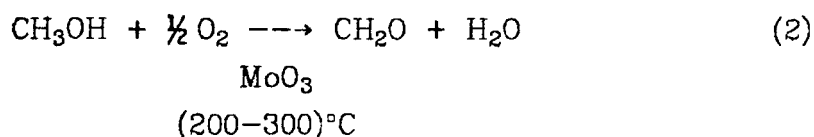
Pure MoO_3 exhibits ~100% *selectivity* but has low activity *(1)*. Addition of Fe_2O_3 to MoO_3 increases the *activity*, with an optimal Mo:Fe ratio of 1.7 *(1)*. Molybdates as well as complex oxide catalysts, K_2MoO_4, $CaMoO_4$, $CoMoO_4$, $Cr_2(MoO_4)_3$, $Fe_2(MoO_4)_3$, and $Bi_2(MoO_4)_3$ are also used for the selective formation (~95%) of formaldehyde from methanol, with the activation energy for these processes varying between 10-20 kcal/mol at 275°C *(1)*. Because of the extreme industrial importance of formaldehyde for plastics, dyes, etc., the highly selective reaction (2) has been the focus of much study *(2- 5)*.

Most of the information concerning the mechanism of reaction (2) to date has been extracted from a variety of infrared spectroscopy, mass spectroscopy, and kinetic isotope studies *(1- 9)*. The following concepts are generally accepted regarding the oxidation of methanol to formaldehyde over MoO_3:

a) The first step consists of dissociative adsorption of methanol to yield surface methoxy and surface hydroxyl species. This has been established by infrared studies which show evidence of a *nonvolatile* surface species with bands at 2925, 2825, and 1440 cm^{-1} assigned to methyl asymmetric stretch, symmetric stretch, and deformation vibrational frequencies (C-H bend), respectively, and a band at 1065 cm^{-1} due to the C-O stretch *(7)*. These band assignments have been confirmed by Sleight *et al.* *(13)*.

b) The rate determining step is the breaking of a C-H bond of the surface methoxy species. This has been established by changes in product distribution from the starting products CH_3OH versus CH_3OD and from CH_3OH versus CD_3OD *(3,6)*.

c) The activation energies for oxidation of methanol over MoO_3 and $Fe_2(MoO_4)_3$ are in the range 16-20 kcal/mol *(1)*.

d) The catalysis by both supported and unsupported single crystals of MoO_3 crystals having a variety of geometries indicates that the basal crystal face [(010) surface] of MoO_3 is responsible for forming formaldehyde H_2CO, while the side surface [(100)] and apical surfaces [(001)] plus (110)] lead to methylal $CH_2(OMe)_2$ and dimethyl ether $(CH_3)_2O$, respectively *(4)*.

e) Mo=O centers have been identified by a number of workers as possible dehydrogenation centers believed to be important in *mild* oxidation *(4,5,8,9)*.

Despite the progress indicated above, there is little known about the *detailed* sequence of reaction steps or the thermochemistry of methanol oxidation over metal oxide catalysts. Thus, one does not know what surface *sites* are required for selective formation of H_2CO and which sites

lead to formation of the acetal, ether, or CO_2. Our goal is to develop a sufficiently detailed understanding of these mechanisms so that one could design new catalysts that would be more selective or more active.

As a basis for the mechanistic considerations of the mild oxidation of methanol by molybdate catalysts, we have carried out a series of *ab initio* quantum chemical calculations [generalized valence bond (GVB) and configuration interaction (CI)] on models of various active sites. These studies provide some new insights concerning mechanisms that we believe move us closer to the above goal. We first outline the relevance of the emerging paradigm concerning transition metal oxides and then examine some details of the mechanism.

SPECTATOR EFFECTS

The molybdate systems lead to bulk structures involving either octahedral or tetrahedral coordination of oxygens about each Mo. As a result, one would expect the most stable surface configurations for such molybdates to be as indicated in **1, 2,** and **3**.

I	2	3a	3b
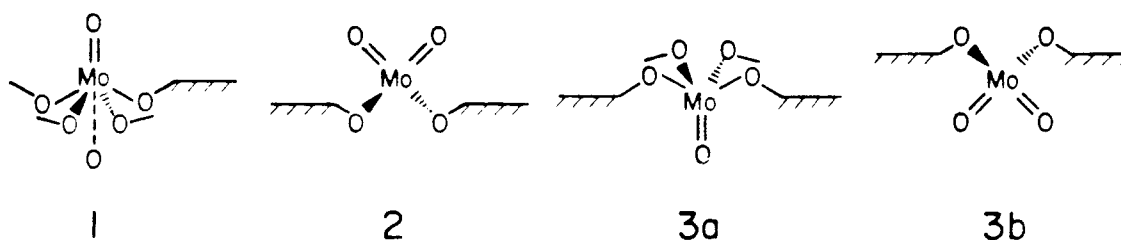
where **1** and **3a** derive from bulk octahedral sites and **2** and **3b** derive from bulk tetrahedral sites. Here each single-bonded O makes a strong single bond to a second Mo (typical bond distances of ~1.95 Å), whereas the oxygen involved in the double bond (Mo=O) is bonded only to the one Mo (typical bond distances of 1.67 to 1.73 Å in the bulk); the next closest oxygen is typically 2.2 to 2.4 Å. All four cases involve Mo^{VI} centers and cases **1** and **2** both involve surface Mo-O double bonds. However, we find that species **1** and **2** lead to extremely different chemistry. This remarkable difference arises from the **spectator oxo effect** *(10,11)*, as discussed below.

Figure 1 shows the bonding for
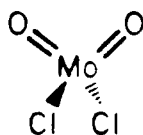
as a model of the dioxo species **2** (with each Cl modeling a bridging oxygen). Here we see that each Mo=O bond has the form of a covalent double bond involving spin pairing of two singly-occupied Mo d orbitals and two

singly-occupied O p orbitals. Denoting the Mo=O axis as z and the MoO_2 plane as yz, the Mo-O sigma bond involves Mo d_{z^2} and O p_z (leading to an overlap of 0.78), while the Mo-O pi bond involves Mo d_{xz} and O p_x (leading to an overlap of 0.64). Two such bonds require four Mo electrons in four orthogonal Mo d orbitals. On the other hand, the two Mo-Cl bonds (modeling single bonds to the two bridging oxygens in molybdates) involve a large amount of ionic character with some 5s-5p character on the Mo. Thus the Mo^{VI} center in **2** should be best visualized in terms of ionic bonds to the two bridging oxygens, while the Mo=O bonds should be considered as covalent double bonds. The requirement of four singly-occupied d orbitals for the two Mo=O bonds leads to an O=Mo=O of 106° (the π bonds would prefer 90°; the σ bonds, 125°) *(11)*. In addition to the two singly-occupied oxygen p orbitals involved in the Mo=O bond, each oxygen has four valence electrons in two nonbonding orbitals (mixture of O 2s and O $2p_y$).

The bonding is quite different when there is only one multiple bonded oxygen, as indicated in Figure 2 (the orbitals are for
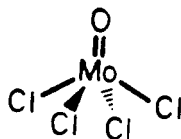
where each Cl models a bridging oxygen of **1**). Here there are *two* pi bonds between Mo and O. Thus, taking the Mo=O axis as z, there is a pi bond involving Mo d_{yz} and O p_y and a pi bond involving Mo d_{xz} and O p_x. In addition, the Mo has a total of four partially ionic bonds to the four Cl, acounting then for the six Mo valence electrons (in this description the Mo d_{z^2} orbital is empty). The two Mo=O pi bonds require two singly-occupied pπ orbitals on the oxygen (p_x and p_y), leaving four electrons for

the O 2s and O $2p_z$ orbitals. With two electrons in O $2p_z$ and none in Mo d_{z^2}, we obtain a Lewis base-Lewis acid bond in the sigma system, leading to a net Mo-O bond involving *six electrons* (four from oxygen and two from Mo). The result is a **partial triple bond** that is much stronger than the double of bond of **2**. Why can't species **2** make two such partial triple bonds? The requirement is *two* singly-occupied metal pi orbitals (π_x and π_y) for *each* super double bond so that there are just not enough Mo pi orbitals to go around for **2**. This is analogous to the difference between O=C=O with two *double* bonds and C≡O with a partial triple bond about twice as strong.

When chemistry occurs at one Mo=O bond, for example,
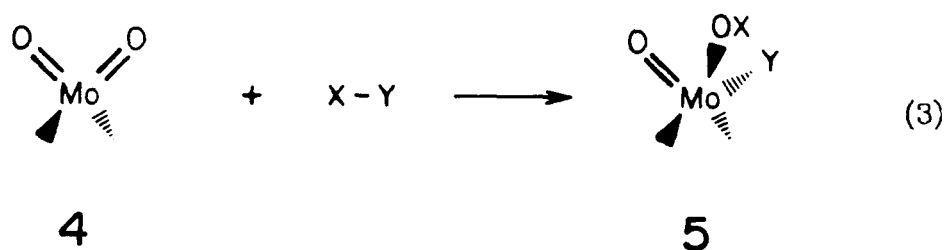
the extra Mo=O bond of **4** would appear to be a spectator to the reaction, but in fact it helps *promote* the reaction. The spectator Mo=O bond changes from a double bond in **4** to a super double bond in **5** when chemistry occurs at the *other* Mo=O bond. This results because the Mo-OX and Mo-Y bonds in **5** are sigma bonds, neither requiring Mo dπ orbitals. As a result, the spectator Mo=O bond in **5** can sequester both Mo dπ orbitals for its own purposes, yielding two pi bonds plus the donor-acceptor sigma bond for an overall *partial triple bond*. Thus the spectator oxo group is stabilized by the reaction, and hence *the spectator oxo group promotes reaction at the adjacent double- bonded group*. Such spectator oxo effects have proved important in homogeneous metathesis catalysis by

-8-

Mo *(10,16,17)* and we suggest below that they are critical in oxidative dehydrogenation. For surface species such as **3a** and **3b,** the Mo=O bonds are protected from direct attack; however, the exposed part of the Mo should act as an electrophile (Lewis acid) that could stabilize the physisorption of species such as CH_3OH.

We should point out here that Trifiro *(5)* has long maintained that Mo=O double bonds are important in oxidation catalysts and has suggested that the dioxo center **2** should be the important center since it can simultaneously extract both hydrogens from methanol,
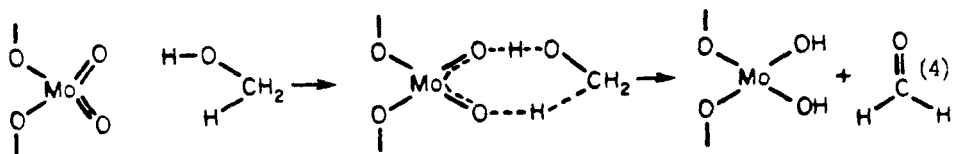
$$\Delta H \approx +31.5 \text{ kcal/mol}$$

Although the simple pictures in (4) make the process *look* plausible, it is in fact very endothermic, $\Delta H \approx +31.5$ kcal. Of course, this mechanism is also inconsistent with the experimental evidence of adsorbed methoxide *vide infra*. The problem is that (4) involves loss of two strong Mo=O pi bonds, but the resulting two unpaired electrons on the Mo are not utilized for any two strong bonds (formally, the Mo is changed from Mo^{VI} where all six valence electrons are involved in bonds to Mo^{IV} where only four electrons are involved in bonds).

THE MECHANISM

Considering the interaction of CH_3OH with the likely surface species, **1**, **2**, and **3** of MoO_3, we find the following energetics for the simplest one-center process,
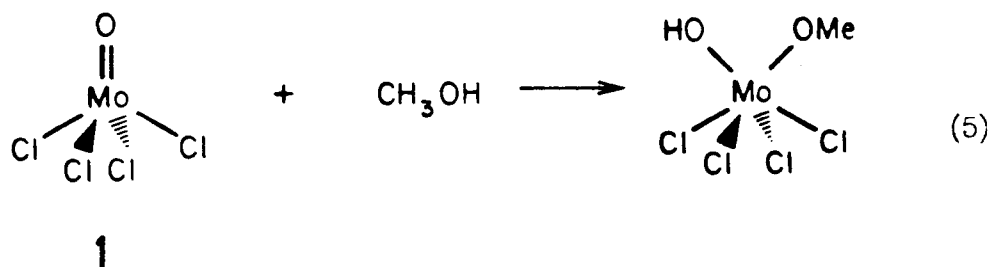
$$\Delta H_5 = +22 \text{ kcal/mol}$$
$$\Delta G_5 = +33 \text{ kcal/mol}$$
$$(25°C)$$
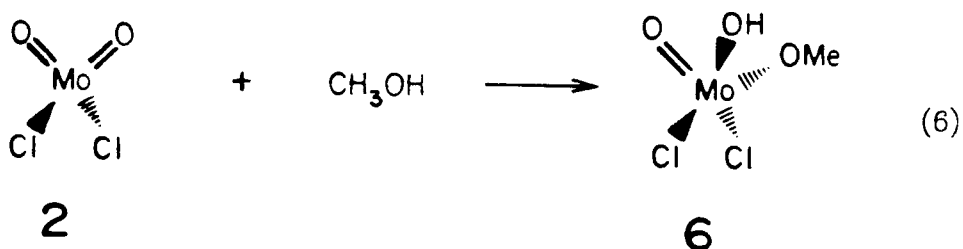
$$\Delta H_6 = -9 \text{ kcal/mol}$$
$$\Delta G_6 = +2 \text{ kcal/mol}$$
$$(25°C)$$

Thus, species **1** with a partial triple bond is *not* effective in activating methanol; however, due to spectator oxo stabilization, *species **2** can activate* CH_3OH *in a one- center process.*

From (4) we see that the Mo-O partial triple bond in (6) cannot extract the H from the bound methoxy to form formaldehyde. The remaining possibility for a one-center process would be β-hydride elimi-

nation of formaldehyde from **6**

$$\Delta H_7 = +30 \text{ kcal/mol}$$

$$\Delta G_7 = +10 \text{ kcal/mol}$$

$$(300°C)$$
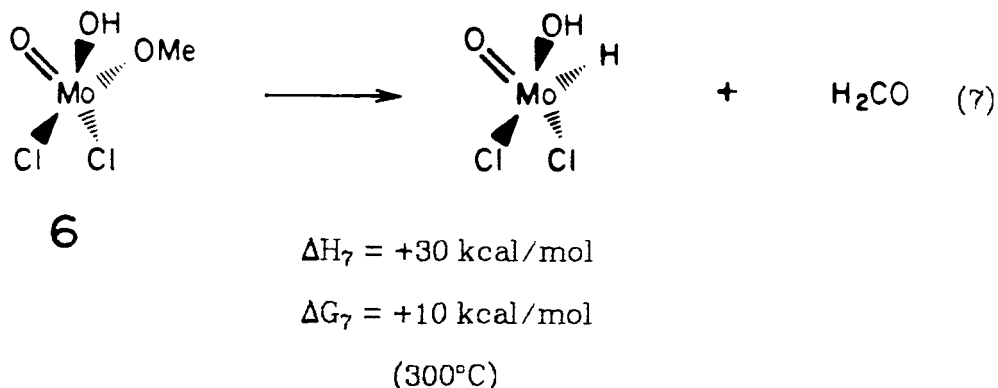
However, we find this process to be quite endothermic, and we believe that the barrier is too high.

Consequently, we must now consider whether a *second* Mo site
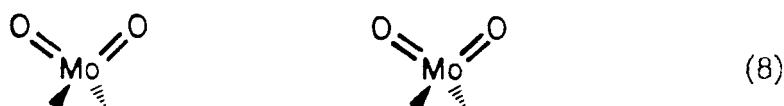
might play a role in the catalytic process. If two dioxo units are arranged so that chemisorption of the CH_3OH to form a methoxy unit places a CH bond sufficiently close to one of the oxo bonds of the *second dioxo unit*, then cleavage of the C-H bond of the chemisorbed methoxy group in **6** to form CH_2O can be facile

$$\Delta H_9 = +6 \text{ kcal/mol}$$

$$\Delta G_9 = +6 \text{ kcal/mol}$$

$$(300°C)$$
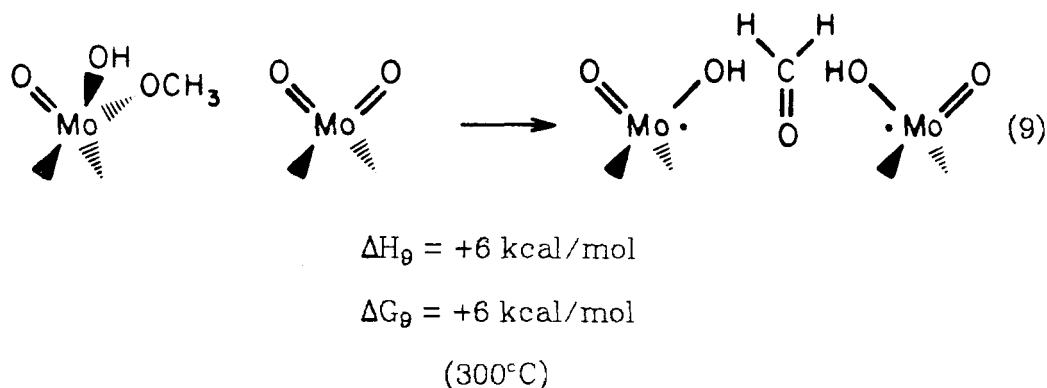
This process is favorable only because it is promoted by the spectator oxo group on this adjacent dioxo unit.

After completion of step (9), subsequent steps involve desorption of formaldehyde, associative desorption of H_2O, e.g.,

(10)
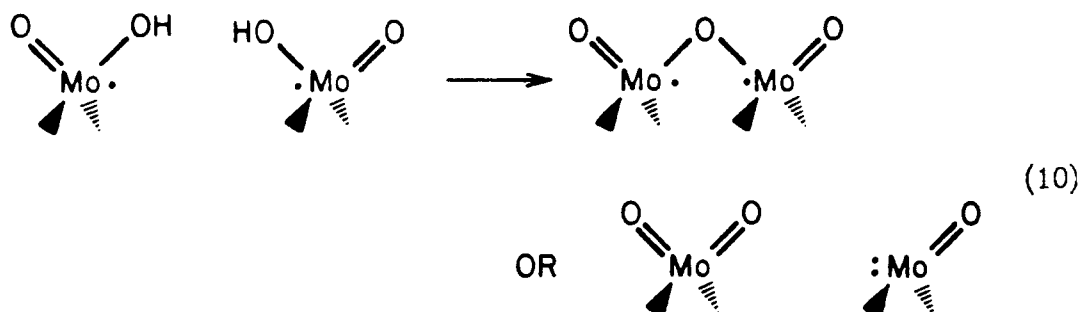
and replenishment of the surface with bulk oxide to reconstruct the active site.

Thus we suggest that *selective oxidation dehydrogenation of* CH_3OH *to* CH_2O *requires a dual set of adjacent* dioxo units with an overall scheme as indicated in Figure 3. For each dioxo unit, one of the two oxygens can extract a hydrogen, with the other oxygen providing the spectator oxo stabilization. The spectator oxo effects are crucial in making the chemisorption step (6) exothermic and keeping the CH chemisorption step (9) only slightly endothermic. In this description one would expect the CH bond cleavage (9) to be the rate-determining step [as proved in recent experiments (5)]. Note that step (9) leads to OH groups on different Mo centers so that there should be an additional barrier to desorbing H_2O [step (10)] after formation and desorption of $H_2C{=}O$. Indeed, this is obtained in temperature programmed reaction studies (7).

Now the question is, does MoO_3 have a surface with the requisite configuration with adjacent dual oxo sites? Indeed, as indicated in Figure 4, examination of the crystal structure (14) of MoO_3 shows that the (010) surface has exactly the configuration needed for the steps in Figure 3 and Scheme I. On the other hand, the other low index faces of MoO_3 do *not*

have the requisite combination of dual dioxo units. This conclusion that dual dioxo units are essential for the catalytic dehydrogenation of CH_3OH is strongly supported by the experimental studies of the Lyon group (Tatibouët and Germain) *(4)*. In the presence of O_2, they find that MoO_3 (010) is highly selective for formation of H_2CO, whereas MoO_3(100) leads to methylal, and MoO_3 [(001) + (101)] are bifunctional [leading to H_2CO and $O(CH_3)_2$].

The (100) surface is shown in Figures 5 and 6, where we see that there are exposed (isolated) dioxo units and buried ones (as in **3b**). Tatibouët and Germain suggest that it is the bifunctionality that is responsible for the production of methylal. The low index faces (001) and (101) are expected to be less stable, and it is not clear what the reconstructed surface is like. However, the observed lack of selectivity is certainly consistent with the expected multifunctionality.

From Figure 5 we see that there are two plausible forms for the Mo (010) surface. The one shown in Figure 4 leads to oxo units pointing out of the surface and would appear to be the most stable surface. Alternatively, shaving the top layer leads to a surface structure as shown in Figure 5 (this leads to breaking of the long, weak 2.33 Å Mo-O bonds). In this case the oxo units point along the surface and down, exposing Lewis base sites. This might physisorb CH_3OH but does not appear plausible for chemisorption. We speculate that this surface may be stabilized under high vacuum environments with low O_2 pressure (vide infra). If so, this would explain the results of the Lyon group which finds no reaction with CH_3OH unless O_2 is present.
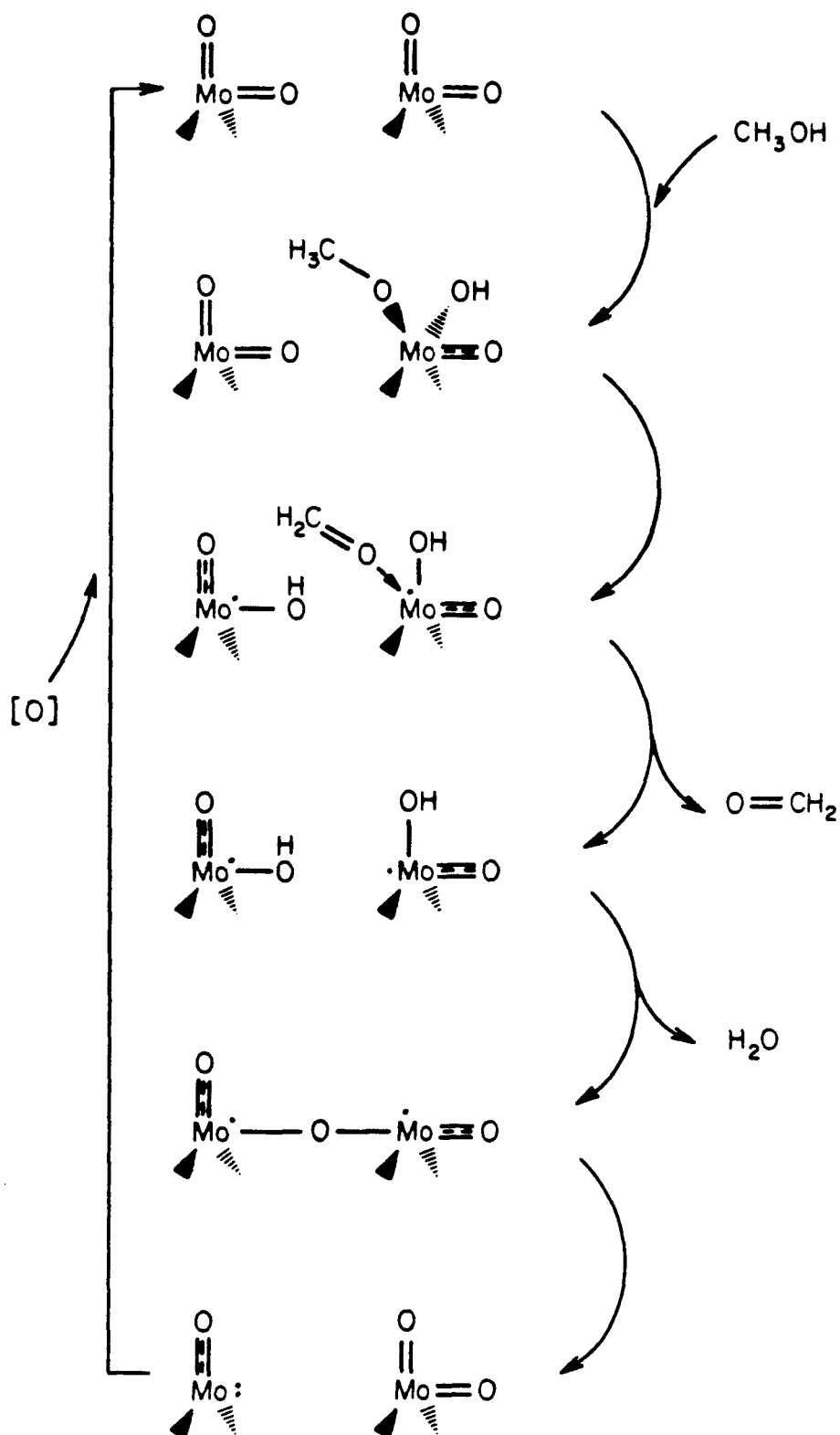
Scheme I. The mechanism for oxidative dehydrogenation on the dual dioxo site of MoO_3 (010).

DISCUSSION

It has sometimes been suggested *(15)* that the (010) surface of MoO_3 may be nonreactive compared with other surfaces because it has no broken chemical bonds. Our mechanism suggests that this simple reasoning is inadequate for MoO_3 (010), and indeed the experiments of Ref. *(4)* provide strong evidence that MoO_3 (010) is the important surface for formation of H_2CO.

The specific mechanism proposed here, involving a dual dioxo catalytic site, is susceptible to many experimental tests. We expect that such interplay between theory and experiment will promote the development of a much more detailed understanding of the fundamental chemical mechanisms of heterogeneous catalytic reactions. We believe that sites involving collections of surface dioxo units are also important in selective oxidation and ammoxidation reactions *(18)*.

$$=\!\!\diagup \;+\; O_2 \longrightarrow \;=\!\!\diagup^{C=O}$$
$$NH_3 \searrow$$
$$=\!\!\diagup^{C\equiv N}$$
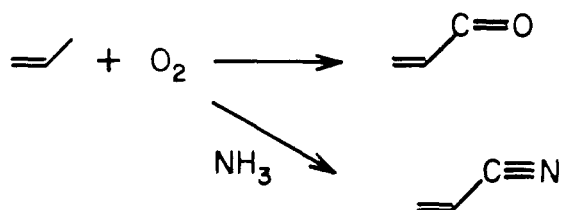
After submission of our original manuscript, a paper from the Dupont group appeared *(19)* that seems to contradict both the conclusions from the experimental studies at Lyon *(4)* and our theoretical studies. Using large single crystals of MoO_3 with large exposed basal planes (010), the Dupont group exposed these surfaces with up to $10^5 L$ of CH_3OH at room temperature and observed no changes in the UPS. This might seem to contradict the results of the Lyon group; however, it should be noted that the Lyon group also found no reaction unless O_2 was present with the CH_3OH (they also used higher temperatures, 200-300°C). A second

consideration is whether UPS is sufficiently sensitive to detect submono-layer adsorption of CH_3OH on MoO_3 (010). Studies on polycrystalline MoO_3 indicated reaction to form CH_2O under conditions where the UPS does not change *(19)*.

ACKNOWLEDGMENTS

REFERENCES

1. Golodets, G. I., "Studies in Surface Science and Catalysis 15. Heterogeneous Catalytic Reactions Involving Molecular Oxygen," Elsevier Publishing Company: Amsterdam, 1983; Chap. XVI.

2. Machiels, C. J., and Sleight, A. W., "Proceedings of the Fourth International Conference on Chemistry and Uses of Molybdenum," Climax Molybdenum Company: Ann Arbor, Michigan, 1982; p 411.

3. Machiels, C. J., *ACS Symposium Series* **178**, 239 (1982).

4. Tatibouët, J. M., and Germain, J. E., *J. Catal.* **72**, 375 (1981); Tatibouët, J. M., Germain, J. E., and Volta, J. L., *J. Catal.* **82**, 240 (1983).

5. Trifiro, F., Notarbartolo, S., and Pasquon, I., *J. Catal.* **22**, 324 (1971).

6. Machiels, C. J., and Sleight, A. W., *J. Catal.* **76**, 238 (1982).

7. Groff, R. P., *J. Catal.* **86**, 215 (1984).

8. Weiss, F., Marion, J., Metzger, J., and Cognion, J. M., *Kinet. Katal.* **14**, 45 (1973).

9. Agaguseinova, M. M., Adzhamov, K. Yu., and Alkhazov, T. G., *Kinet. Katal.* **17**, 1556 (1976).

10. Rappé, A. K., and Goddard III, W. A., *Nature* **285**, 211 (1980); *J. Am. Chem. Soc.* **102**, 5114 (1980); *ibid.* **104**, 448 (1982).

11. Rappé, A. K., and Goddard III, W. A., *J. Am. Chem. Soc.* **104**, 297, 3287 (1982).

12. Allison, J. N., and Goddard III, W. A., to be published.

13. Sleight, A. W., Staley, R. H., and Chowdry, V., private communication.

14. Kihlborg, L. *Arkiv Kemi* **21,** 155 (1983).

15. Firment, L. E., and Ferretti, A., *Surf. Sci.* **129,** 155 (1983).

16. (a) Schrock, R. R., Rocklage, S., Wengrovious, J. H., Rupprecht, G., and Fellmann, J., *J. Mol. Catal.* **8,** 73 (1980); (b) Wengrovious, J. H., Schrock, R. R., Churchill, M. R., Missert, J. R., and Youngs, W. J., *J. Am. Chem. Soc.* **102,** 4515 (1980).

17. Muetterties, E. L., and Band, E., *J. Am. Chem. Soc.*, **102,** 6574 (1980).

18. Burrington, J. D., Kartisek, C. T., and Grasselli, R. K., *J. Catal.*, **81,** 489 (1983).

19. Ohuchi, F., Firment, L. E., Chowdry, U., and Ferretti, A., *J. Vac. Sci. Technol. A* **2,** 1022 (1984).
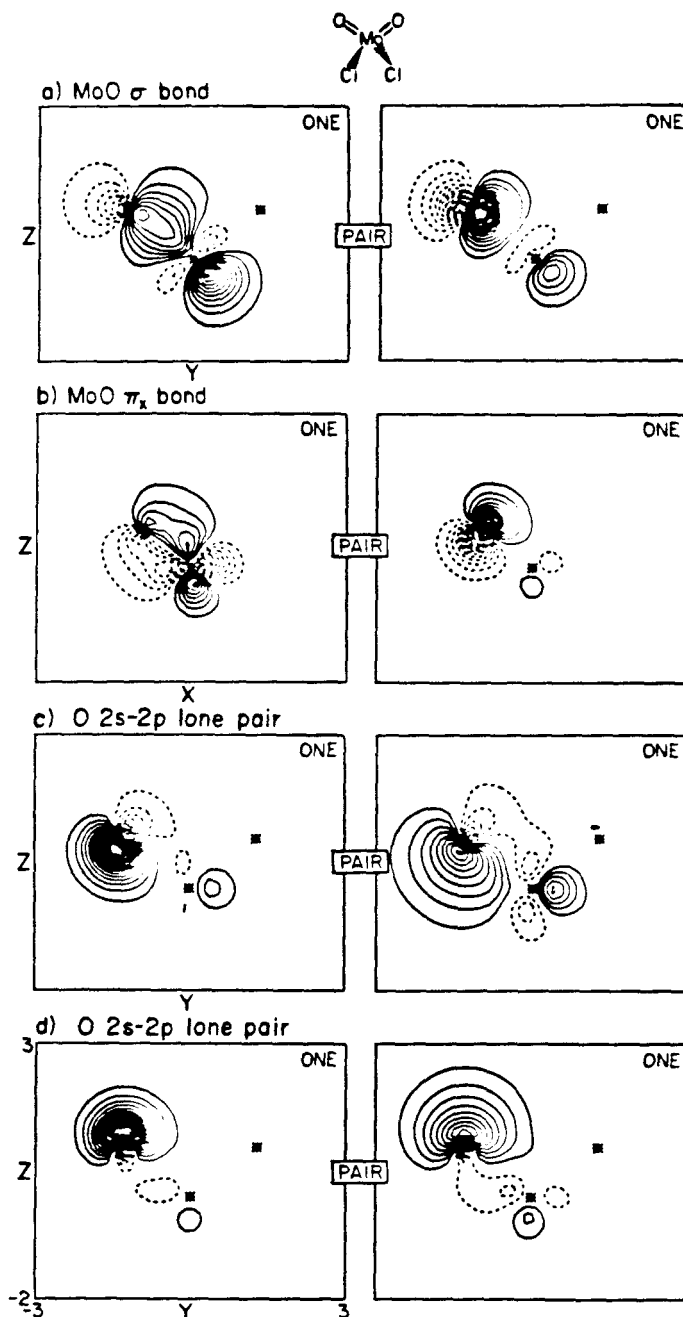
FIG. 1. GVB orbitals for the electron pairs involving the left Mo=O double bond in species **2**. Dotted contours indicate negative amplitude. Increments between contours are 0.050 a.u.; the zero contour is *not* shown.
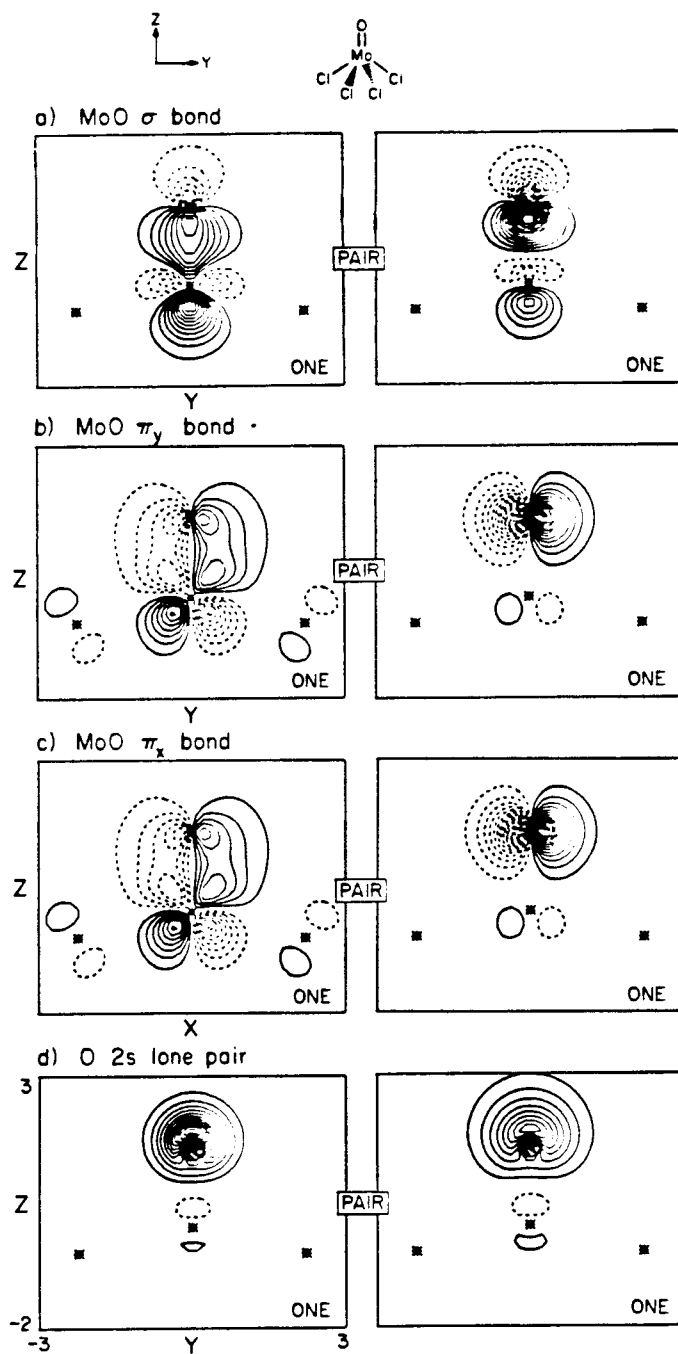
FIG. 2. GVB orbitals for the electron pairs involving the triple bond for species **1**. (Same plotting conventions as in Figure 1.)
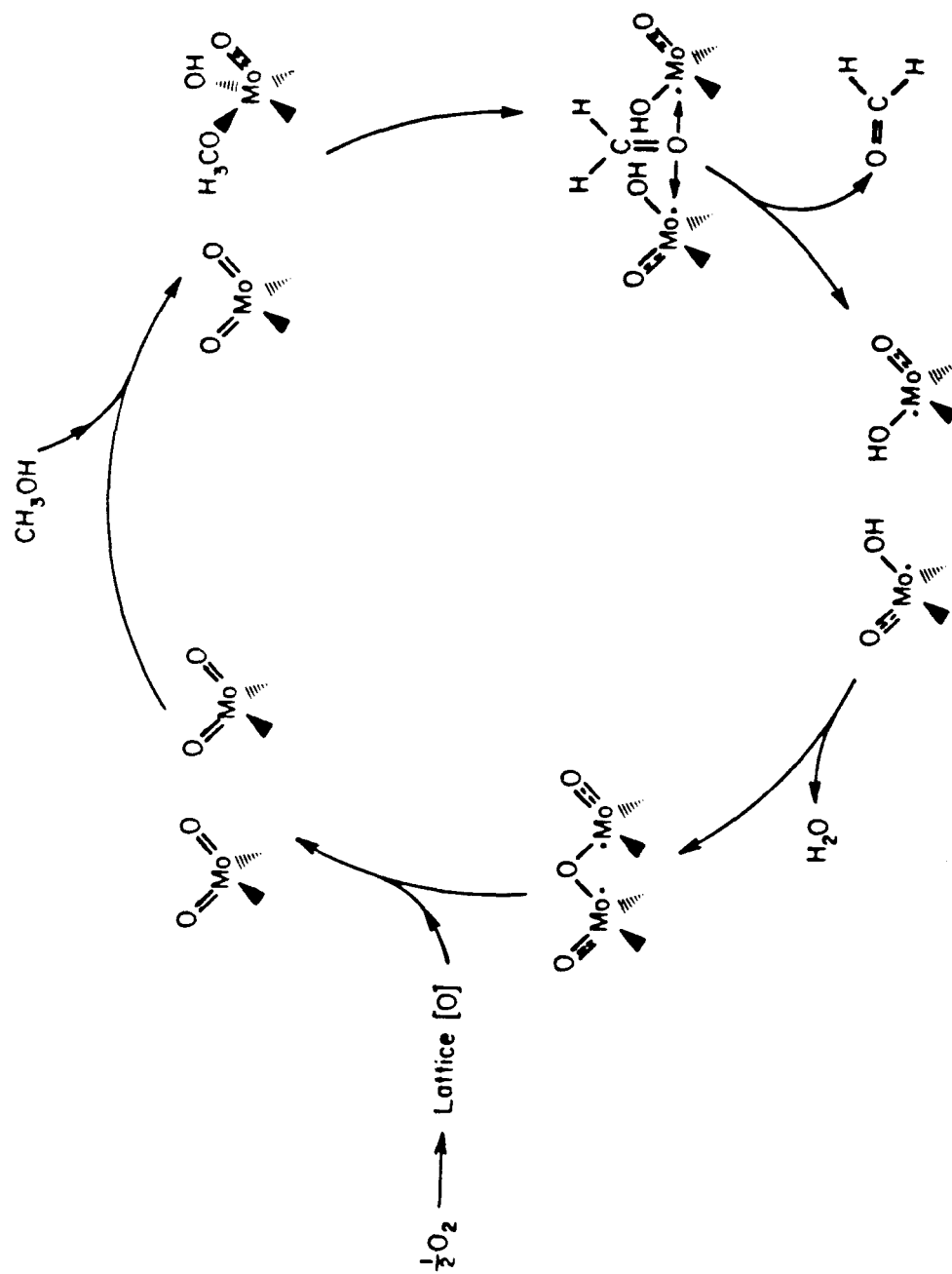
FIG. 3. The sequence of reaction steps for the dual dioxo catalytic site.

-20-

SIDE VIEW

TOP VIEW
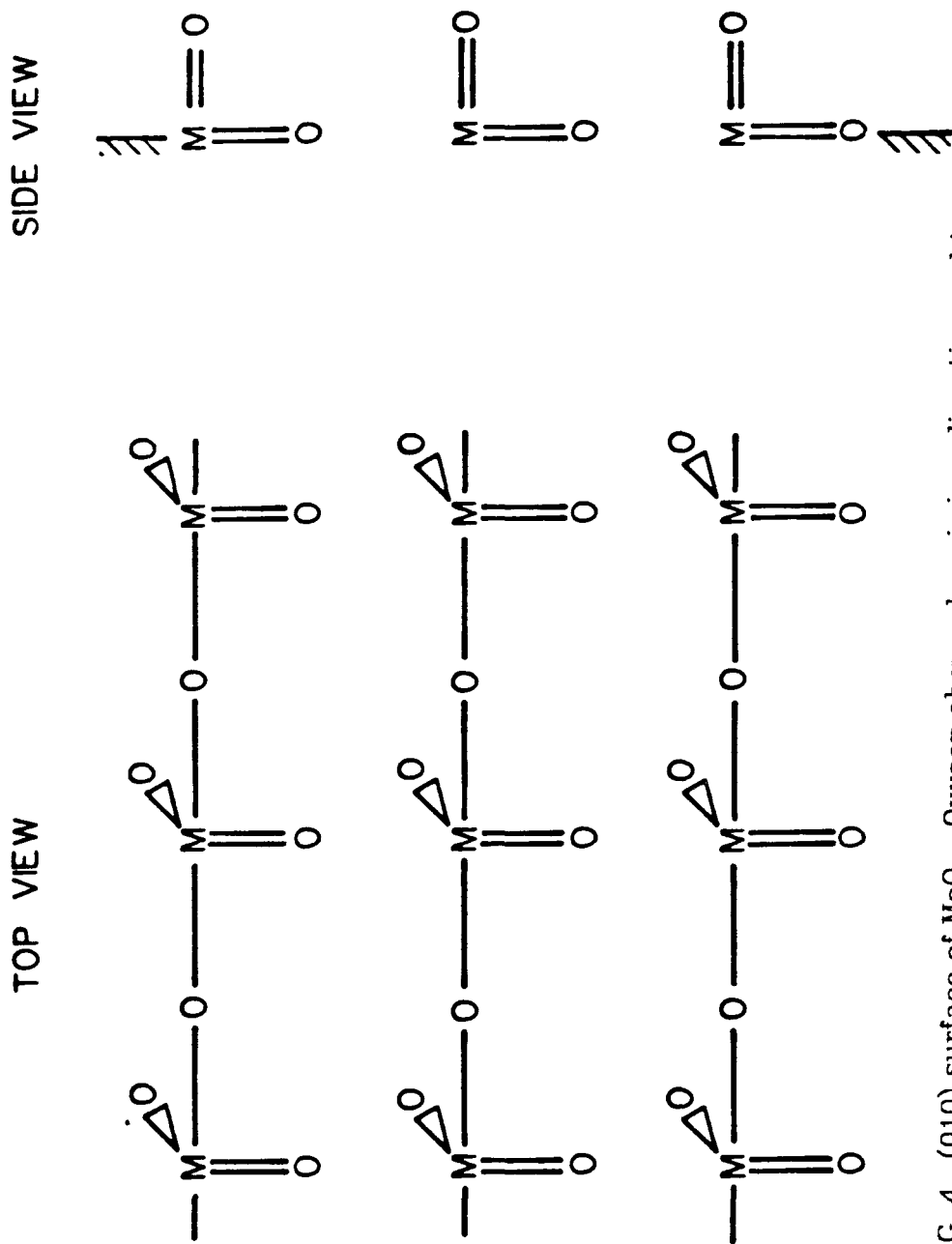
FIG. 4. (010) surface of MoO_3. Oxygen above plane is in y direction and is double-bonded to Mo in plane.

FIG. 5. Side views of the (010) and (100) surfaces of molybdenum triox-ide, MoO_3. Plots were made using the PLUTO program (Sam Motherwell, University Chemistry Laboratory, Cambridge, England) as follows: Pack-ing range: a = -1.5 to 1.5; b = 0.0 to 1.0; c = 0.0 to 1.0. Scale factor: 15 (15 mm $\equiv$ 1 Å). Mono 1500 (single plot with perspective drawing as seen from a distance of 1500 mm). The view shown is the MoO_3 (010) surface whose image has subsequently been rotated about the fixed plotter axes x,y,z (z axis rotation, 90°; x-axis rotation, 83°).

MOLYBDENUM TRIOXIDE (MoO₃) SURFACES

(OIO) surface with Lewis acid sites exposed

(OIO) surface with oxo groups exposed

(100) surface showing both Lewis acid sites and oxo groups exposed
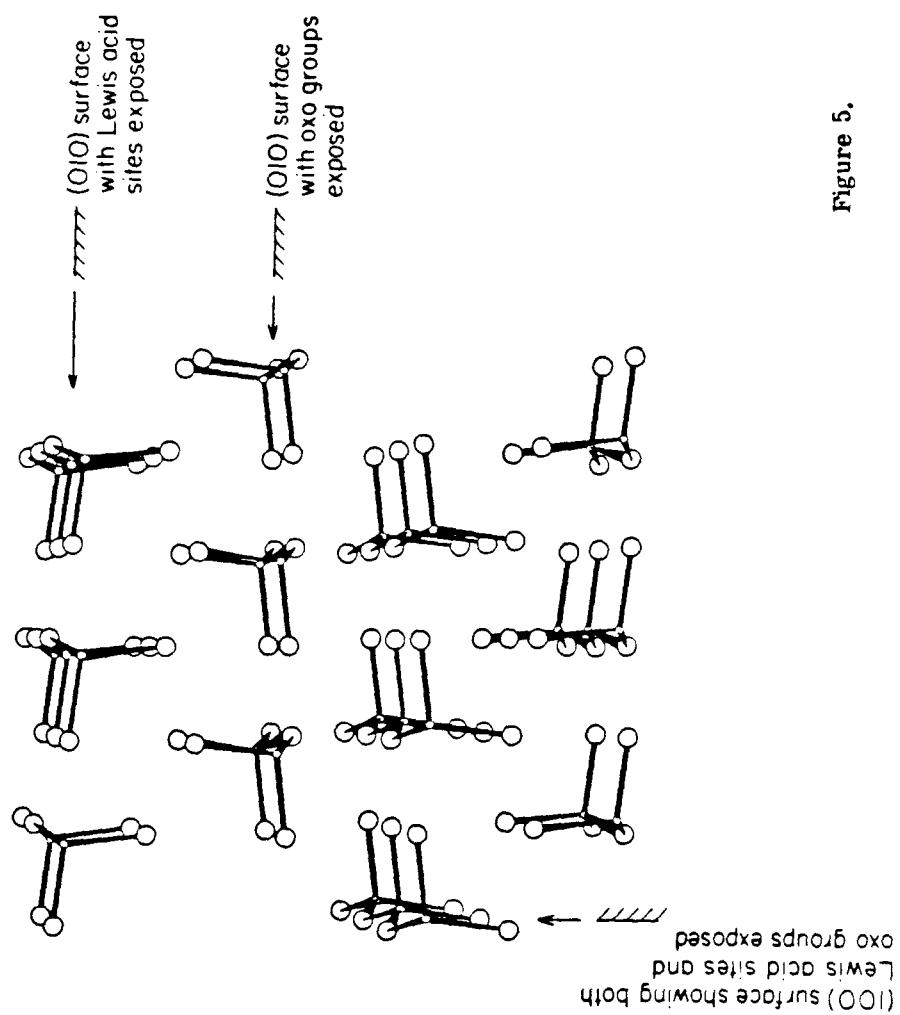
Figure 5.

MOLYBDENUM TRIOXIDE, MoO_3 (100) SURFACE

Lewis acid site
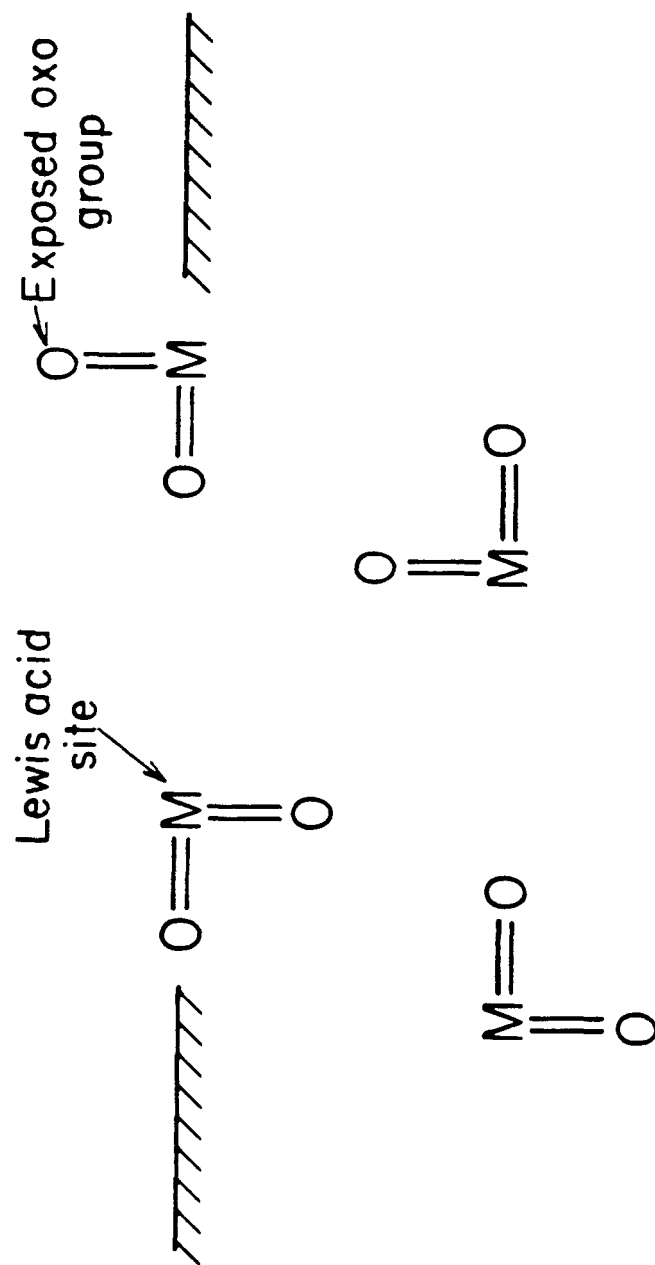
Exposed oxo group

FIG. 6. Schematic diagram of $MoO_3(100)$ side face. For this bifunctional face there are pairs of alternating Lewis acid sites and exposed oxo group sites.

APPENDIX TO CHAPTER 1

Concerning recent results of Ohuchi *et al.*[1] for CH$_3$OH exposure to MoO$_3$ powder and to the MoO$_3$ (010) crystal surface, the following observations have been made.[1]

Using UPS and XPS, adsorption of CH$_3$OH was *not* detected on MoO$_3$ powder surfaces at room temperature up to exposures of 10^{10}L. Microbalance results showed a low probability of adsorption with saturation coverage (1 × 10^{14} molecules/cm^2) reached after 10^{10}L. In spite of high background pressures, reaction products were observed in the TPD at 385, 485, and 520K corresponding to H$_2$CO, CH$_3$OH, and H$_2$O, respectively.[1]

Using UPS, it was determined that the MoO$_3$ (010) crystal surface was inert to CH$_3$OH adsorption at room temperature up to exposures of 10^5L. Only physisorbed CH$_3$OH at 150K was detected in the UPS which desorbed physically intact at 220K. No reaction products were detected in the TPD.[1]

To summarize, work done by Ohuchi *et al.*[1] indicated CH$_3$OH adsorption was not detected on MoO$_3$ powder; however, reaction products were observed. Also, the MoO$_3$ (010) crystal surface was believed to be inert to CH$_3$OH adsorption. Only physisorbed CH$_3$OH was found and *no* reaction products were detected.

The above study may be interpreted as weak with respect to several issues:

1) There was failure to detect *adsorbed* CH$_3$OH on the MoO$_3$ powder, which apparently did produce reaction products. This lack of detection would seem unusual as high doses of CH$_3$OH were used and the UPS technique has a relatively high surface sensitivity.

2) There was failure to quantitatively compare the activities of MoO_3 powder with the MoO_3 (010) surface via TPD.

3) It is not clear whether the MoO_3 powder and the MoO_3 (010) crystal surface samples were *fully oxidized*. Even though the sample can be reoxidized in the pretreatment chamber, it is transferred to the UHV chamber *without exposure to air*. There is no specific mention in this paper of reoxidization of the catalyst or the addition of O_2 to the feed. The MoO_3 powder sample was prepared by decomposition of molybdenum oxalate in air at 670K, and the MoO_3 (010) crystal was prepared according to any one of three methods described in a previous paper by Firment and Ferretti.[2]

A fully oxidized MoO_3 sample is necessary for stoichiometric surfaces (vide supra). Firment and Ferretti[2] discuss three methods for removing carbon contamination from the MoO_3 (010) crystal (which was prepared via the Bridgman technique):

a) Oxygen cleaning of air-cleaved crystals;

b) Ion bombardment followed by reoxidation;

c) Scraping followed by annealing at 770-850K.

For the first two methods of crystal preparation (a,b), strenuous reoxidation conditions (10^2 Pa O_2 at 770K for 0.5 hr) were found to be necessary to insure stoichiometry at the MoO_3 (010) surface.[2] Attempts at reoxidation at lower temperatures or at lower O_2 pressures failed to produce stoichiometric MoO_3 (010) surfaces.[2]

If the MoO_3 surface is not fully oxidized, the heating of "oxygen-deficient" crystals in vacuum induces reduction, as the surface is labile.[2] Other works[3,4] stress the importance of having fully oxidized MoO_3

catalysts. Fully oxidized catalysts have been shown to be the most active and selective. Without the presence of O_2 in the feed, catalyst activity decreases.[4]

The partial oxidation of CH_3OH over a commercial ferric molybdate catalyst in a lean methanol-air mixture was investigated by Edwards *et al*.[5] Temperatures just below normal reaction temperatures were used in order to help understand the surface chemistry. At 170°C and 1 atm., the principal products were formaldehyde, water, dimethylether, methyl formate, and methylal. These species were identified by analyzing the chromatogram of reaction products at 170°C.

Structure-sensitive catalytic oxidation of methanol over unsupported and graphite-supported MoO_3 crystals has been studied.[7-9] Vapor phase reactions of diluted methanol-oxygen mixtures $MeOH/O_2$ 8.2/19.7 were carried out at 1 atm. and 200-300°C. Very pure orthorhombic MoO_3 was sublimed and flat crystalline needles were collected. Different crystallographic orientations were found by electron diffraction patterns.[7] The MoO_3 crystal faces studied were the (010) basal face, the [(001) + (101)] apical faces, and the (100) side face. Gas chromatography was used for product analysis. The results are shown below in Table 1.[9]

TABLE 1.

MoO$_3$ surface	Product	
	with O$_2$	without O$_2$
(010) basal face	Formaldehyde	
[(001) + (101)] apical faces	formaldehyde dimethylether	methylal dimethylether
(100) side face	methylal	dimethylether

We can see from Table 1 that the (010) basal face is active only *in the presence of oxygen* -- the dehydrogenation sites produce formaldehyde. The [(001) + (101)] apical faces are bifunctional with or without O$_2$. The (100) side face dehydrogenates with O$_2$ to produce CH$_2$O and dehydrates without O$_2$ to produce dimethylether. For dehydrogenation sites the Mo=O bonds must point out from the surface. For dehydration exposed Mo cation (Lewis acid) sites are required.

CHAPTER 2

PART A:

ACTIVE SITES ON MOLYBDATE SURFACES,

MECHANISTIC CONSIDERATIONS FOR SELECTIVE OXIDATION

AND AMMOXIDATION OF PROPENE

Introduction

Various catalysts based on molybdates have been used both for *selective oxidation of propene to acrolein*

$$H_2C=CH{\nearrow}^{CH_3} + O_2 \xrightarrow[\substack{Bi_2O_3 \cdot nMoO_3 \\ 320°C}]{} H_2C=CH{\nearrow}^{HC=O} + H_2O \qquad n = 2, 3 \tag{1}$$

and *ammoxidation of propene to acrylonitrile*,

$$H_2C=CH{\nearrow}^{CH_3} + O_2 + NH_3 \xrightarrow[\substack{Bi_2O_3 \cdot nMoO_3 \\ 430°C}]{} H_2C=C{\big\langle}^{CN}_{H} + H_2O \tag{2}$$
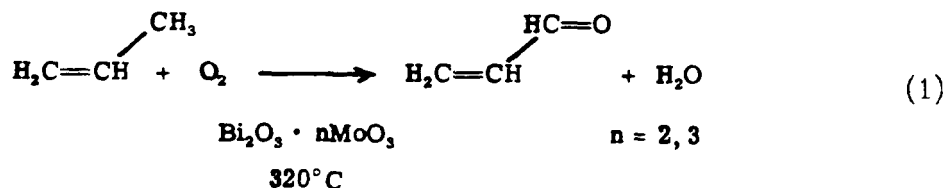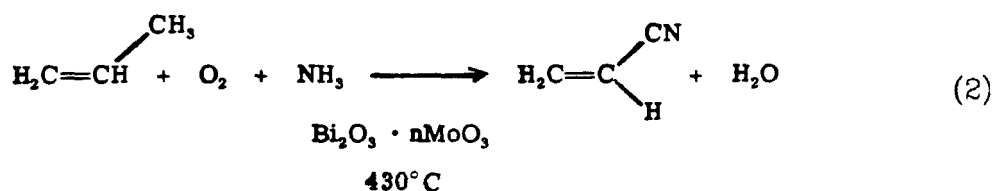
Numerous experimental studies have provided mechanistic information about these catalytic reactions; however, there are as yet many uncertainties concerning the character of the active site and its relation to the details of the mechanism. In this paper we will use the results of *ab initio* quantum chemical calculations [generalized valence bond (GVB) and configuration interaction (CI)] to help analyze the details of the reaction mechanisms and the relation of various reaction steps to specific surface sites.

In the following sections we discuss the principle of spectator oxo promotion that we find to play a crucial role in promoting particular reaction steps; we then examine the details of selective oxidation; and, finally, we outline preliminary results on ammoxidation .

Spectator Oxo Effects

Molybdates lead to bulk structures involving either octahedral or tetrahedral coordination of oxygens about each Mo. On various surfaces, the most stable configurations for such molybdates are likely to be

| 1 | 2 | 3 |
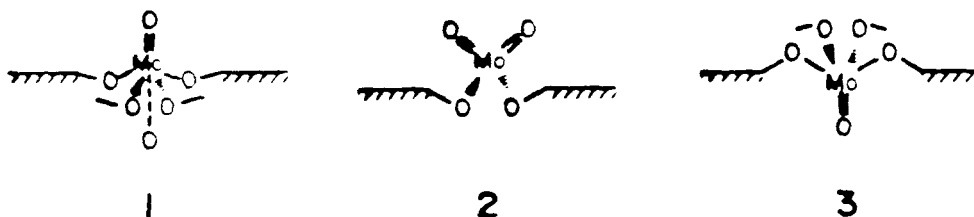
where **1** and **3** correspond to bulk octahedral sites and **2** to bulk tetrahedral sites. Here there are four (**1**) and (**3**) or two (**2**) single bonds to oxygen atoms that have a single bond to another Mo center, and one (**1**) and (**3**) or two (**2**) double bonds to oxygens that are not bonded to other Mo atoms. Typically the M-O single bond lengths are ~1.95 Å and the Mo-O double bond lengths are 1.67 to 1.73 Å. In addition, the octahedral site **1** would have a sixth oxygen neighbor at 2.2 to 2.4 Å (1). All three surface structures are formally Mo^{VI} and all involve Mo-O double bonds. However, we find that these species lead to extremely different chemistry. Thus, in selective oxidation of propene, a critical step is trapping of an allyl radical at an Mo=O bond. However, we find that only for species **2** is this process strongly exothermic.

ΔH $\Delta G_{(400°C)}$

(kcal / mol)

-2 +21 (3)

-35 -12 (4)
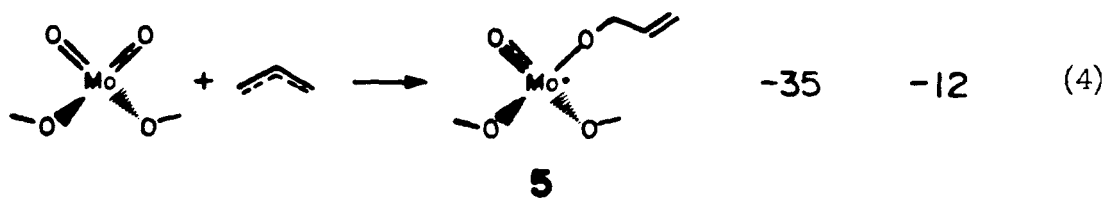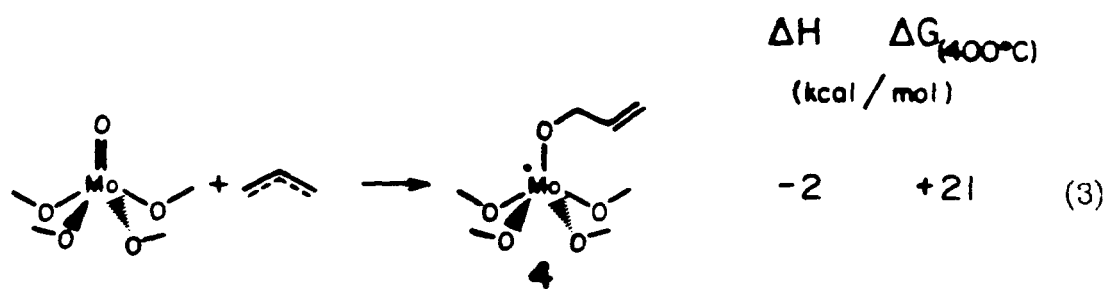
This remarkable difference arises from the spectator oxo effect (2,3), as discussed below.

Figure 1 shows the bonding for **2'**

2'
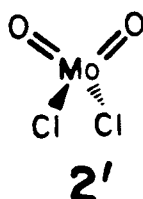
as a model of **2**. Here we see that each Mo=O bond has the form of a covalent double bond involving spin pairing of two singly-occupied Mo d orbitals and two singly-occupied O p orbitals. Denoting the Mo=O axis as z and the MoO_2 plane as yz, the Mo-O sigma bond involves Mo d_{z^2} and O p_z orbitals, while the Mo-O pi bond involves Mo d_{xz} and O p_x orbitals . Two such double bonds require four electrons in four orthogonal Mo d orbitals. On the other hand, the two Mo-Cl bonds (modeling single bonds to bridging oxygens in molybdates) involve a large amount of ionic character with some 5s-5p character on the Mo. Thus the Mo^{VI} center in **2** should be best visualized in terms of ionic bonds to the two bridging oxygens, while the Mo=O bonds should be considered as covalent double bonds. The requirement of two singly-occupied d orbitals for each Mo=O bond leads to an O=Mo=O angle of 106° (the π bonds would prefer 90°; the σ bonds, 125°) (3). In addition to the two singly-occupied p orbitals involved in the Mo=O bond, each oxygen has four valence electrons in two nonbonding orbitals (mixture of O 2s and O $2p_y$).

The bonding is quite different when there is only one double bond, as indicated in Figure 2 (the orbitals are for **1'**

$$
\begin{array}{c}
O \\
\parallel \\
\overset{\displaystyle Mo}{}
\end{array}
$$

Cl — Mo — Cl
Cl   Cl

1'
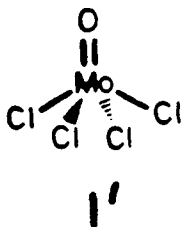
where each Cl models the bridging oxygens of **1**). Here there are *two* pi bonds between Mo and O. Thus the Mo has a total of four ionic bonds to the four Cl, two singly-occupied $d\pi$ orbitals (d_{xz} and d_{yz} if the Mo=O axis is z) used in the two Mo=O pi bonds and an empty d_{z^2} orbital. The two Mo=O pi bonds require two singly-occupied $p\pi$ orbitals on the oxygen (p_x and p_y), leaving four electrons in the O 2s and O $2p_z$ orbitals. With two electrons in O $2p_z$ and none in Mo d_{z^2}, we obtain a Lewis base-Lewis acid bond in the sigma system, leading to a net bond involving six electrons (four from oxygen and two from Mo). [As indicated in Figure 2, there is some charge transfer from Mo to O in the π bonds and from O to Mo in the σ bond, but the net description remains a *six- electron* bond.] The result is a partial triple bond or a **super double bond** that is much stronger than the double bond of **2**. Why can't species **2** make two such super double bonds? The requirement is *two* singly-occupied metal pi orbitals (π_x and π_y) for *each* super double bond so that there are just not enough Mo pi orbitals to go around (analogous to the difference between O=C=O with two *double* bonds and C=O with a partial triple bond about twice as strong).

Based on the above arguments, we expect reaction (4) to be much more favorable than reaction (3) because (3) involves attack on a stronger bond. However, there is a *second* equally important factor involved in the difference in reaction enthalpies for (3) and (4). The extra Mo=O bond of **2** would appear to be a spectator to reaction (4), but in fact

it helps *promote* the reaction. The reason is that in the product, **5,** this
spectator group is free to utilize two Mo dπ orbitals to form a super dou-
ble bond, whereas in the reactant, **2,** the second Mo=O bond (the one
involved directly in the reaction) requires one of these dπ orbitals. Thus
the spectator Mo=O bond changes from a double bond to a super double
bond when the allyl reacts with the *other* Mo=O bond. The net result then
is that reaction (4) is more favored than (3) by 33 kcal.

This spectator oxo promotion is a general effect, so that considering

versus

(5)

(6)
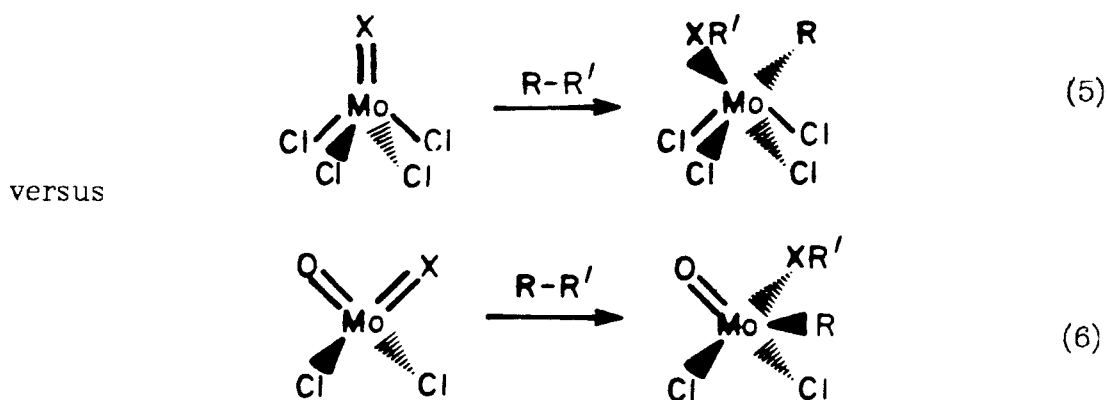
*the spectator oxo group promotes reaction at the adjacent double-
bonded group in (6) by* ≈ *33 kcal with respect to (5).*

We find a similar but smaller spectator effect of ≈16 kcal for imido
groups, promoting reactions such as

(7)
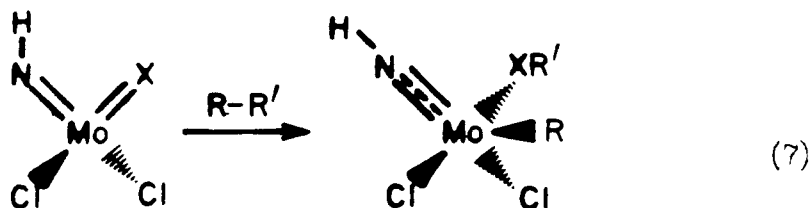
Thus, as shown in Figure 3, **6** has a (bent) Mo=NH double bond involving
two singly-occupied N p orbitals (both perpendicular to the NH bond)
paired up to form a sigma bond and a pi bond to the Mo (utilizing an Mo

$d\pi$ orbital and an Mo $d\sigma$ orbital). Here the N 2s lone pair is not involved in bonding. However, for **7,** the Mo=NH bond is linear, leading to two Mo-N pi bonds. There is also a Lewis base-Lewis acid sigma bond between N and Mo; however, in this case it involves the N 2s pair (the N $2p_z$ orbital being involved in the NH bond) rather than the pz pair as for O. The result is an Mo-NH super double bond about half as super as the Mo=O super double bond.

In the next section we will use this concept of the *spectator effect* in examining likely pathways for selective oxidation of propene to acrolein.

Mechanistic Studies on Selective Oxidation

For selective oxidation (1) and ammoxidation (2) of propene by bismuth molybdates,

i)   It has been well established that the rate-determining step is allyl hydrogen abstraction to yield allyl radical;[4,5]

ii) It is generally acknowledged that the Bi oxide site is involved in this initial step since Bi_2O_3 will abstract the H but does not do oxidation, while MoO_3 will do oxidation of allyl but is ineffective at allyl H abstraction);[6-9] and

iii) Grasselli, Burrington, and co-workers[9] have proposed a detailed mechanism involving trapping of the allyl radical from (i) at a dioxo Mo site

$$(8)$$
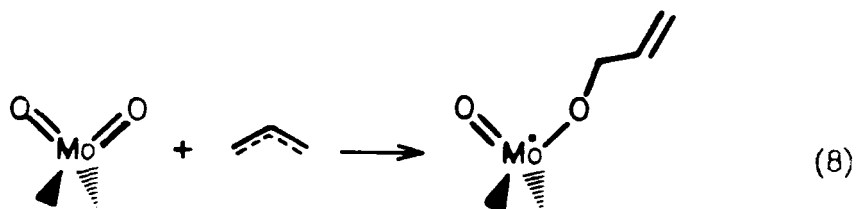
followed by β-hydride elimination to form acrolein

$$(9)$$
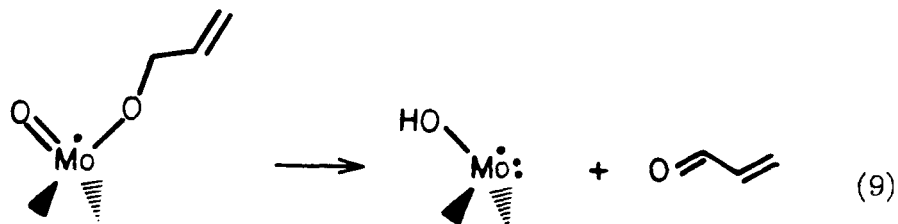
As additional evidence for the role of the dioxo site, they carried out experiments using labeled allyl alcohol (rather than propene) that could be most simply interpreted in terms of reaction at a dioxo site followed by interchange of allyl between spectator oxo and alkoxy oxygens (10).

(10)
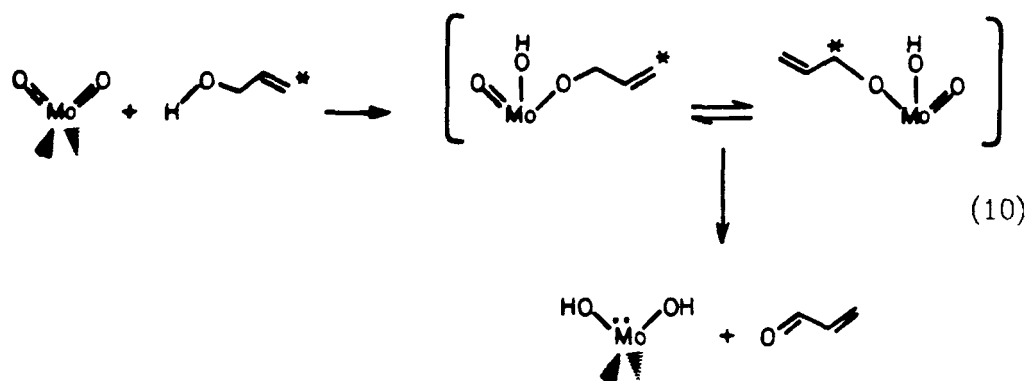
In order to explore further the details of these mechanisms, we calculated the energetics for some of the reaction steps.

Concerning trapping of an allyl at a surface molybdate site, we find that the process for the dioxo unit (4) is quite favorable, whereas the process for the monoxo unit (3) is less favorable. This results from the spectator oxo stabilization present in the dioxo unit and agrees with the basic tenet (8) of the Grasselli-Burrington mechanism. However, one-center steps such as (9) for propene and (10) for allyl alcohol involving reaction *with* the spectator oxo group are unfavorable. For example, the step in (9) is endothermic by ~45 kcal and the step in (10) is endothermic by ~25 kcal. As a result, we were led to the idea that the *collections of adjacent dioxo units* are *critical* to the *selective oxidation process.* * *This idea is illustrated in Figure 4 where step b corresponds to (8). Rather than the one- center process (10), we propose that the β- hydride abstraction is by an adjacent dioxo unit* as in Figure 4c. The stabilization due to the spectator oxo group of the second center is critical in keeping the free energy charge negative.

---

* This conclusion is buttressed by recent results that were reported after the original theoretical analysis and submission of our paper (10).

The first question to ask concerning the mechanism in Figure 4 is whether the crystal structure is compatible with adjacent surface dioxo units. Figure 5 shows the (010) surface of $\alpha-Bi_2(MoO_4)_3$ [corresponding to the parent Scheelite structure, $CaWO_4$] (11). Here we see that there are adjacent dioxo centers along the crystal surface.

With these adjacent dioxo units, we would expect allyl transfer steps such as

(11)
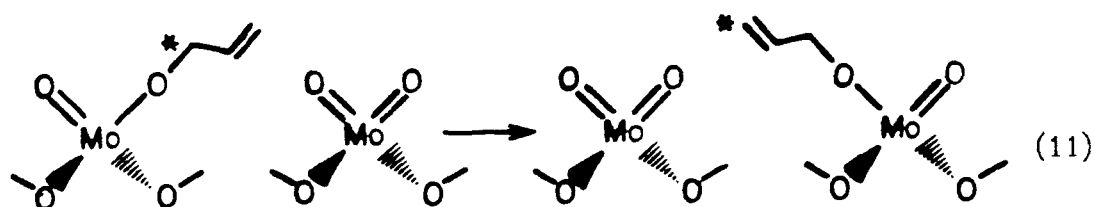
to be facile. This should lead to equilibration of the C1 and C3 carbons and hence a fixed ratio of

(12)
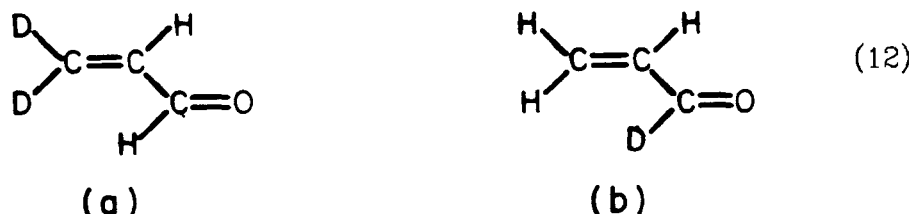
regardless of whether the starting propene is

(13)
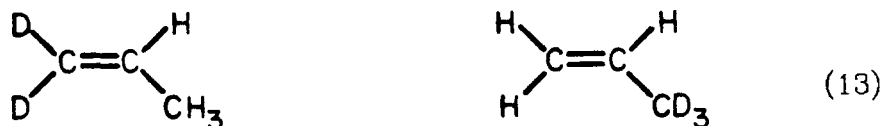
or whether the starting allyl alcohol is

(14)
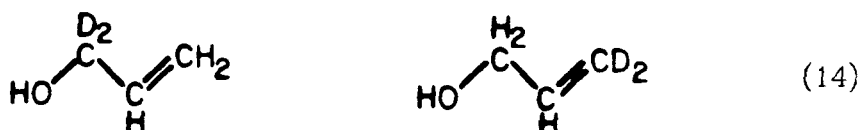
This is consistent with abundant experimental evidence (Grasselli *et al.*) *(9) that the ratio of products (12a) to (12b) is 70% to 30%, independent*

of starting material in (13) or (14).

It is important to note that $\alpha-Bi_2(MoO_4)_3$ has this active site with adjacent Mo dioxo groups. Such sites do *not* exist in the parent Scheelite structure (6) (CaWO_4), but with Bi, two adjacent Ca sites out of each six are vacant (indicated by dotted circles in Figure 5), leading to the special active site.

The availability of several adjacent Mo dioxo units suggests the *possibility* of step (a) in Figure 4 in activating the propene. It is generally accepted that this activation occurs on a Bi site since MoO_3 is not effective in abstracting the allyl hydrogen. However, Bi *is essential* to the existence of the chain of Mo dioxo units in Figure 5, and hence it is possible that the *activation* is actually *by a Mo dioxo unit that exists because of the Bi- induced vacancies and not actually on a Bi oxide site*. These ideas are consistent with the fact that allyl iodide is readily converted to acrolein over *bismuth- free* MoO_3, while the conversion of propene to acrolein over MoO_3 is inactive (~2% yield) (7). The C-I bond strength as in C_3H_5I is 43.5 kcal/mol, whereas the C-H bond strength as in C_3H_6 is 87.5 kcal/mol (7). Therefore it may be postulated that an important differential factor in the breaking of the C-H bond of propene may be the extra stabilization needed that is provided by the Bi-induced configuration of Mo dioxo sites. This is supportive of the idea of nonadditivity of the active sites of the *two* separate oxides, Bi_2O_3 and MoO_3, and the requirement for active sites of Bi, Mo, and O to act together (as a unit) for the conversion of propylene to acrolein (8).

The isotope studies *(vide supra)* have been used to establish that a π-allyl species is initially formed and, indeed, scrambling may occur at this stage (9). This may well be the case, and we cannot address the issue

of σ-allyl versus π-allyl directly since we have not yet studied π-allyl complexes. However, the formation of π-allyl is *not required* in our mechanism. Equilibration via steps as in (12) involving only σ-allyls as stable species are mechanistically equivalent to π-allyl. [The energy estimates of Figure 4 do *not* include any special stabilization due to Bi.]

In Figure 4 we quote current estimates of the reaction enthalpies for the various steps in our mechanism. There are numerous uncertainties here (12), and with the present uncertainties we certainly cannot say that the mechanism is confirmed. However, each step is approximately thermoneutral and hence the scheme is certainly energetically plausible. Assuming an energy barrier of 10 kcal for the reverse of step (a), Figure 4, leads to allyl H-abstraction as the rate-determining step, in agreement with experiment (the estimated $E_{act} = 19$ kcal would be close to the experimental value of $E_{act} = 22$ kcal).

Summarizing, we agree with Grasselli *et al.* (9) that Mo dioxo units are essential in selective oxidation; however, we find that single dioxo units cannot complete the reaction. We propose that selective oxidation requires a collection of at least three adjacent dioxo units to enter into three potentially endothermic reaction steps, facilitating the desired reaction. Indeed, we find for $Bi_2(MoO_4)_3$ that the dioxo units should be ideal for carrying out the sequence of steps involved in selective oxidation. Using this idea that multiple dioxo sites are required, one might be able to develop strategies for promoter additives and for preparative

techniques based on enhancing the probability of such sites. Perhaps the role of such sites could be tested using bidentate or multidentate ligands, e.g.,
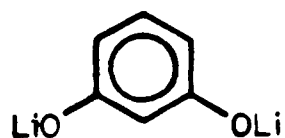
that would bond only to specific configurations.

Ammoxidation

In mechanistic studies of ammoxidation by Bi-molybdates, Grasselli et al.[9] have suggested a critical role of bis-imido sites,

Indeed, assuming an active site analogous to that in Figure 5 but with oxo groups replaced by imido groups leads to a scheme analogous to Figure 4, where spectator imido groups play the role of spectator oxo groups in steps (a), (b), and (c) of Figure 4.

At intermediate NH_3 pressures, oxo-imido species
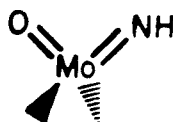
are probably present on the surface. Because of the difference between spectator-oxo and spectator-imido effects, reaction at the N is greatly favored over reaction at the oxygen. Thus, for allyl trapping by N, ΔH = -30 kcal, whereas for allyl trapping by O, ΔH = -20 kcal [see (ii)a, (ii)b]. Thus, in thermodynamic equilibrium, only reaction at the N would be observed. Kinetic data of Grasselli et al.[10] have been interpreted to indicate that allylic N insertion is approximately three times *faster* than allylic O insertion, i.e., $\dfrac{K(\text{acrylonitrile})}{K(\text{acrolein})} \sim 3$. Comparing the theory with experiment suggests kinetic control with an activation energy of $\Delta H^{\ddagger}$ = 0 for (ii)a and $\Delta H^{\ddagger} \approx 2$ kcal for (ii)b. We are currently in the process of examining the energetics for various possible catalytic sequences involved in ammoxidation.

	ΔH	$\Delta G_{(400°C)}$
	(kcal/mol)	
i)	-35	-12
ii)	-30	-7
	-20	+3
iii)	-23	0
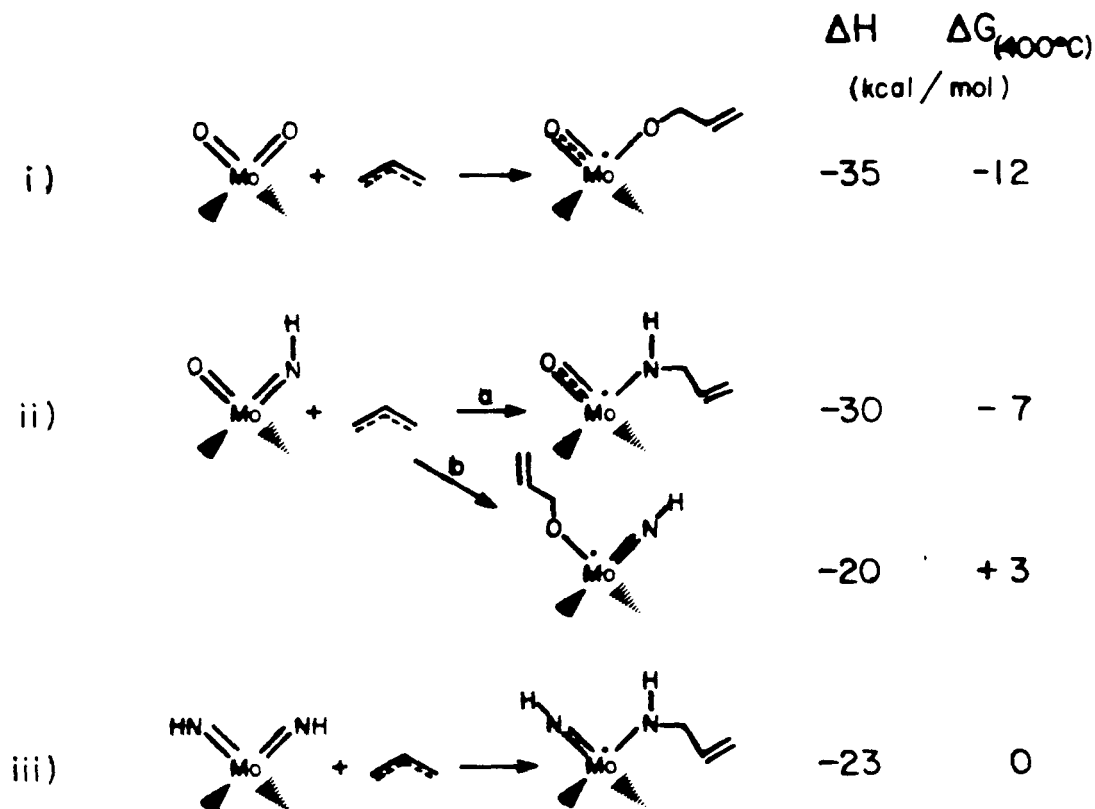
Acknowledgments

We would like to thank Bob Grasselli, Jim Burrington, and Keith Hall for spirited discussions of various aspects of chemistry on molybdates. We also gratefully acknowledge partial support of this work from the Department of Energy (under a contract with the Jet Propulsion Laboratory) and the Donors of the Petroleum Research Fund of the American Chemical Society. One of the authors (JNA) wishes to acknowledge support in the form of a fellowship from the Fannie and John Hertz Foundation.

References

1. Kihlborg, L. *Arkiv Kemi* 1963, 21, 357-364.

2. Rappé, A. K.; Goddard III, W. A. *Nature* 1980, 285, 311; *J. Am. Chem. Soc.* 1980, 102, 5114; *ibid.* 1982, 104, 448.

3. Rappé, A. K.; Goddard III, W. A. *J. Am. Chem. Soc.* 1982, 104, 3287.

4. (a) Keulks, G. W.; Krenzke, L. S.; Noterman, T. M. *Adv. Catal.* 1978, 27, 183; (b) Brown, F. R.; Makovsky, L. E.; Rhee, K. H., *J. Catal.* 1977, 50, 162, 385; (c) Patterson, T. A.; Carver, J. C.; Leyden, D. E.; Hercules, D. M., *J. Phys. Chem.* 1976, 80, 1700; (d) Matsuura, I.; Schut, R.; Kirakawa, K. *J. Catal.* 1980, 63, 152; (e) Holm, V.; Clark, A. *ibid.* 305 (1968); (f) McCain, C. C.; Gough, G.; Godin, G. W. *Nature* 1963, 198, 989; (g) Wragg, R. D.; Ashmore, P. G.; Hockey, J. A. *J. Catal.* 1971, 22, 49; (h) Portefaix, J. L.; Figueras, F.; Forissier, M. *ibid.* 1980, 63, 307.

5. Otsubo, T.; Miura, H.; Morikawa, Y.; Shirasaki, T. *J. Catal.* 1975, 36, 240.

6. Sleight, A. W. In "Materials Science Series - Advanced Materials in Catalysis"; Burton, J. J., Ed.; Academic Press: New York, 1977; p. 181.

7. Grzybowska, B; Haber, J.; Janas, J. *J. Catal.* 1977, 49, 150-153.

8. Martin, W.; Lunsford, J. H. *J. Am. Chem. Soc.* 1981, 103, 3728-3732

9. Grasselli, R. K.; Burrington, J. D. *Advan. Catal.* 1981, 30, 133; Burrington, J. D.; Kartisek, C. T.; Grasselli, R. K. *J. Catal.* 1980, 63, 235; *ibid.* 1982, 75, 225.

10. Burrington, J. D.; Kartisek, C.T.; Grasselli, R. K. *J. Catal.* 1984, 87, 363-380

11. van der Elzen, A. F.; Rieck, G. D. *Acta Cryst. B* 1972, 29, 2433.

12. Our current estimates for σ-allyl are currently based on calculations for CH_3 with corrections to allyl based on Benson-type estimates.[13] In addition, we have not yet estimated the stability of the π-allyl species. Most important, we have not calculated the transition states and energy barriers for any of the steps.

13. Benson, S. W. "Thermochemical Kinetics;" Wiley: New York, 1976.
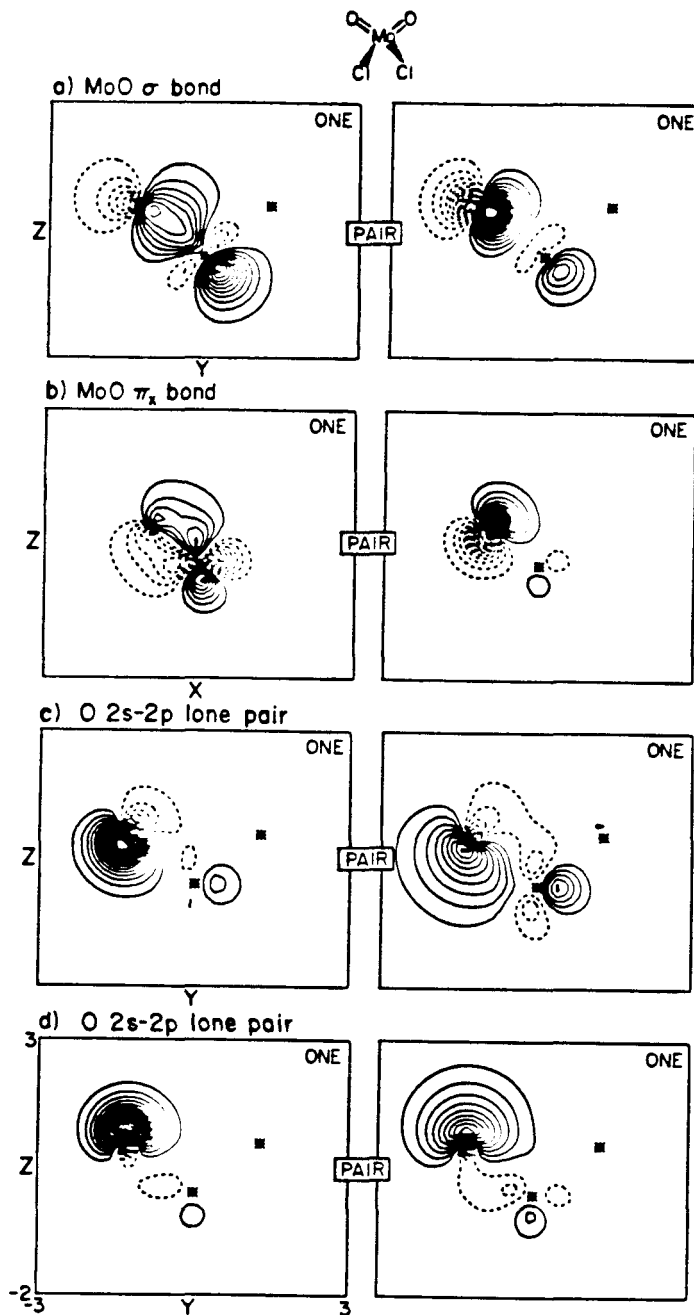
Figure 1. GVB orbitals for the four electron pairs involving the left Mo=O double bond in species **2**. Dotted contours indicate negative amplitude. Increments between contours are 0.050 a.u.; the zero contour is *not* shown.
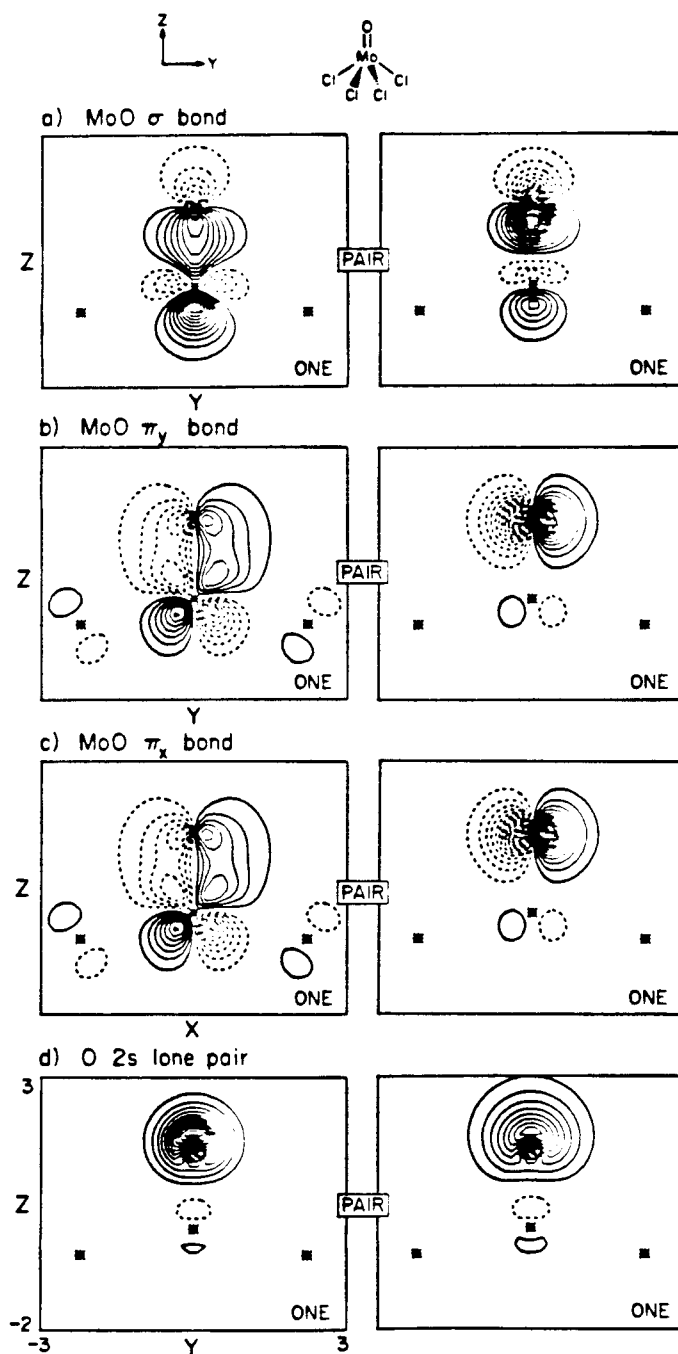
Figure 2. GVB orbitals for the four electron pairs involving the Mo=O super double bond for species **1**. (Same plotting conventions as in Figure 1.)
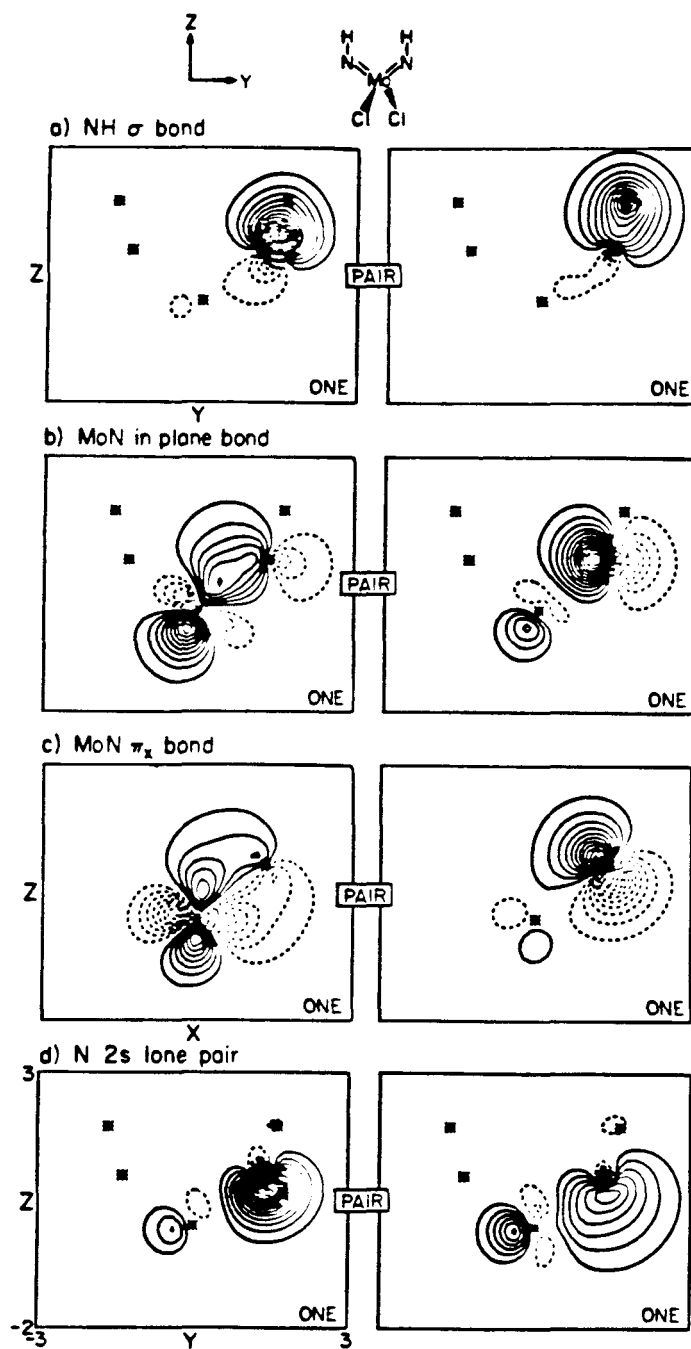
Figure 3. The GVB orbitals for the four electron pairs in the right Mo=NH bond of species **5.** (Same plotting conventions as in Figure 1.)
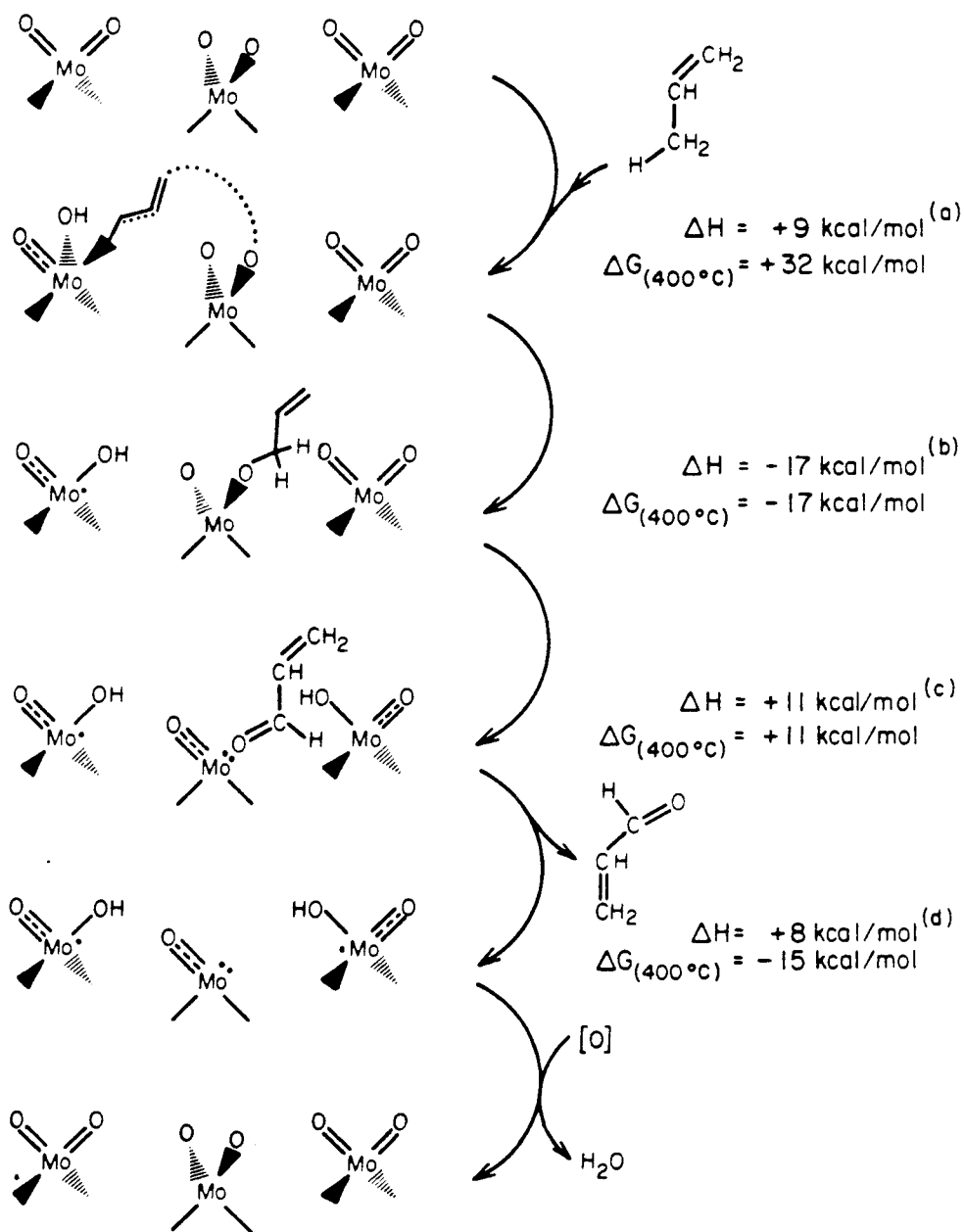
Figure 4. The multiple dioxo mechanism for selective oxidation.
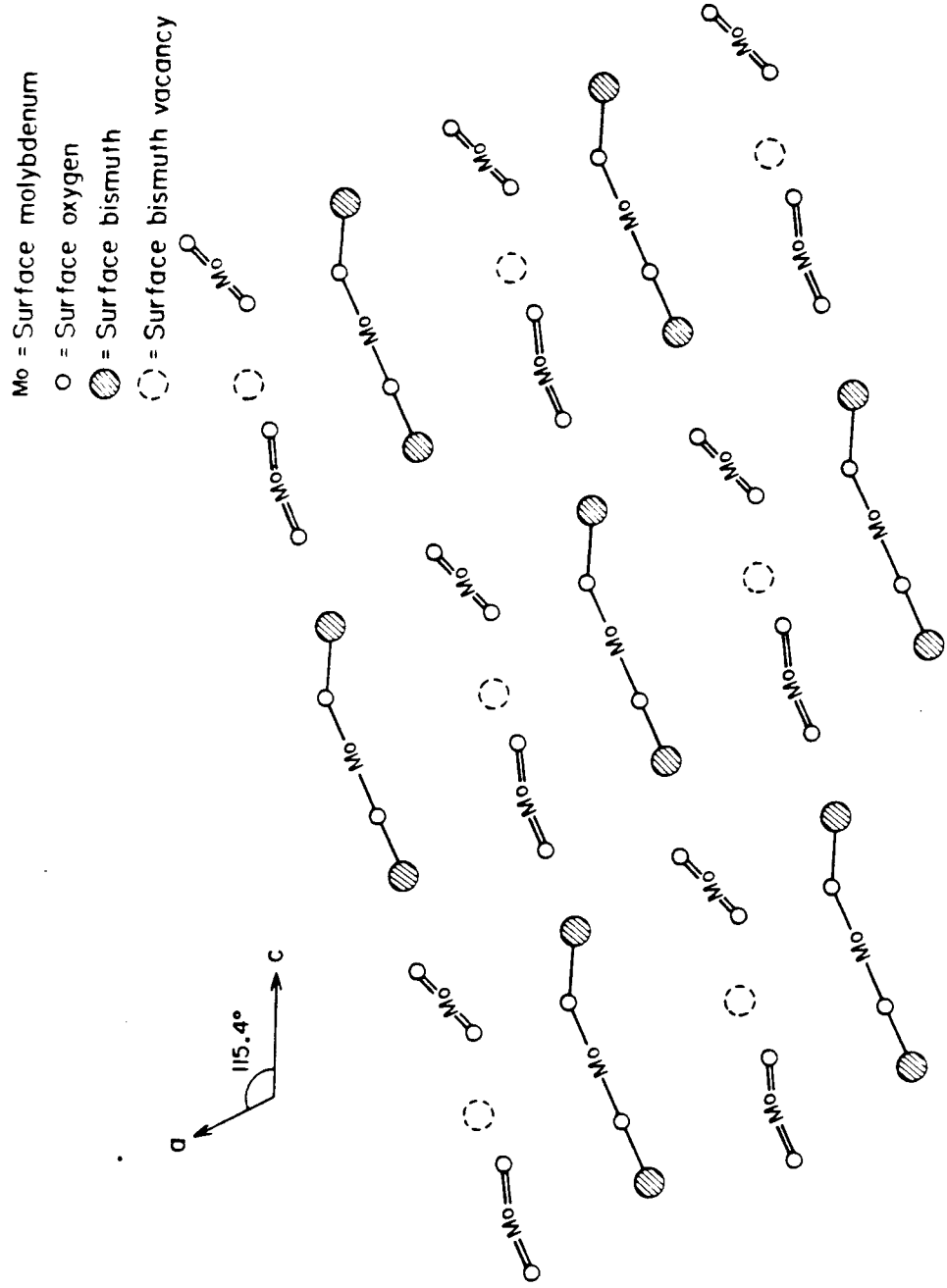
Figure 5. The (010) surface of α–$Bi_2(MoO_4)_3$ [corresponding to the (001) surface of the parent Scheelite structure, $CaWO_4$].

CHAPTER 2

PART B:

ADDENDUM ON AMMOXIDATION

Addendum on Ammoxidation

Ammoxidation of propene to form acrylonitrile is a more complex process than the selective oxidation of propene to produce acrolein. In order to form acrylonitrile, the activation of ammonia is involved as well as an overall cleavage of *three* carbon-hydrogen bonds in the reactant molecue, propene. The overall reaction is shown in (15).

$$\overset{=}{\diagdown} \; + \; NH_3 \; + \; \tfrac{3}{2}O_2 \; \longrightarrow \; \overset{=}{\diagdown}{}^{C\equiv N} \; + \; 3H_2O \qquad (15)$$

$$Bi_2O_3 \cdot nMoO_3$$
$$430°C$$
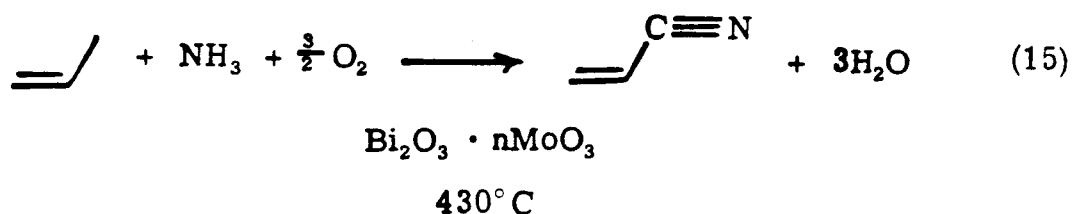
A similarity does exist between ammoxidation and selective oxidation inasmuch as the activation energy for both processes is ~20 kcal.[1,2] Because of this, as well as the fact that deuterated propene produces the isotopic distribution expected based on H or D abstraction from either end of an allylic intermediate, it is believed that for both reactions the rate determining step involves α-hydrogen abstraction from propene to form an allylic intermediate.[2] The catalytically active sites which consist of molybdenum dioxo groups are believed to activate ammonia. At low partial pressures of feed, ammonia may react with the dioxo group to produce a molybdenum oxo-imido species as shown in reaction (16).

$$+ \text{ NH}_3 \xrightarrow{\Delta H = +8 \text{ kcal}} \quad + \text{ H}_2\text{O} \qquad (16)$$
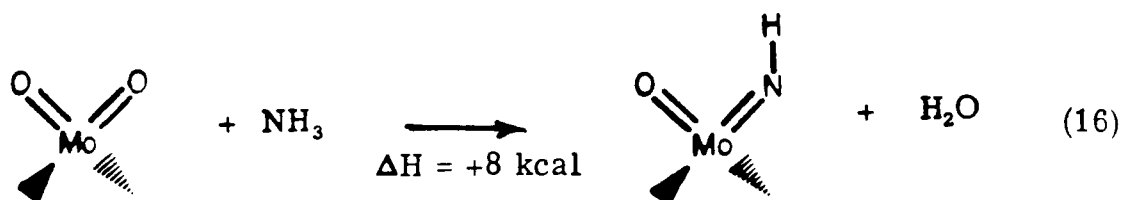
At higher partial pressures of feed, the bis-imido species has been postulated to be present on the catalytically active surface. This is shown in reaction (17).[3]

$$+ \text{ NH}_3 \xrightarrow{\Delta H = +18 \text{ kcal}} \quad + \text{ H}_2\text{O} \qquad (17)$$
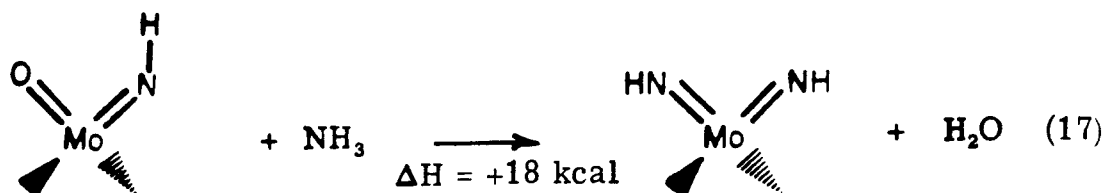
From our calculations, we note that the addition of the second ammonia molecule to the oxo-imido species in reaction (17), ($\Delta H = +18$ kcal), to produce the bis-imido species is thermodynamically less favored than the addition of the first ammonia molecule to the dioxo species in reaction (16), ($\Delta H = +8$ kcal).

A comparison of ammoxidation using isotopically labeled propene, allyl alcohol and allyl amine shows that the favored formation of N vs. O

σ-allylic intermediate occurs.[4] Grasselli *et al.*[4] have recently shown that the collapse of allyl on N is favored by about 3:1 over O insertion. Indeed, our calculations support this idea as we show the conversion of O-allyl to N-allyl species is exothermic by 10 kcal (18).

$$\Delta H = -10 \text{ kcal} \tag{18}$$
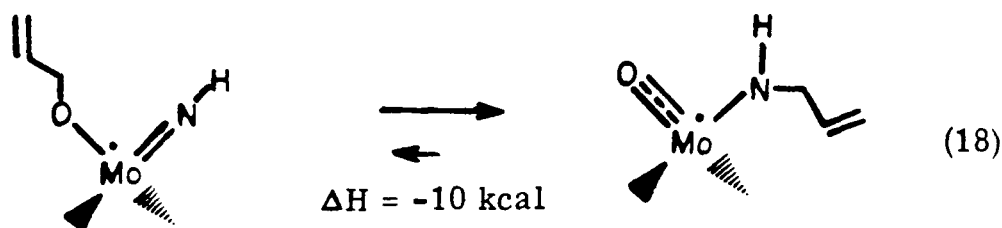
The bismuth-molybdate crystal structure is described as a defect crystal structure (containing cation vacancies) of the parent scheelite crystal structure, $CaWO_4$.[5] However, bismuth molybdate is an active catalyst for the oxidation and ammoxidation of propene, whereas scheelite has been found to be inactive. We have seen in Chapter 2, Part A that several molybdenum dioxo units are necessary in order to convert propene to acrolein over α-bismuth molybdate, $Bi_2Mo_3O_{12}$ (2:3 ratio of bismuth to molybdenum). Previously, there has been speculation regarding the concept of site isolation in order to account for selectivity.[6] Indeed, we have verified the concept (Chapter 2, Part A) and find "chains" of reactive dioxo units along the α-bismuth molybdate surface, clustered in units of two. For ammoxidation, experimental results indicate that β-bismuth molybdate, $Bi_2Mo_2O_9$ (1:1 ratio of bismuth to molybdenum), is *initially* the most active and the most selective catalyst; however, the activity of the catalyst is quickly lost. The β-phase is incongruent and stable only between 550°C and 670°C. At temperatures less than 550°C it

decomposes slowly into α and γ-phases.[6] The fact that the β-phase, which has a molybdenum dioxo unit clustering of degree four, is initially the most selective and active may be significant. We have previously shown in Part A that for propene oxidation to acrolein, two hydrogen abstractions from propene are needed and that three adjacent molybdenum dioxo units are required. Therefore, for propene ammoxidation to acrylonitrile, where three hydrogen abstractions from propene must occur, it seems reasonable that at least four adjacent molybdenum dioxo units may be necessary in order to complete the chemistry. This may be one of the reasons why the β phase of bismuth molybdate is the most selective phase for ammoxidation.

It has been found that ammoxidation catalysts with superior properties commonly contain bismuth, molybdenum and oxygen as well as small amounts of other elements such as alkali metals, alkaline earth metals, phosphorus, arsenic or antimony. These catalysts are referred to as multicomponent molybdate (MCM) catalysts, many of which have been patented. Recently, studies have been made to measure the activity and selectivity of MCM catalysts as the bismuth content and the cation vacancy concentration are independently varied. From these studies, it has been concluded that *selectivity* to acrylonitrile is high for all catalysts as long as they contain bismuth, and that the catalytic *activity* increases with increasing cation vacancy concentration.[7] In addition to improving lattice oxygen diffusion, it is generally believed that the cation defects generate higher order Mo=O centers in the crystal which are the centers for olefin chemisorption.

We believe that the fundamental principles discussed in Chapter 2 for the selective oxidation of propene -- namely, active surface sites contain-

ing multiple dioxo units as well as spectator oxo and imido effects -- may apply to other catalytic mechanisms. Indeed, these ideas should serve to provide a basis for further research regarding the ammoxidation of propene.

References

1) Callahan, J. L.; Grasselli, R. K.; Milberger, E. C.; Strecker, H. A. *Ind. Eng. Chem. Prod. Res. Dev.*, **9,** 134, 1970.

2) Schuit, G. C. A. *J. Less. Com. Met.* **36,** 329, 1974.

3) See Reference 9, Part A.

4) See Reference 10, Part A.

5) See Reference 11, Part A.

6) Gates, B. C.; Katzer, J. R.; Schuit, G. C. A. In "Chemistry of Catalytic Processes," McGraw-Hill: New York, 1979: p.366.

7) Brazdil, J. F.; Glaeser, L. C.; Grasselli, R. K. *J. Catal.* **81,** 142, 1983.

CHAPTER 3

DESCRIPTIVE BONDING IN Mo^{IV}, Mo^V, and Mo^{VI} COMPLEXES

INTRODUCTION

The study of molybdenum complexes containing imido and nitrido ligands are of great interest because of their role in catalytic processes, e.g., the ammoxidation of propene to acrylonitrile and the conversion of dinitrogen to ammonia. Molybdenum complexes containing oxygen ligands also play a key role in catalytic oxidation reactions such as the oxidation of methanol to formaldehyde and the oxidation of propene to acrolein.

Even though the crystal structures of many molybdenum-nitrogen and molybdenum-oxygen containing complexes have been characterized, there remains great uncertainty about the exact mode of bonding between the ligand and the metal. As a result, there is little information regarding the favored geometries of the ligand, particularly as relevant for the reaction intermediates and transition states involved in the chemical transformations.

In Section 3.1 we present a detailed description of molybdenum-ligand bonding and geometries for complexes with a *single* nitrido, imido and oxo group. Here we focus on three systems,
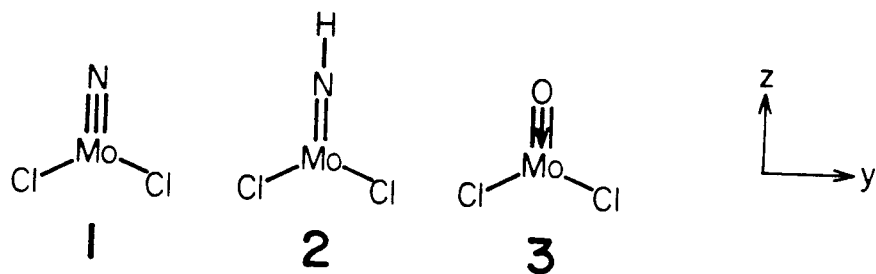
where molybdenum is bonded to two chlorine atoms as well as to one multiply-bonded ligand. We compare and contrast the exact nature of

the multiple bond in complexes **1, 2,** and **3.** Metal-imido ligands may be linear or they may be bent. Section 3.2 analyzes the bonding between molybdenum and the imido group for both the linear and the bent imido forms. In Section 3.3, the bonding and geometries of dioxo, oxo-imido, and bis-imido terminally attached ligands to molybdenum in complexes,
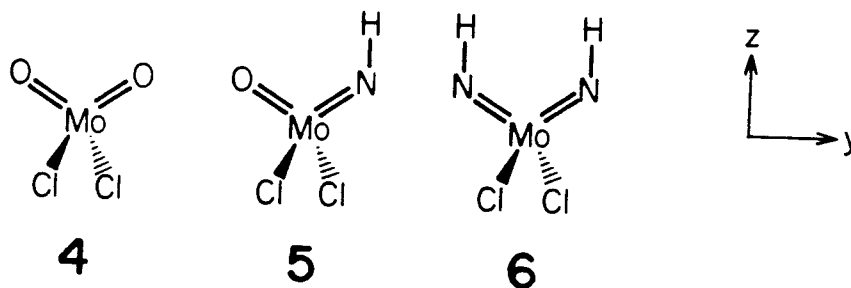
4, 5, and **6** are discussed. These complexes have *two* multiply-bonded ligands attached to molybdenum. For these molecules, detailed analysis is made concerning the mode of bonding when two oxo groups are attached to one molybdenum **4,** when one oxo group and one imido group is attached to one molybdenum **5,** and when two imido groups are attached to one molybdenum **6.** In Section 3.4, we describe the covalent bonding of ligand X to molybdenum in complexes such as,
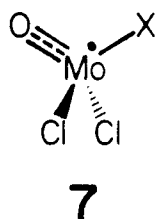
with X = H, CH_3, OH, OCH_3, and NH_2. By varying the ligand X, this sys-

tematic study allows for a direct comparison of Mo-X bond energies for molybdenum complexes as shown in **7**.

Section 3.5 concerns the *trans*-influence in which model square planar molybdenum complexes,
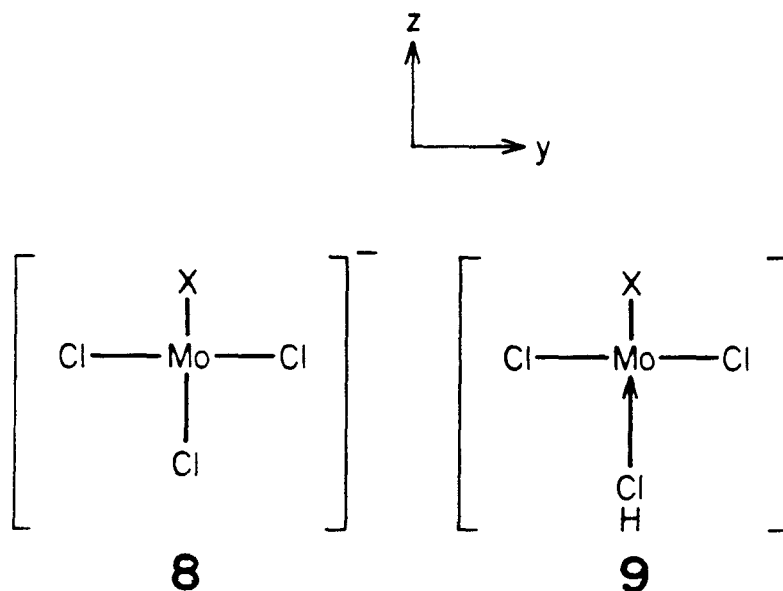
8 and **9** are studied. Model trichloro molybdenum complexes, $[(Cl)_3Mo-X]^-$, are used and the ligand *trans* to X is optimized. We observe the change in bond length of the *trans* chloride as a function of ligand X, for X = NH, O, N.

3.1. Molybdenum-Ligand Multiple Bonds, Mo=X with X = N,NH,O

In molybdenum-dichloro complexes, two of the six valence electrons on the Mo are used for partially ionic bonds to the two Cl ligands. This leaves four electrons on the Mo for bonding to other ligands, i.e., we have a choice of Mo ($d\sigma$, $d\pi_y$, $d\pi_x$, $d\delta_{xy}$, $d\delta_{x^2-y^2}$) orbitals into which four electrons are to be placed.

Consider the molybdenum-nitrogen bond in $(Cl)_2Mo\text{-}(N)$ **1**. Nitrogen has an (s^2p^3) ground state with electrons in three separate p orbitals, and we have four molybdenum d electrons available. Thus, we expect a triple bond (σ, π_x, π_y) with the molybdenum retaining an unpaired electron of $d\delta$ symmetry as shown below,
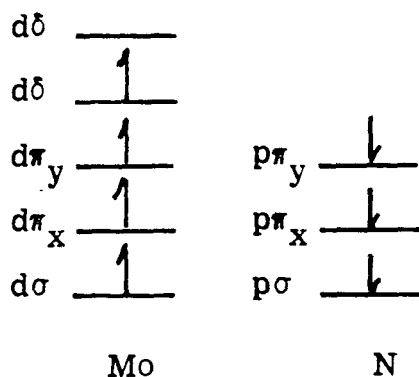
Triple Bond Between Molybdenum and Nitrogen

The metal-nitrogen bond in $(Cl)_2Mo\text{-}(N)$ is a *triple* covalent bond (two π bonds plus one σ bond) between Mo $4d(xz, yz, z^2)$ and nitrogen $2p(x, y, z)$ orbitals.

Consider the linear molybdenum-imido bond as in $(Cl)_2Mo\text{-}(NH)$ **2**. Nitrogen atom (s^2p^3) forms a σ bond with hydrogen, leaving two p electrons on nitrogen, each in separate π orbitals. Thus we expect a double bond with the molybdenum retaining two unpaired electrons of $d\delta$

symmetry.

$d\delta$ ↑

$d\delta$ ↑

$d\pi_y$ ↑ $p\pi_y$ ↓

$d\pi_x$ ↑ $p\pi_x$ ↓

$d\sigma$ ←2s   ↑↓
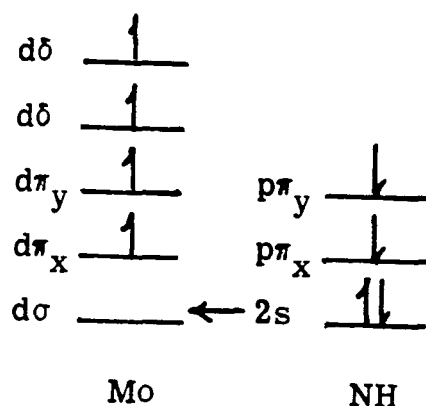
Mo   **NH**

"Double" Bond Between Molybdenum and Linear Imido

The metal-nitrogen bond in $(Cl)_2Mo$-(NH) may be described as a covalent *double* bond (two π bonds) between Mo $4d(xz,yz)$ and nitrogen $2p(x,y)$ orbitals, plus a weaker σ donor interaction between the nitrogen 2s orbital which delocalizes toward the empty Mo d_{z^2} orbital. For linear imido, the N $2p_z$ orbital is bound to hydrogen.

In the Mo d^1 system, $(Cl)_2Mo$-(N) **1**, we calculate a metal-nitrido (Mo≡N) bond length of 1.58 Å, whereas for the triplet Mo d^2 system, $(Cl)_2Mo$-(NH) **2**, the linear metal-imido bond length is 1.66 Å - 0.08 Å longer than the nitrido case. Consistent with this, our previous work indicates a bond length of 1.60 Å for the covalently triple-bonded $^4\Sigma^-$ Mo≡N diatomic molecule.[1] These data are in accord with the experimental results, as it is well known that metal-nitrido bond distances are consistently shorter than the corresponding metal-imido bond distances in isoelectronic complexes.[2] For example, in the two d^0 Mo^{VI} 18-electron complexes, $(S_2CNEt_2)_2Cl_2Mo$-(NR) and $(S_2CNMe_2)_3Mo$-(N), the metal-imido Mo≡NR bond length is 1.73 Å, while in the metal-nitrido Mo≡N complex, the bond length is 1.64 Å.[3,4]

The change in metal-nitrogen bond length of imido relative to nitrido is due to radically different bonding descriptions for the imido $(Cl)_2Mo$-(NH) versus the nitrido $(Cl)_2Mo$-(N) complexes. The main difference in bonding between linear imido and nitrido ligands is contained within the sigma system. For linear imido the sigma system consists of the N2s orbital delocalizing toward an empty Mo d_{z^2} orbital. Mulliken population analysis shows that for the two-electron sigma bond in imido, 1.74 electrons are on nitrogen and only 0.26 of an electron is on molybdenum. However, for nitrido the sigma bond between nitrogen and molybdenum contains 1.15 electrons on nitrogen and 0.85 of an electron on molybdenum.

To summarize, the reason that the imido bond is longer than the nitrido bond can be explained by looking at the bonding description within the sigma system. Molybdenum-imido (linear imido) ligands consist of two covalent π bonds and a weaker N2s σ donor, whereas molybdenum-nitrido ligands consist of three covalent metal nitrogen bonds.

Consider the molybdenum-oxygen bond as in $(Cl)_2Mo$-(O) **3**. Free ground state oxygen starts with four p electrons (s^2p^4) distributed among three p orbitals. We find that the dπ orbitals of the molybdenum are used to make π covalent bonds to the oxygen. This leaves a doubly-occupied Op_z orbital pointing towards an empty Mo dz^2 orbital.
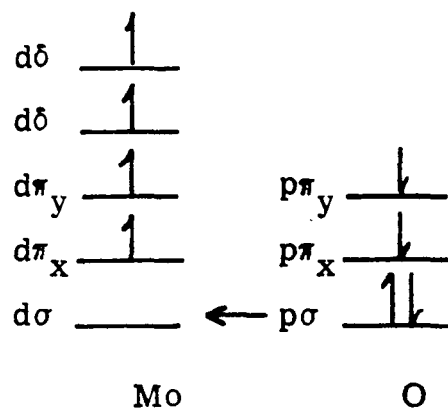
"Triple" Bond Between Molybdenum and Oxygen

In the triplet Mo d^2 system (Cl)$_2$Mo-(O) **3**, the molybdenum oxygen bond is essentially a *triple* bond, analogous to the triple bond in the CO diatomic (Figure 1), i.e., two π bonds and a dative σ bond between O2p$_z$ and Mo4d$_{z^2}$ orbitals.
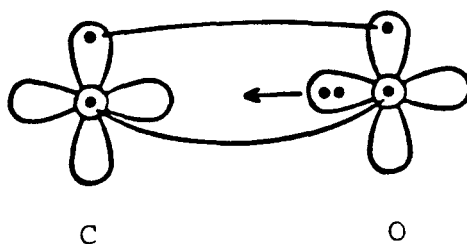
Figure 1. Description of partial triple bond between C and O.

Mulliken population analyses for the metal-oxo dative σ bond show that there are 1.37 electrons on oxygen and 0.63 of an electron on molybdenum.

Orbital contour plots for the nitrido covalent triple bond in $(Cl)_2Mo$-(N) **1** and the linear imido (covalent double bond plus N2s σ donor) in $(Cl)_2Mo$-(NH) **2** as well as for the oxo triple bond in $(Cl)_2Mo$-(O) **3** are shown in Figures 2, 3, and 4.

In further agreement with experiment, we calculate the metal-nitrido and metal-oxo bond distances to be nearly equal - 1.58 Å for Mo$\equiv$N and 1.59 Å for Mo$\equiv$O. (Experimental difference is estimated to be ± 0.02 Å.[5])
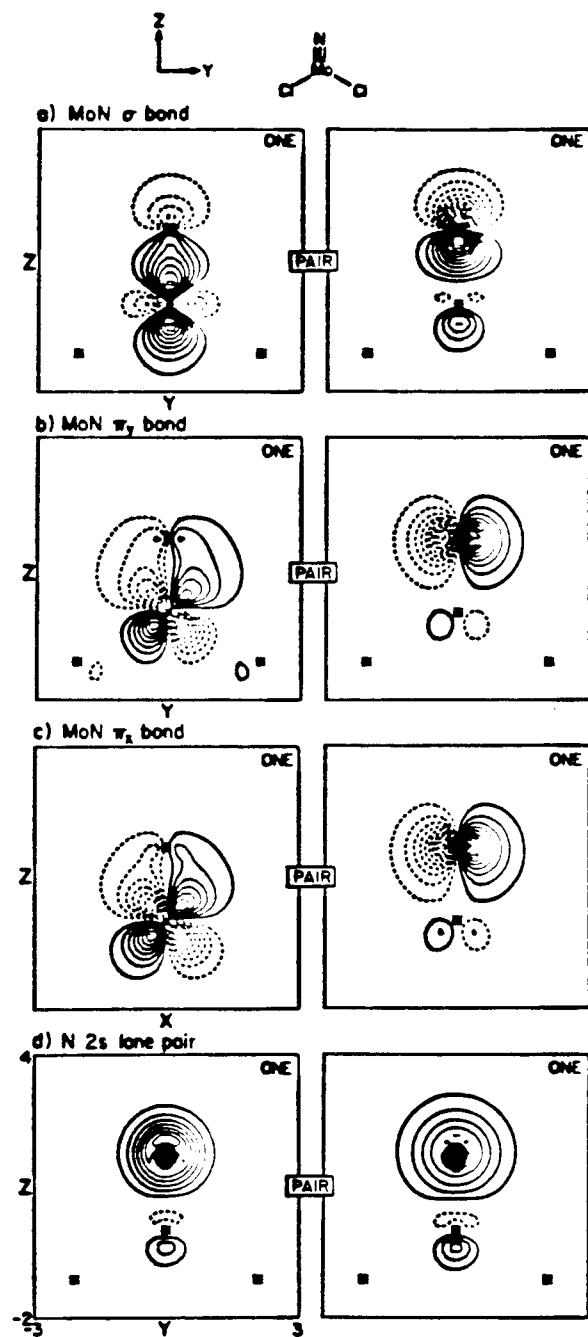
Figure 2. GVB orbitals for the electron pairs involving the Mo≡N bond.
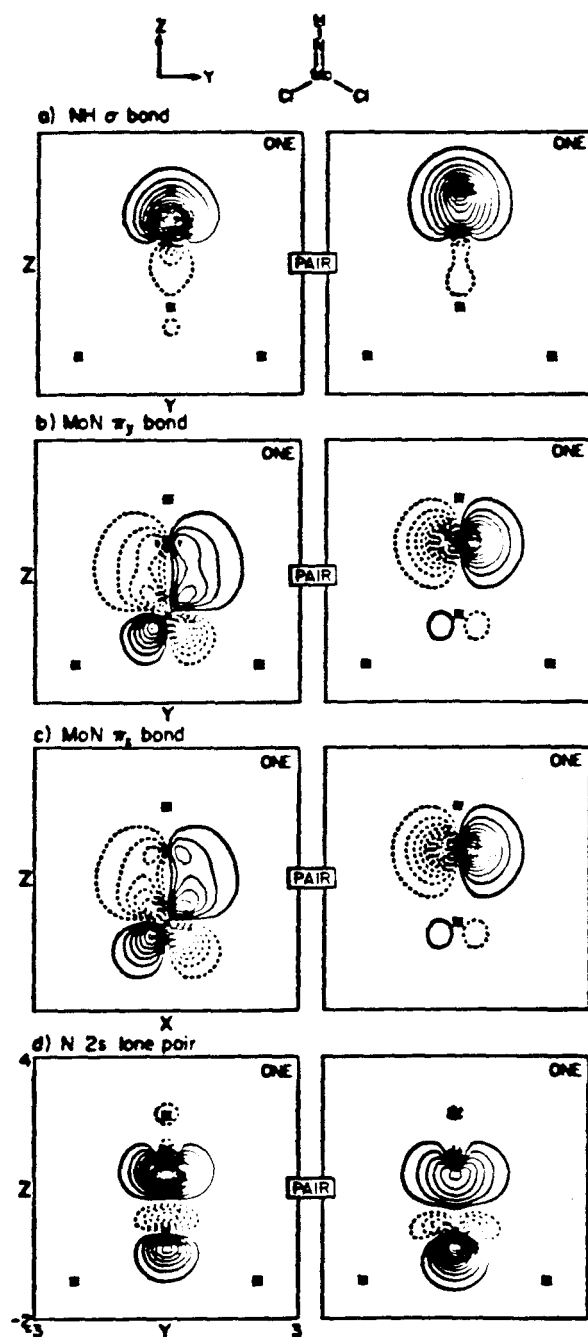
Figure 3. GVB orbitals for the electron pairs involving the Mo≡NH bond.
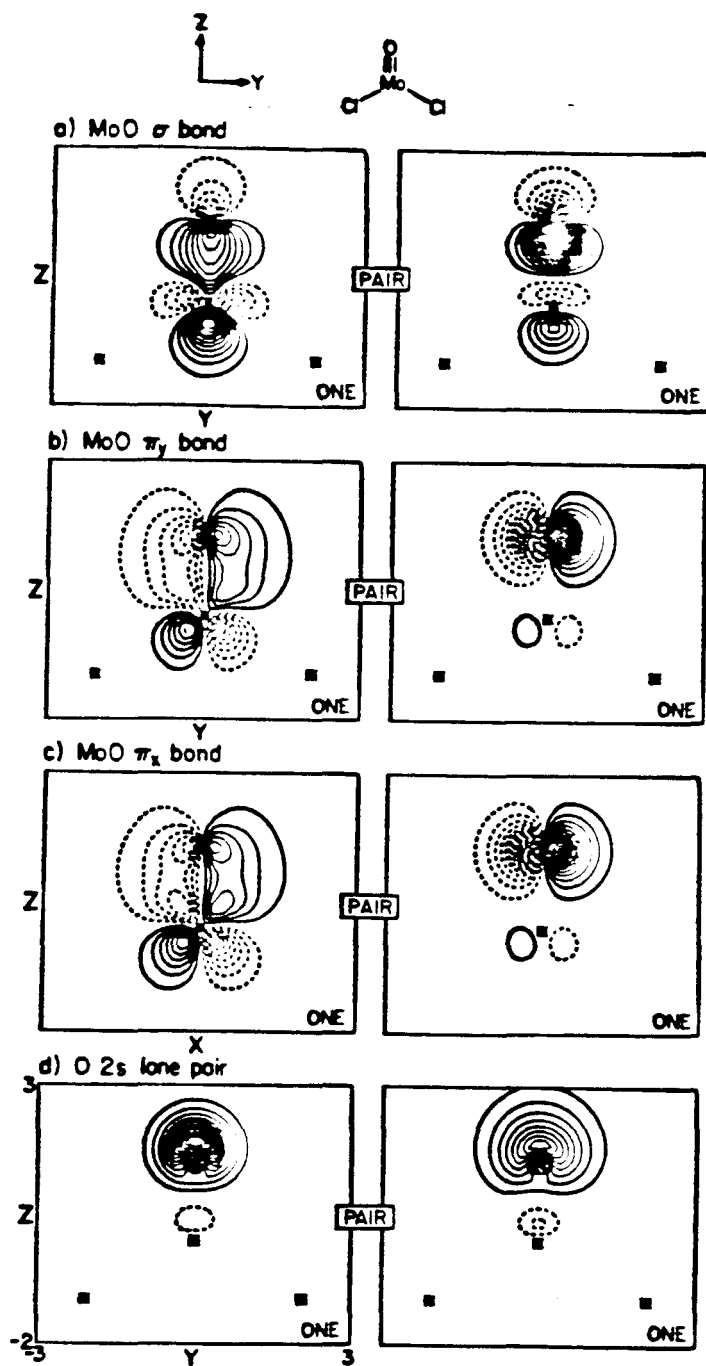
Figure 4. GVB orbitals for the electron pairs involving the Mo≡O bond.

3.2. Bent Imido or Linear Imido Ligands?

The terminal *linear* bonding mode **2a** is the most commonly found form in crystal structures of organoimido complexes, e.g., $Ta(N^tBu)(NMe_2)_3$.[2] However, a *few* structures which contain *bent* terminal imido ligands, e.g., $(S_2CNEt_2)_2Mo(NPh)_2$, are known **2b** (Mo-N-R angle = 139°).[2]

Terminal Linear Imido	Terminal Bent Imido
2a	**2b**
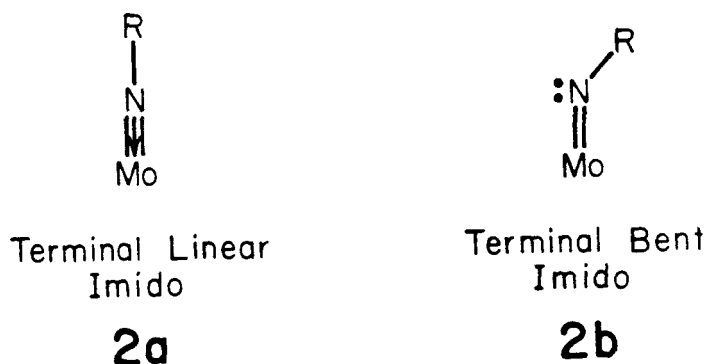
We show that linear metal-imido bonds such as **2a** consist of two covalent π bonds between molybdenum and nitrogen and a doubly-occupied N2s sigma donor orbital pointing towards the empty Mo d_{z^2} orbital (*vide infra*). Using the $(Cl)_2Mo(NH)$ d^2 system as a model and simultaneously stretching the Mo-N bond while varying the Mo-N-H angle provides us with energetics as a function of geometry. In Figure 5 we see that for longer Mo-N distances, the favored Mo-N-H angle changes from 180° (linear) to ~120° (bent). At shorter distances, the linear imido form is more stable by about 20 kcal, while at longer distances the bent imido form becomes the favored form. These data are reflected in Figure 6 where the Mo-N bond energy is plotted as a function of internuclear distance R(Å) for both the linear and bent imido forms. For R ≤ 2.1 Å, the linear imido form **2a** is lower in energy; however, for R > 2.1 Å the bent imido form **2b** is the more stable.

When the bonding orbitals for bent imido **2b** (Figure 7) are compared with those of the linear form **2a** (Figure 3), we can clearly see what has happened. *Bent* imido consists of a (1σ + 1π) covalent bond between molybdenum and nitrogen (*not* two covalent π bonds as for linear imido) and an N2s lone pair which is no longer pointing toward molybdenum. With the bent form we no longer require the N2p$_z$ orbital to be bonded to hydrogen so **2b** is free to make a covalent σ bond with the Mo d$_{z^2}$ orbital.

dδ ___↿___

dδ ___↿___

dπ_x ___↿___   pπ_x ___⇂___

dσ ___↿___   pσ ___⇂___

Mo   NH
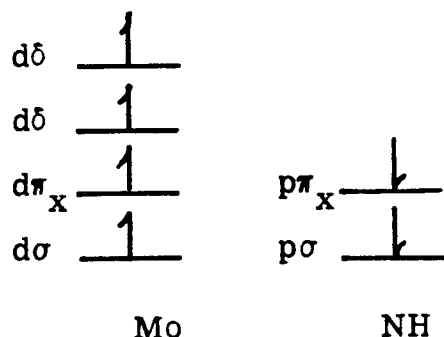
Double Bond Between Molybdenum and Bent Imido

The fact that this bonding description is favored for the longer R bent imido form is not surprising, as the overlap for a sigma bond is larger than for a pi bond at such distances.

In summary, consistent with the experimental results, we find that the most stable electronic imido isomer is the short R linear form which consists of two pi bonds and an N2s sigma donor orbital pointing from nitrogen toward molybdenum.[12]
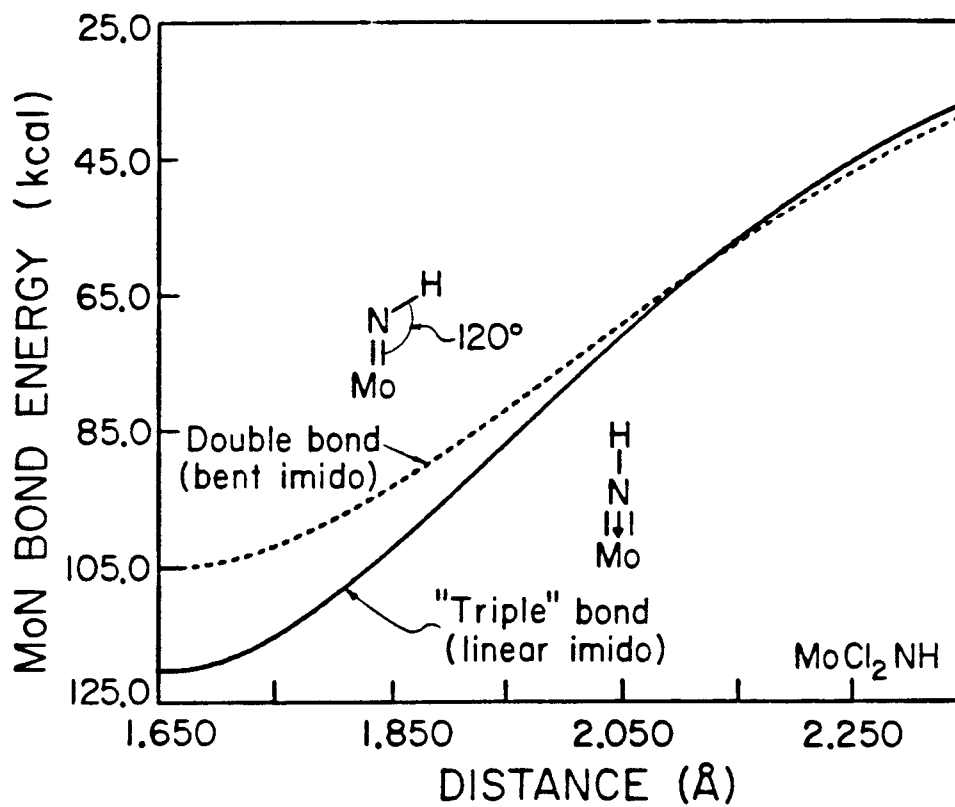
Figure 6. Mo-N bond energy (kcal/mol) as a function of distance for linear and bent imido forms.
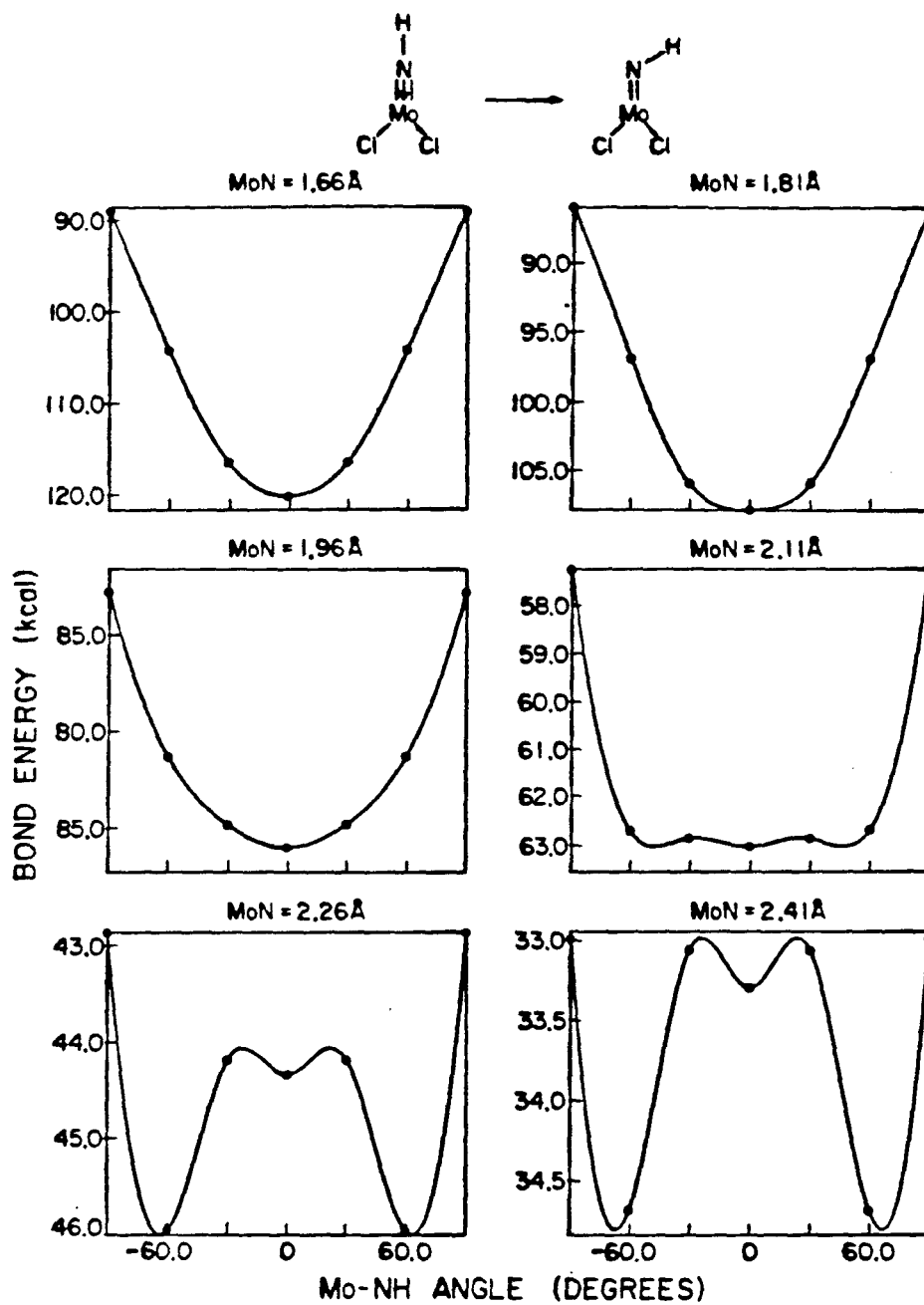
Figure 5. Mo-N bond energy (kcal) as a function of Mo-N-H angle (degrees).
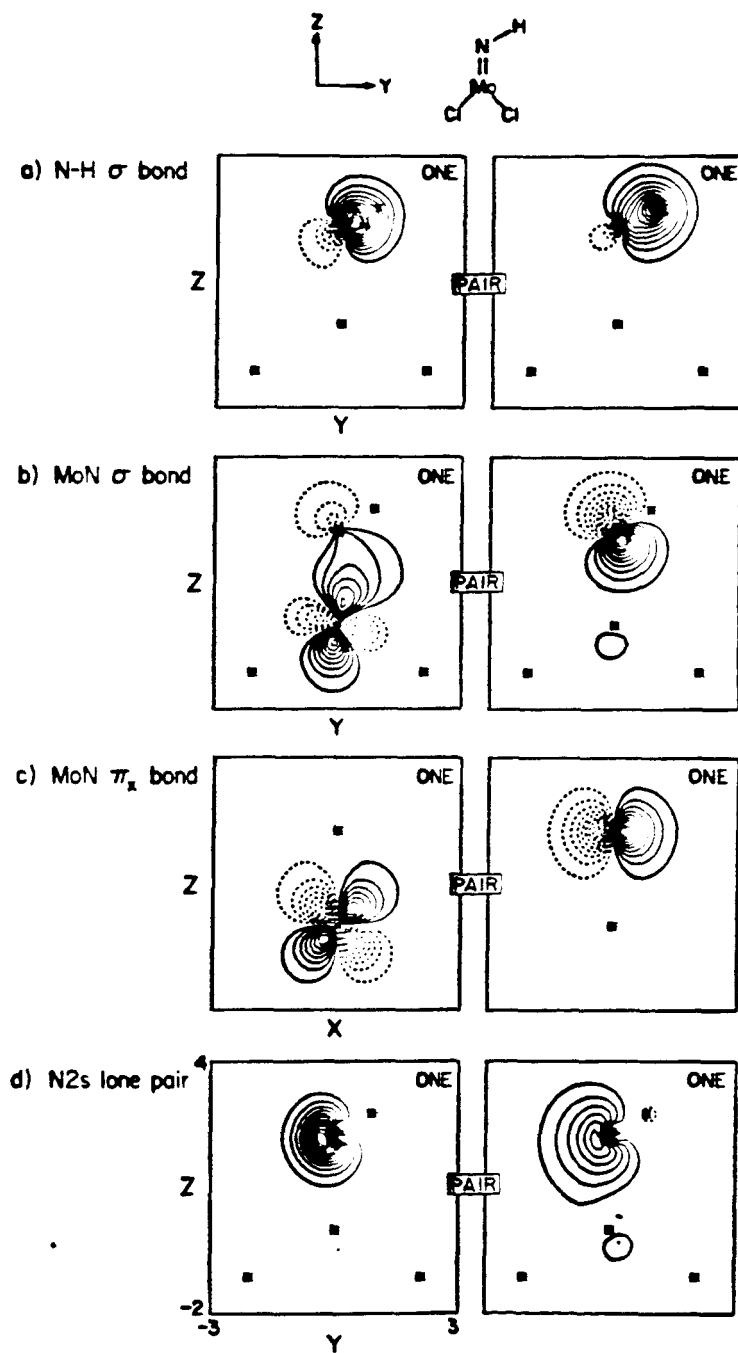
Figure 7. GVB orbitals for the electron pairs involving bent imido Mo=NH.

3.3. Combinations of Two Molybdenum Oxo or Imido Bonds on One Metal

In the Mo d^0 complexes,
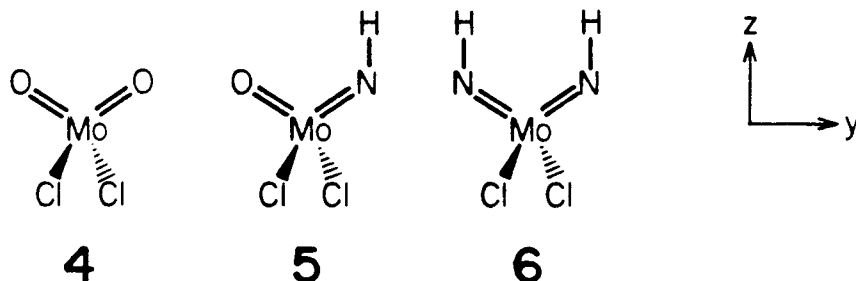
there are four singly-occupied d orbitals available to bond to the oxo and/or imido ligands. Both oxygens in $(Cl)_2Mo-(O)_2$ **4** form one sigma bond and one out-of-plane pi bond concurrently. Both oxygen lone pairs of each oxygen delocalize *only slightly* into the same Mo 4dπ-like orbital. The optimized geometry for the molybdenum-oxygen bond length is 1.61 Å and the optimized oxygen-molybdenum-oxygen bond angle is 106°.

When *one* of the molybdenum oxo double bonds in **4** is broken, i.e., "snapped off" (without readjusting fragment geometry), the mono oxo triplet Mo d^2 fragment is left, with the oxo ligand at 53° with respect to the normal. The remaining spectator oxo ligand can form *two* pi bonds plus one sigma bond. For convenience in getting transferrable energies for use on surfaces, we have calculated "snap" bond energies, i.e., energies with respect to the frozen fragment.

Orbital contour plots of $(Cl)_2Mo-(O)_2$ **4** doubly-bonded oxo ligands and the $(Cl)_2Mo-(O)$ triply-bonded oxo ligand are shown in Figures 8 and 9, respectively.

In the oxo-imido complex $(Cl)_2Mo-(O)(NH)$ **5**, molybdenum is bonded to one oxo ligand and to one imido ligand. The molybdenum oxo bond consists primarily of one sigma bond and one out-of-the-plane (xz) pi bond; however, there is considerable delocalization of the oxygen 2p lone pair onto the metal with some mixing of Mo 4d π-like character. Therefore, one can consider the molybdenum oxo bond in $(Cl)_2Mo-(O)(NH)$ to be of slightly higher bond order than the analogous molybdenum oxo bond in $(Cl)_2Mo-(O)_2$. Indeed, looking at the energetics of reaction (1)

$$\Delta E = -10.7 \text{ kcal}$$
$$(Cl)_2Mo-(O)_2 + (Cl)_2Mo-(NH)_2 \xrightarrow{\hspace{3cm}} 2[(Cl)_2Mo-(O)(NH)], \quad (1)$$
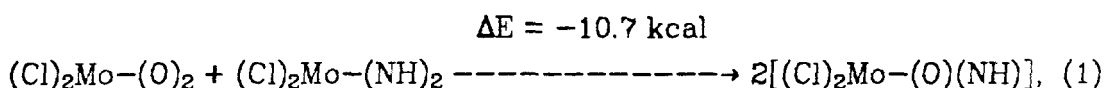
it can be concluded that the oxo-imido species has ~5 kcal/mol more stability than expected with respect to the two more nearly doubly-bonded dioxo and bis-imido reactants.

Table I lists the Mulliken populations for the various GVB pairs of the oxo and imido complexes under discussion (two electrons = GVB pair). Also listed are Mulliken populations for Mo, O, N, H, and Cl atoms in these complexes.

Of particular interest is the shift in the distribution of electron density in the oxygen 2p lone pair from oxygen to molybdenum of nearly 0.2 electrons (0.23 electrons versus 0.40 electrons) as we proceed from the dioxo complex to the oxo-imido complex. This shift occurs because the adjacent imido group allows for delocalization of electron density from oxygen to molybdenum. Such stabilization of the oxo group is not possible in the dioxo complex as both oxo groups *compete* for the same empty Mo $4d\pi$-like orbital (see Table I).

The molybdenum imido bond in $(Cl)_2Mo-(O)(NH)$ is a double bond with

one in-the-plane bent sigma bond and one out-of-the-plane (xz) pi bond. For the linear imido bond, as in $(Cl)_2Mo-(NH)$, the N2s orbital delocalizes onto the metal. However, for the bent imido bond, as in $(Cl)_2Mo-(O)(NH)$, we find that the N2s orbital is mostly localized on nitrogen (Table I). The optimized molybdenum-nitrogen bond distance for the bent imido in the oxo-imido complex is 1.68 Å; the optimized oxygen-molybdenum-nitrogen angle is 108°; and the molybdenum-nitrogen-hydrogen angle is 142°. Orbital contour plots of $(Cl)_2Mo-(O)(NH)$ are shown in Figures 10a,b.

In the bis-imido complex $(Cl)_2Mo-(NH)_2$ **6**, molybdenum is symmetrically bonded to two imido ligands. The molybdenum imido double bond consists of one bent sigma bond and one out-of-the-plane (xz) pi bond. The N2s lone pair is slightly delocalized onto molybdenum in much the same way as for the analogous molybdenum oxo-imido complex (see Figures 10b, 11). The optimized nitrogen-molybdenum-nitrogen angle is 110° and the molybdenum-nitrogen-hydrogen angle is 142°.

Although the terminal linear arrangement of the Mo-N-R bond is the most common, cases of nonlinear geometries are known.[2] Most nonlinear Mo-N-R angles range from 155° and upwards. However, for $(S_2CNEt_2)_2Mo(NPh)_2$, an Mo-N-C angle of 139° has been observed.[6] It is also believed that many more imido structures may possess a bent terminal ligand if they are correctly formulated.

Optimized geometries at the GVB-RCI level for the molybdenum complexes are discussed in Chapter 5 and are shown in Figure 12 and Table II.

We see from Table III that for complexes **1** and **2** of the form $[(Cl)_2]Mo-X$ there is an intrinsic Mo-O multiple bond strength of 155 kcal, and an intrinsic Mo-NH multiple bond strength of 120 kcal. This means that a molybdenum oxygen triple bond is stronger than a linear
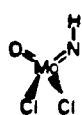
molybdenum imido "triple" bond (two π bond plus N2s σ donor) by ~35 kcal.

For complexes **3** → **6** in Table III of the form $[(Cl)_2(X')]Mo-X$, the situation is not as simple. The amount of energy needed to break bond M-X will depend upon the stabilization ability of the *remaining* X' ligand in the $[(Cl)_2(X')]Mo$ fragment. With a fixed Cl-Mo-Cl angle of 112°, a comparison can be made between bond energies relative to the "relaxed" remaining fragment and to the "snap" remaining fragment. These bond energies are shown in the first and second columns of Table III, respectively. From these data we deduce the relaxation energy for imido [complexes **3** and **5** in Table III] is 16 kcal. Therefore, it is 16 kcal lower in energy to have a geometrically relaxed linear imido normal fragment in $[(Cl)_2(NH)]Mo$ than it is to have a bent imido fragment at 54° with respect to normal and an Mo-N-H angle of 142°. (Bis-imido parent compound HN-Mo-NH angle is 110°, and oxo-imido parent compound HN-Mo-O angle is 108°.)

In complexes **4** and **6** in Table III, the geometric relaxation for the oxo ligand in the remaining fragment $[(Cl)_2(O)]Mo$ is 5 kcal. Therefore, a normal oxo ligand is 5 kcal more stable than an oxo ligand 53° with respect to the normal. (Dioxo parent compound O-Mo-O angle is 106°.)

In summary, relaxation energy for imido is 16 kcal. When the orbitals involved in molybdenum imido multiple bonds are analyzed, it is the geometric imido relaxation which allows for electronic relaxation. When imido is in the relaxed linear normal position, the N2s sigma donor can point toward molybdenum and donate electron density into Mo d_{z^2} orbital, thus providing extra electronic stability for the system.

Table I. Mulliken Populations of GVB Pairs.

Elec. Config.	Molecule	Bond	Center [a]	Orbital			
				π_x	$\bar{\pi}_y$ (2p lone pair)	σ (bond in plane)	$2s$
	$(Cl)_2Mo-(O)_2$						
d^0		M=O	O	8.441	1.266	1.747	1.368	1.921
		(two)	Mo	10.500	0.700	0.236	0.618	0.0075
			Cl	7.310	0.034	0.017	0.014	0.004
		overlap			0.6386	0.8630	0.7777	0.9023
	$(Cl)_2Mo-(O)(NH)$						
d^0		Mo=O	O	8.468	1.350	1.596	1.390	1.967
			Mo	10.575	0.623	0.404	0.596	0.016
			Cl	7.334	0.027	0	0.014	0.017
		overlap			0.6738	0.8163	0.7766	0.9279
						N-H		
		Mo=NH	N	7.675	1.090	1.356	1.289	1.804
			Mo	10.575	0.854	0.006	0.707	0.196
			Cl	7.334	0.056		0	0
			H	0.615	0	0.639	0	0
		overlap			0.5940	0.8465	0.7625	0.8779
	$(Cl)_2Mo-(NH)_2$						
d^0		Mo=NH	N	7.694	1.148	1.345	1.293	1.767
		(two)	Mo	10.643	0.820	0	0.675	0.243
			Cl	7.355	0.032	0	0.032	0
			H	0.630	0	0.655	0	0
		overlap			0.6148	0.8461	0.7554	0.8722

a) Mo (Z = 42) effective potential used with Zn (Z = 30) core. Neutral Mo ≡ 12 electrons.

Cl (Z = 17) effective potential used with Ne (Z = 10) core. Neutral Cl ≡ seven electrons.

Table II. Geometries for Molybdenum Dichloro Complexes.

Molecule	Ground State	Bond Distance (Å) (Mo-X)	Bond Angle (deg) Cl-Mo-Cl	X-Mo-X[a] X'-Mo-X
$(Cl)_2Mo\text{-}(O)$	$^3A_2$ $(xy, x^2 - y^2)$	1.59	123	-
$(Cl)_2Mo\text{-}(NH)$	$^3A_2$ $(xy, x^2 - y^2)$	1.66	127	-
$(Cl)_2Mo\text{-}(N)$	$^2A_2$ (xy)	1.58	133	-
$(Cl)_2(O)Mo\text{-}(O)$	singlet	1.61	112	106
$(Cl)_2(NH)Mo\text{-}(O)$	singlet	1.61	112	108
$(Cl)_2(O)Mo\text{-}(NH)$	singlet	1.68	112	108
$(Cl)_2(NH)Mo\text{-}(NH)$	singlet	1.68	112	110

[a] X, X' = O, NH.

Table III. Adiabatic "Relaxed" and Vertical "Snap" Bond Strengths for Molybdenum Dichloro Complexes (kcal/mol).

Complex No.	Molecule	Adiabatic Bond Energy "relaxed" (kcal/mol)	Vertical Bond Energy "snap" (kcal/mol)
	Remaining Fragment	Cl-Mo-Cl $\angle = 180°$	Cl-Mo-Cl $\angle = 123°$
1	$[(Cl)_2]Mo\text{-}(O)$	139	155
2	$[(Cl)_2]Mo\text{-}(NH)$	104	120
	Remaining Fragment	Cl-Mo-Cl $\angle = 112°$ NH,O ligand on remaining fragment "relaxed"	Cl-Mo-Cl $\angle = 112°$ NH,O ligand on remaining fragment "frozen"
3	$[(Cl)_2(NH)]Mo\text{-}(O)$	119	135
4	$[(Cl)_2(O)]Mo\text{-}(O)$	104	109
5	$[(Cl)_2(NH)]Mo\text{-}(NH)$	88	104
6	$[(Cl)_2(O)]Mo\text{-}(NH)$	85	89

Figure 8. GVB orbitals for the electron pairs involving the left Mo=O double bond.

Figure 9. GVB orbitals for the electron pairs involving the Mo≡O triple bond.
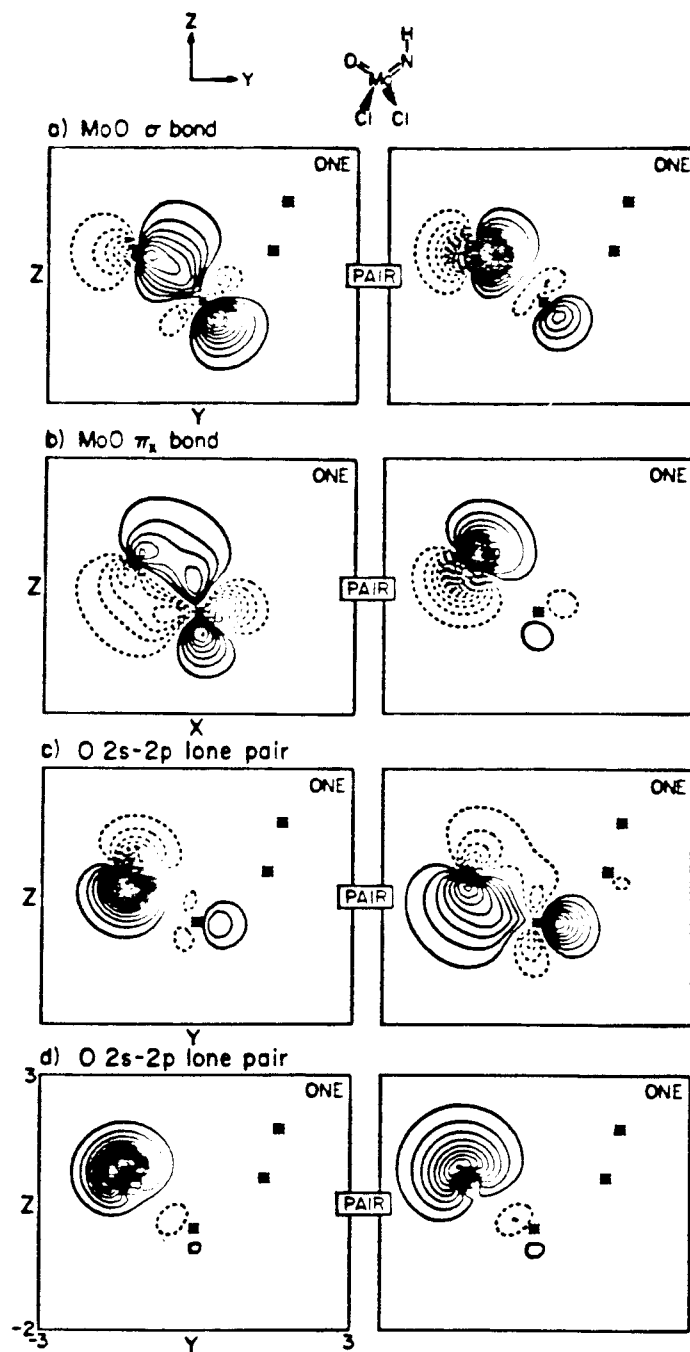
Figure 10a. GVB orbitals for the electron pairs involving the Mo=O double bond.
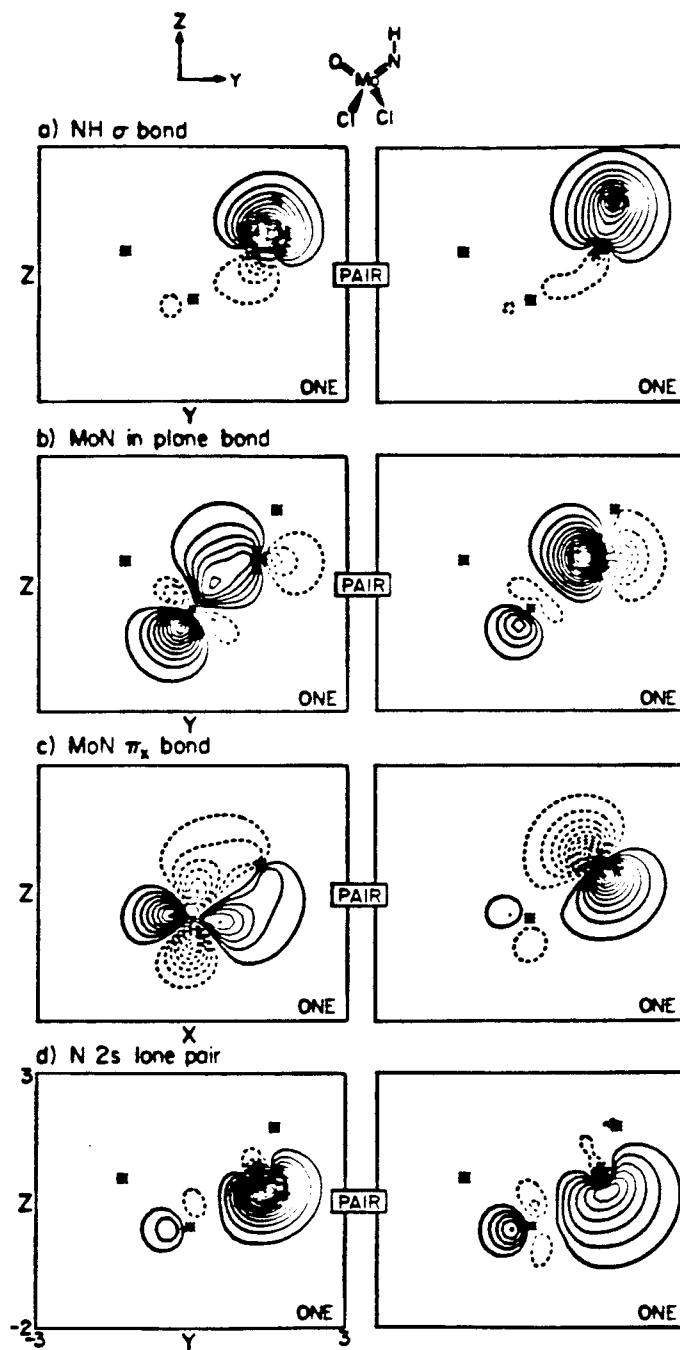
Figure 10b. GVB orbitals for the electron pairs involving the Mo=NH bond.
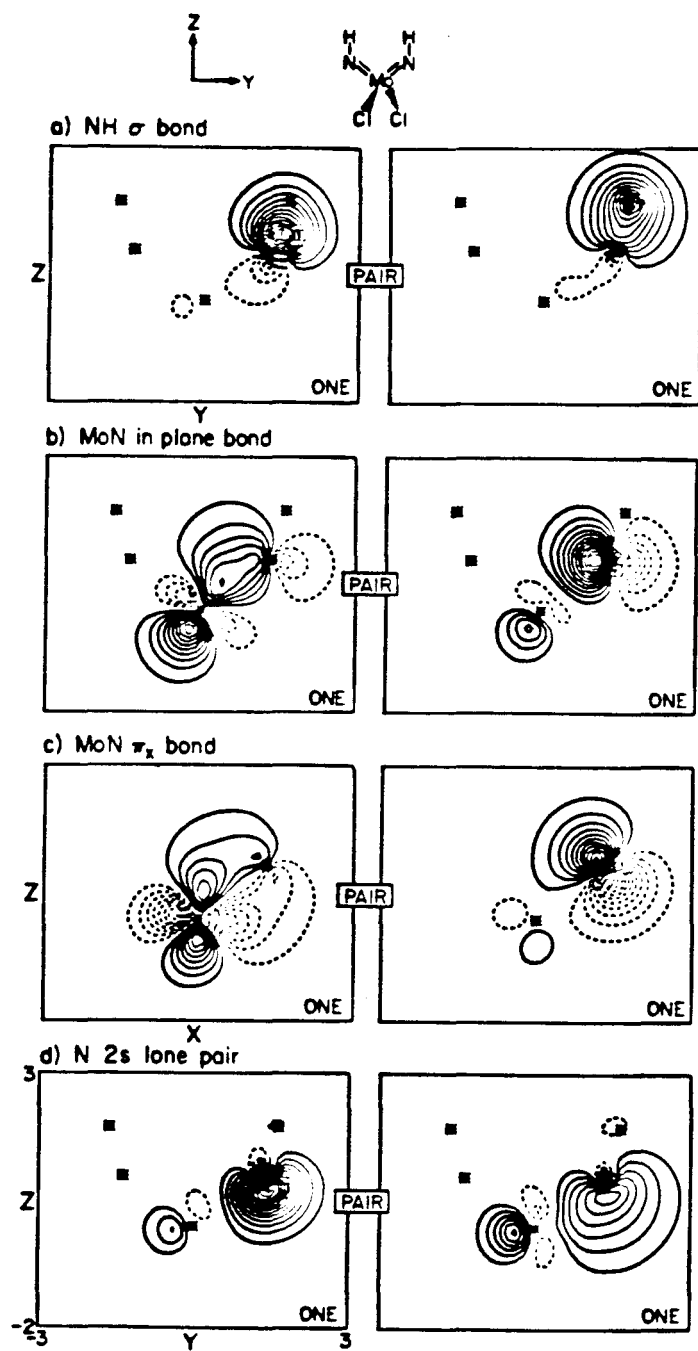
Figure 11. GVB orbitals for the electron pairs involving the right Mo=NH double bond.
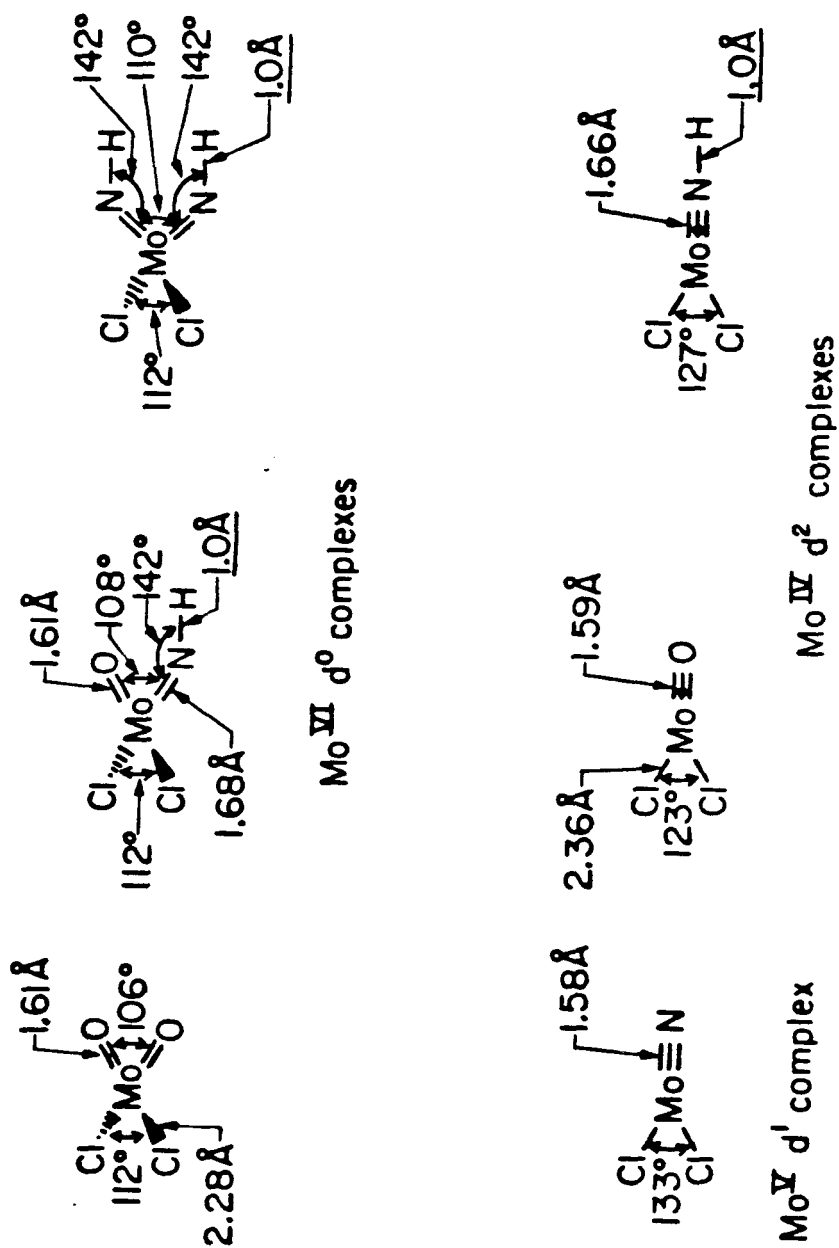
Figure 12. Optimized geometries of Mo[VI], Mo[V], and Mo[IV] dichloro complexes.

3.4. Molybdenum-Ligand Single Bonds, M-X With X = H, CH₃, OH, OCH₃, and NH₂

In this section we will consider Mo-ligand *single* covalent bonds for H, CH_3, OH, OCH_3, and NH_2 ligands using dichloro oxo complexes of the form $(Cl)_2(O)Mo-(X)$.

7
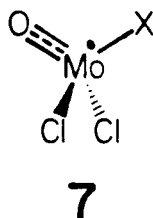
The optimized geometries of these four-coordinate radical complexes are shown in Figure 15. In all cases, molybdenum is triply-bonded to one oxo group (two π bonds and one σ bond), and the complex has a ground state symmetry of either $^1A'$ and $^2A''$ (Figures 13b, 14). The mode of bonding between molybdenum and the ligand X influences whether the ground state symmetry is A' or A''. As an example, compare the situation with X = OH with that of X = CH_3. In Figure 13a the orbitals for Mo-OH in $(Cl)_2(O)Mo-(OH)$ indicate the Mo-O covalent bond is between Mo $d\pi_x$ and $O2p_x$ orbitals. This leaves a singly-occupied orbital on molybdenum of A' symmetry. However, for Mo-CH₃ in $(Cl)_2(O)Mo-(CH_3)$, the Mo-C covalent bond is between the Mo $d\sigma$ and C $2p_\sigma$ orbitals (Figure 14). This leaves a singly-occupied orbital on molybdenum of A'' symmetry.

In summary, for complexes such as **7**, when X = CH_3, H the Mo-X covalent bond is of sigma character, leading to a $^2A''$ ground state; however, when X = OH, OCH_3, or NH_2, the Mo-X covalent bond is of pi character, leading to a $^2A'$ ground state.

Vertical "snap" bond energies for the Mo-X bonds in $(Cl)_2(O)Mo-(X)$
appear in Table IV and increase in the order Mo-CH$_3$ < Mo-H < Mo-NH$_2$ <
Mo-OCH$_3$ < Mo-OH.

Table IV. Bond Distances and Vertical "Snap" Bond Energies for $(Cl_2O)Mo-(X)$ Mo^V Complexes.

Ground State	Molecule	R(Mo-X) Å	Bond Energies (Mo-X) (kcal/mol)
$^2A''$	$(Cl_2O)Mo-(CH_3)$	2.06	41
$^2A''$	$(Cl_2O)Mo-(H)$	1.68	45
$^2A'$	$(Cl_2O)Mo-(NH_2)$	1.82	53
$^2A'$	$(Cl_2O)Mo-(OCH_3)$	1.77	64
$^2A'$	$(Cl_2O)Mo(OH)$	1.77	68
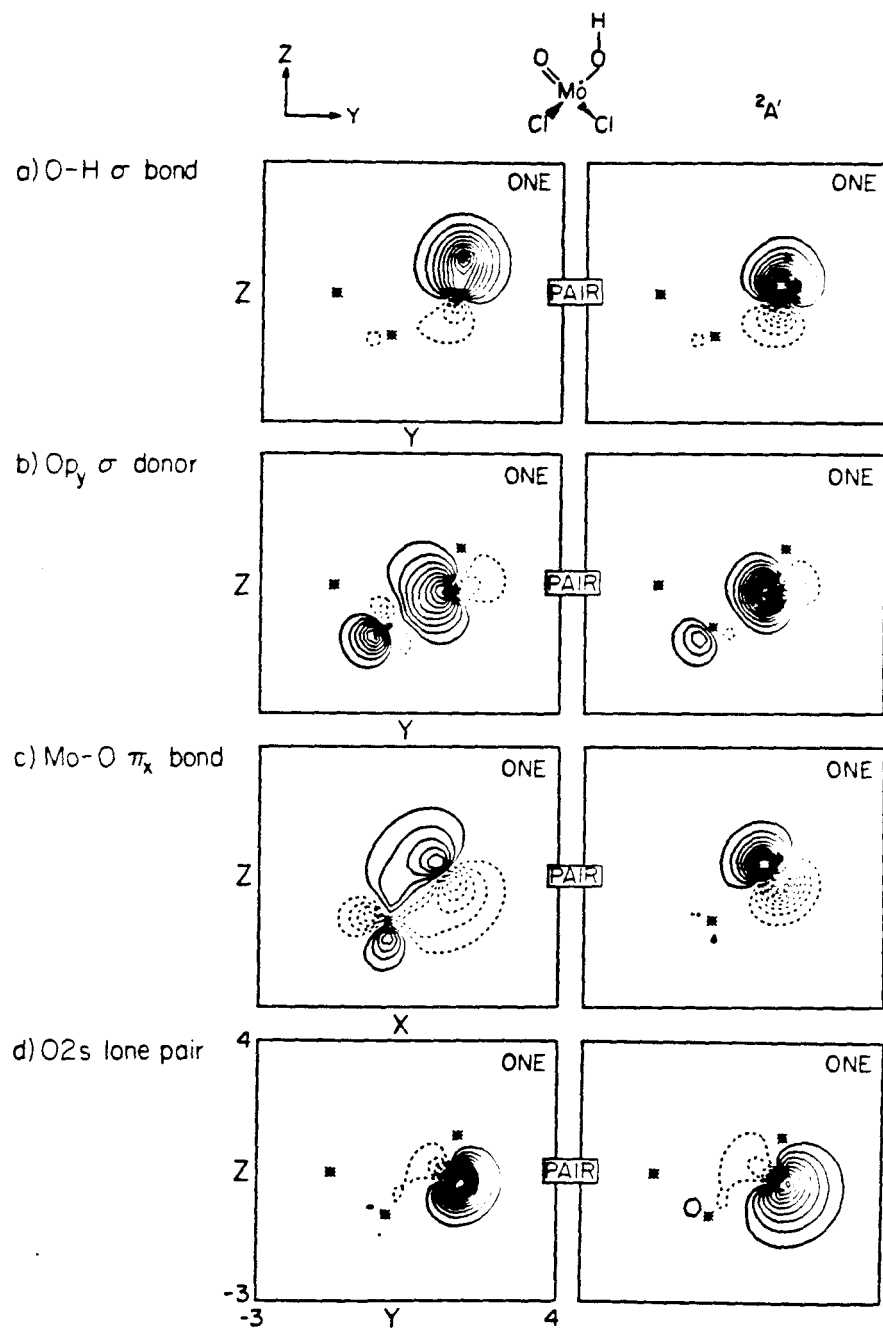
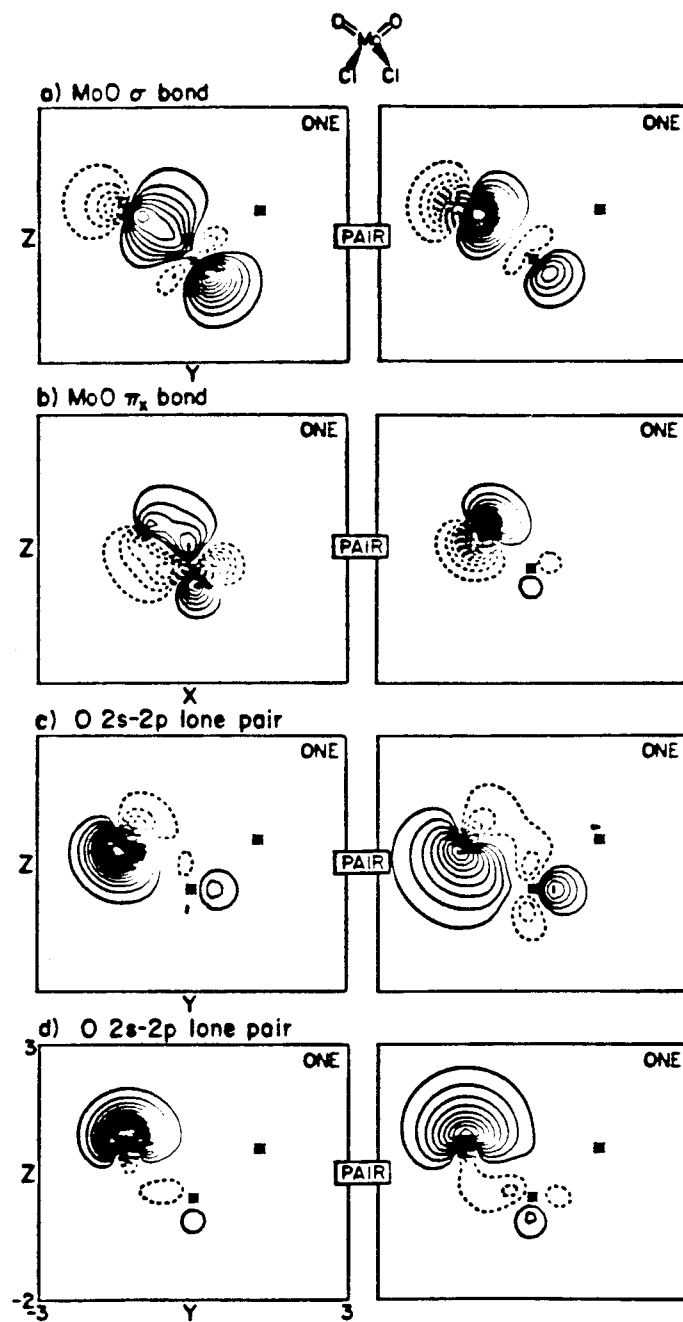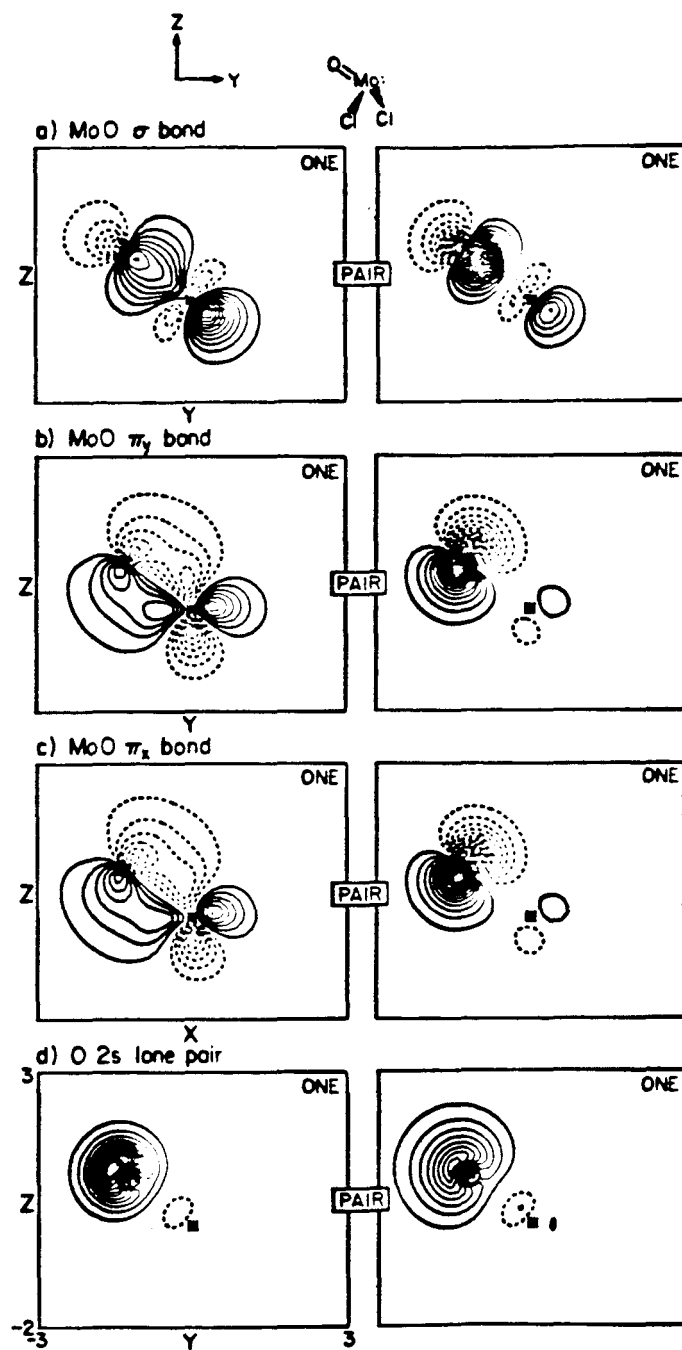Figure 13a. GVB orbitals for the electron pairs involved in Mo-OH.
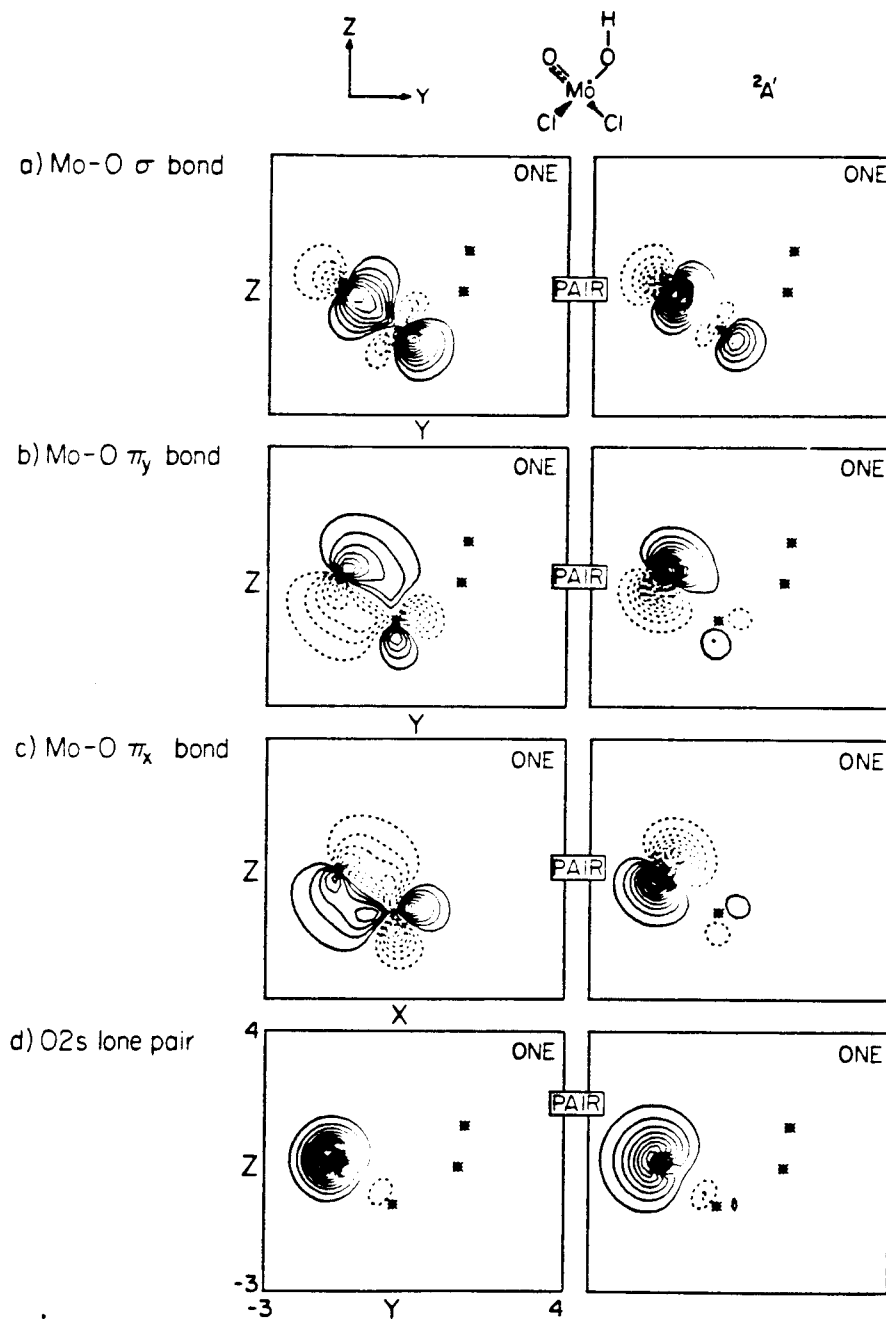
Figure 13b. GVB orbitals for the electron pairs involved in the left Mo≡O bond.
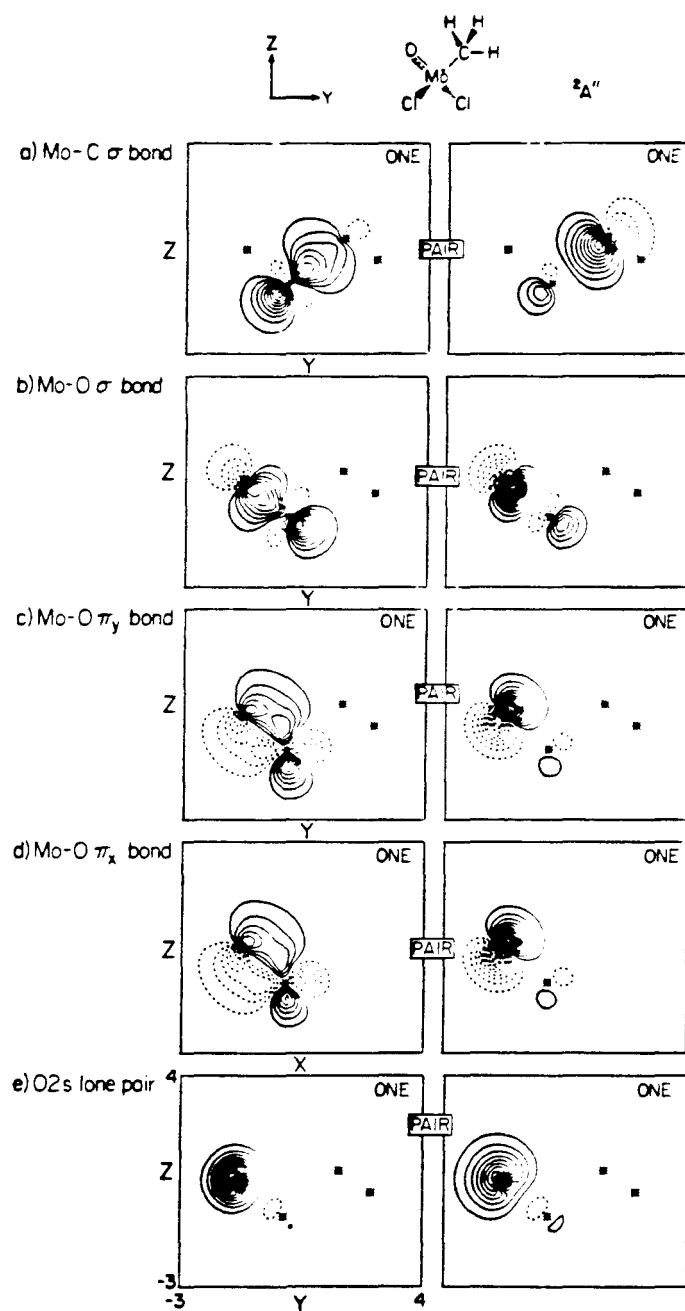
Figure 14. GVB orbitals for the electron pairs involved in the Mo-C sigma bond and the electron pairs involved in the left Mo≡O bond.
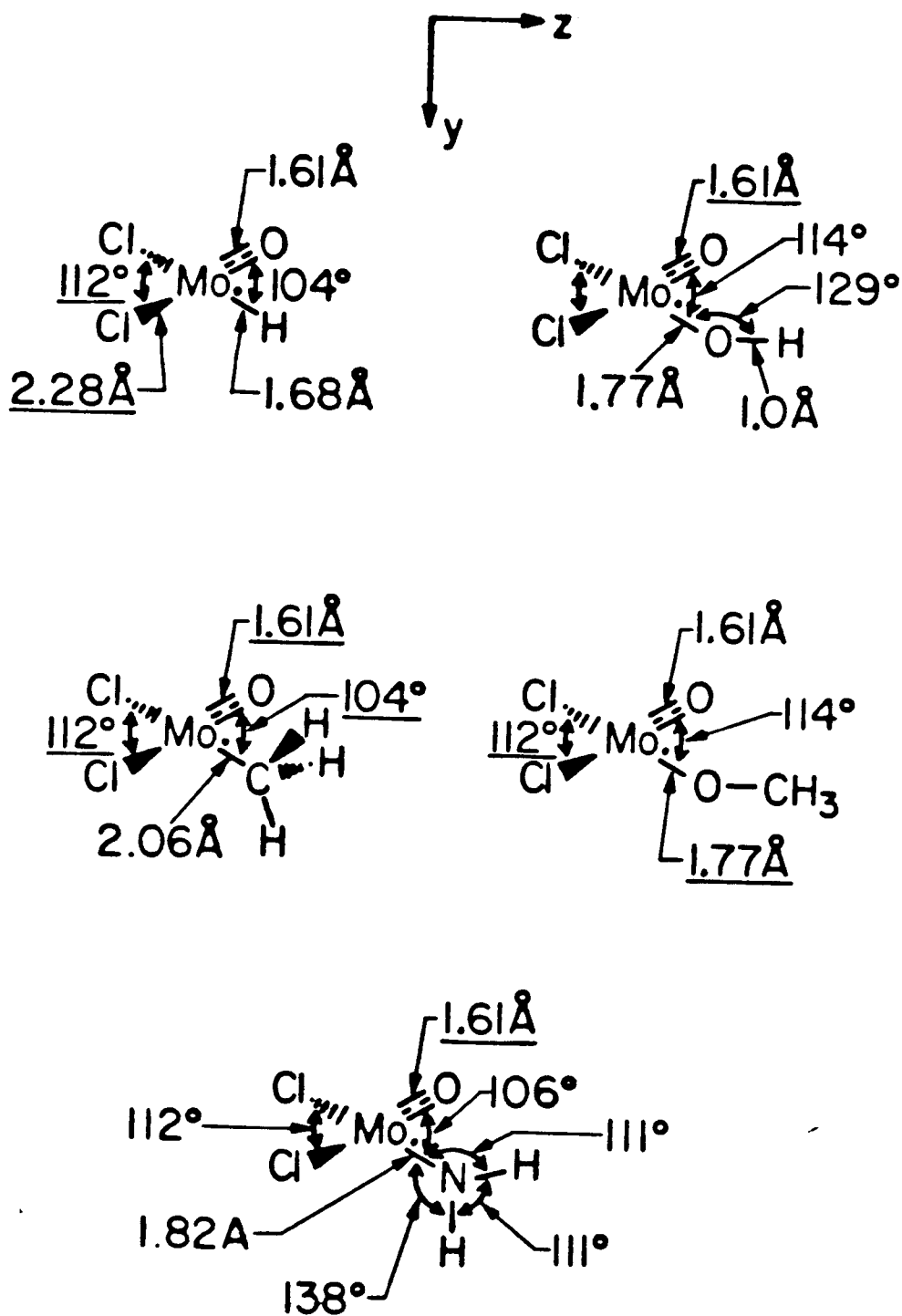
Figure 15. Geometry of Mo^V dichloro oxo radical complexes.

3.5. *trans*-Influence in Model Square Planar Molybdenum Complexes. The Variation in Bond Lengths of Mo-Cl Bonds *trans* to Mo-X, with X = NH, O, N

The *trans*-influence of a ligand in a metal complex was defined in 1966 by Pidcock *et al.*[7] as the extent to which that ligand weakens the bond *trans* to itself in the equilibrium state of that complex. When many crystal structures of similar metal complexes are studied and it is determined that a bond M-L *trans* to a ligand X is abnormally long compared with normal bond lengths, a strong *trans*-influence is ascribed to the ligand X.[8,9]

Several factors should be taken into account when evaluating a *trans*-influence.

1) The variations in bond length of M-L may be on the order of experimental error in bond length determination.[7] This is particularly true of some of the early X-ray structure determinations.

2) Bond lengths in crystals are influenced by intramolecular interactions. Also, bonds which are chemically equivalent in solution may be crystallographically distinct and often show significant differences in length.[10,11]

3) Steric effects caused by adjacent bulky ligands influence bond lengths.

Because of these considerations, there is a need for crystal structure determination which would provide the least ambiguous information. Square planar complexes of the type *cis*-ML_2XX' allow for a comparison between *cis* and *trans* M-L bond lengths, and isomeric pairs, e.g., *cis* and *trans* ML_2X_2 allow for comparison of *trans*-influences of L and X. The idea is to systematically change ligands in order to allow for a quantitative

comparison of the *trans*-influence.

By analyzing many crystal structures it has been observed that the nitrido ligand exerts a very strong *trans*-influence (0.30-0.35 Å), while the oxo ligand exerts a smaller *trans*-influence of ~0.10 Å.[12] However, the imido ligand exerts virtually no *trans*-influence (0.0-0.03 Å).[12] For example, there is a strong *trans*-influence for $(S_2CNMe_2)_3Mo-(N)$ but no *trans*-influence exists for $[(Cl)_2(S_2CNMe_2)_2]Mo-(NR)$.[12]

In order to anwer some of the above questions GVB(4/8) calculations have been carried out on a series of $[ML_3X]^-$ and $ML_2L'X$ square planar model complexes. The coordinate system used is shown in Figure 16 below.
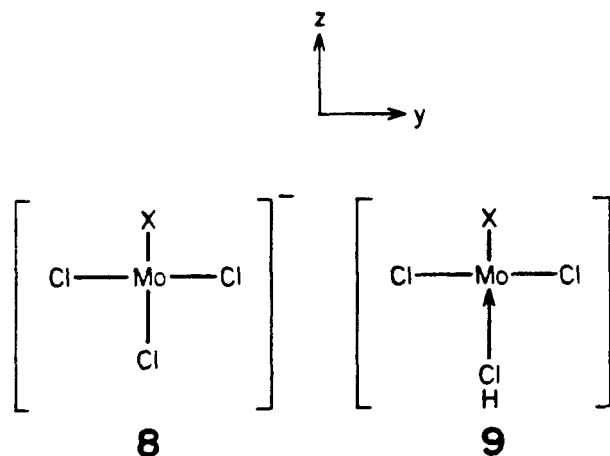
Figure 16. The coordinate system used for $[(Cl)_3Mo-X]^-$ and $[(HCl)(Cl)_2Mo-X]$ square planar systems.

Both *cis* and *trans* Mo-Cl bond lengths were optimized. The Mo-X bond length with X = NH,O,N was held constant in order to simplify the interpretation of results. These structures are shown in Figure 17, and the optimized M-L *(cis* and *trans)* bond lengths along with chosen M-X distances are indicated in Table V. In the series of complexes 1→3 listed in Table VI, we see as the X ligand is varied from NH → O → N, the Mo-Cl bond

trans to X becomes longer. Comparing Mo–Cl$_{trans}$ bond distances with Mo–Cl$_{cis}$ bond distances we find the overall magnitude of the *trans*-influence of complexes 1→3 is 0.10 Å. Looking at analogous complexes where the *trans* ligand is Mo←ClH, there is an overall *trans*-influence of 0.16 Å (see Table VI).

These results are consistent with the experimental trends which show a *trans*-influence order of imido < oxo < nitrido. However, our calculations indicate a magnitude of about one-half of the experimental *trans*-influence. This can be explained, as we are *only* measuring the electronic influence, as in our model [(Cl)$_3$MoX]$^-$ complexes solvent effects, counter ion effects and resulting interactions originating from bulky ligands are not accounted for. We may therefore reasonably suggest that roughly one-half of the total observed *trans*-influence is due purely to electronic effects.

Previously, the ability of a ligand M-X to produce a *trans*-influence has been related to the properties of the M-X sigma bond.[13,14] In a number of Pt(II) square planar complexes, a general qualitative comparison has been made between metal (pσ) overlap integrals and trends in M-L bond lengths -- the larger the M-X metal-ligand pσ overlap, the bigger the *trans*-influence.[13]

Looking in detail at the nature of the molybdenum sigma bonding orbital in M-X complexes 1→3, it is apparent that the Mo d$_{z^2}$ orbital forms the sigma bond with the ligand M-X. As the Mo d character in the sigma bond increases, so does the *trans*-influence, i.e., the *trans*-influence order is Mo=NH < O < N (Table VI). Therefore, for these systems there appears to be little correlation between Mo p character in the σ system of M-X and the *trans*-influence.

Table V. Optimized *cis* and *trans* Bond Distances in $[(Cl)_3Mo-X]^-$ and $[(HCl)(Cl)_2Mo-X]$ Complexes.

Elec. Config.	Complex	#	Mo–Cl$_{trans}$ (Å)	Mo–Cl$_{cis}$ (Å)	Mo-X (Å)
d^2	$[(Cl)_3Mo=NH]^-$	1	2.48	2.53	1.66
d^2	$[(Cl)_3Mo=O]^-$	2	2.49	2.49	1.59
d^1	$[(Cl)_3Mo\equiv N]^-$	3	2.57	2.52	1.58
d^2	*trans*-$(HCl)(Cl)_2Mo=NH$	1'	2.99	2.53	1.66
d^2	*trans*-$(HCl)(Cl)_2Mo=O$	2'	3.08	2.49	1.59
d^2	*trans*-$(HCl)(Cl)_2Mo\equiv N$	3'	3.18	2.52	1.58

Table VI. Magnitude of *trans*-Influence as a Function of Mo-X.

Complex	#	Relative *trans*-influence (Å) with respect to imido = 0
$[(Cl)_3Mo=NH]^-$	1	0.00
$[(Cl)_3Mo=O]^-$	2	+0.05
$[(Cl)_3Mo\equiv N]^-$	3	+0.10
trans-$(HCl)(Cl)_2Mo=NH$	1'	0.00
trans-$(HCl)(Cl)_2Mo=O$	2'	+0.09
trans-$(HCl)(Cl)_2Mo\equiv N$	3'	+0.16
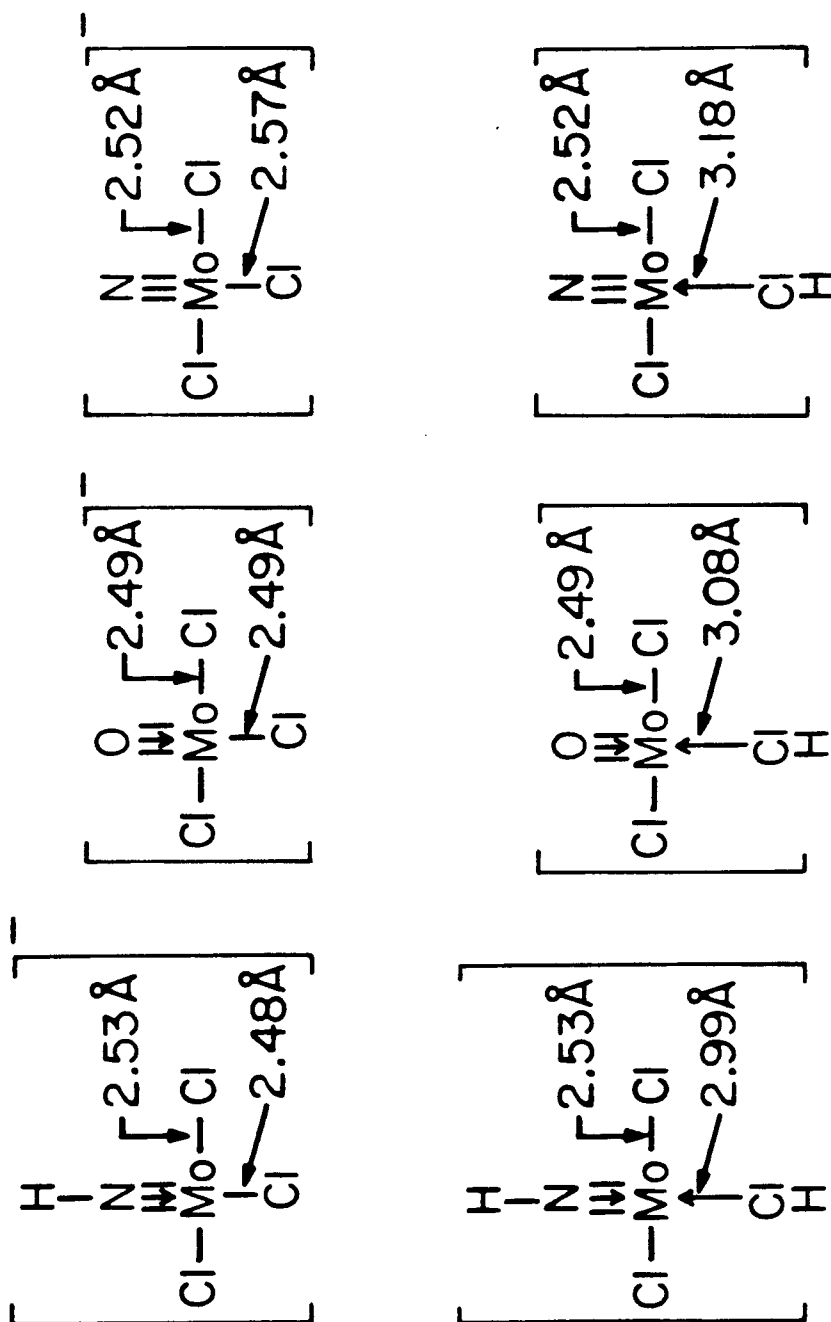
Figure 17. Model [(Cl)₃Mo–X]⁻ and [(HCl)(Cl)₂Mo-X] complexes.

References

1) J. N. Allison and W. A. Goddard III, *Chem. Phys.*, **81**, 263-271 (1983).

2) W. A. Nugent and B. L. Haymore, *Coordination Chemistry Reviews*, **31**, 123-175 (1980).

3) B. L. Haymore, unpublished results.

4) M. W. Bishop, J. Chatt, J. R. Dilworth, and B. D. Neaves, *J. Organomet. Chem.*, **213**, 109-124 (1981).

5) G. V. Gaeden and B. L. Haymore, *Inorg. Chem.*, **22**, 157 (1983).

6) B. L. Haymore, E. A. Maatla, and R. A. D. Wentworth, *J. Am. Chem. Soc.*, **101**, 2063-2068 (1979).

7) A. Pidcock, R. E. Richards, and L. M. Venanzi, *J. Chem. Soc. A*, 1710 (1966).

8) K. F. Purcell and J.C. Kotz, *Inorganic Chemistry* (W. B. Saunders Co., Philadelphia, 1977).

9) J. M. Pratt and R. G. Thorp, *Advan. Inorg. Chem. Radiochem.*, **12**, 375 (1969).

10) M. Black, R. H. B. Mais, and P. G. Owston, *Acta Cryst. B*, **25**, 1753 (1969).

11) M. A. Spinnler and L. N. Becka, *J. Chem. Soc. A*, 1194 (1967).

12) B. L. Haymore, private communication.

13) R. McWeeny, R. Mason, and A. D. C. Towl, *Discuss. Faraday Soc.*, **47**, 20 (1969).

14) S. S. Zumdahl and R. A. Drago, *J. Am. Chem. Soc.*, **90**, 6669 (1968).

CHAPTER 4

THE LOWER ELECTRONIC STATES OF MoN

The following Chapter has been published in *Chem. Phys.*, **81**, 263 (1983).
(1984).

I. Introduction

A number of systems with double and triple M-C and M-O bonds (where M is a transition metal) have now been characterized experimentally [1] and theoretically [2] and have been shown to play a role in catalytic reactions [1-3]. Although M-N double and triple bonds are believed to play a role in some catalytic processes (e.g., Mo=NR and Mo≡N in nitrogenase [4] and Mo=NR in ammoxidation catalysts [5]), few such cases have been studied experimentally or theoretically. On the experimental side, Dunn and co-workers [6] have examined the spectra of a number of transition metal nitrides, one of which is Mo≡N. As part of a project to examine the role of Mo-N moieties in catalytic reactions, we have examined the ground and excited states of Mo≡N and compared the results with current experimental data.

II. Character of the Mo≡N bond

Mo has an s^1d^5 ground state with six electrons in separate orbitals, while N has an s^2p^3 ground state with electrons in three separate p orbitals. Thus we expect a triple bond (σ, π_x, π_y) with the Mo retaining three unpaired electrons (δ_{xy}, $\delta_{x^2-y^2}$, and σ) leading to a $^4\Sigma^-$ state. An important question is whether the Mo part of the σ-bond involves the 5s orbital, the 4d orbital, or some hybrid combination. As indicated in Figure 1, we find indeed that at large R (5.0 Å) the σ-bond involves a nearly pure 5s orbital but that the character changes rapidly to 4d-like at 2.5 Å and remains 4d-like at R_e (1.60 Å). At R_e the triple bond is highly covalent and involves Mo d-like orbitals in all three bonds (see Figures 1 and 2). This leaves the two dδ orbitals and a 5s-like orbital for three nonbonding valence electrons. This nonbonding σ orbital is shown in Figure 3 where we see that it changes from $4dz^2$-like at large R to 5s-like at R_e.

Because of the disparity between the sizes of the $4dz^2$ and $5s$ orbitals, plots of contours with equal amplitude spacing lead to numerous contours for $4dz^2$ but few for $5s$, providing the illusion of $4d$ character in an orbital that is mainly $5s$. In order to help display the full character of orbitals with $5s$ character, several of the plots in Figures 1 and 3 contain contours at 0.0250 a.u. spacing rather than 0.050 a.u. spacing, as indicated in the lower left portion of each figure.

In order to provide a more quantitative description of the atomic character of these orbitals, we have calculated Mulliken populations for the MoN σ bond and for the Mo σ nonbonded, singly-occupied orbital of the full GVB wavefunction. These results are shown in Table I and Figure 4. At R_e, GVB calculations indicate there are 0.76 Mo d-electrons in the σ bond, which decreases to 0.04 Mo d-electrons at $R = 5.00$ Å. As the d character *decreases* in the σ bond, the d character *increases* in the singly-occupied Mo σ nonbonded Mo orbital (from 0.10 ẽ at $R_e = 1.6$ Å to 0.94 ẽ at $R = 5.0$ Å). In Figure 4 we see that at $R = 2.47$ Å the number of electrons in the σ bond are equal to the number in the nonbonding orbital. In the next section we will find that the total dipole moment is a maximum at this point.

From Figure 4 we see that the *total number* of Mo d-electrons in the σ bond plus Mo nonbonding orbital is essentially unity for $R > 3.0$ Å but drops to 0.80 near R_e.

The reason for the change in character of the σ bond is as follows. The exchange energy for Mo(^{7}S) in the s^1d^5 configuration is

$$E^{ex} = -10 \, K_{dd} - 5 \, K_{sd} \, ,$$

where[†]

[†] Based on all-electron ab initio calculations.

$$K_{dd} = 0.540 \text{ eV}$$

$$K_{sd} = 0.306 \text{ eV} .$$

If the s orbital is used in a perfect valence bond to another atom, the exchange energy becomes

$$E^{ex}(\text{s bond}) = -10 \, K_{dd} - \frac{5}{2} K_{sd} ,$$

and the bond energy can be written

$$D(\text{s}-\text{bond}) = D_s - \frac{5}{2} K_{sd} = D_s - 0.765 \text{ eV} ,$$

where D_s is the bond strength ignoring exchange terms.

If, instead, a d orbital is used in a perfect valence bond to another atom, the exchange energy becomes

$$E^{ex}(\text{d bond}) = -8 \, K_{dd} - \frac{9}{2} K_{sd} ,$$

and the bond energy will be written as

$$D(\text{d}-\text{bond}) = D_d - 2 \, K_{dd} - \frac{1}{2} K_{sd} = D_d - 1.233 \text{ eV} .$$

Thus, at large distances where D_s and D_d are both small, the exchange terms favor bonding to the s orbital. On the other hand, for short R, the intrinsic bond strength (D_d) is much larger for a d orbital (D_d) than for an s orbital (D_s) , as an s orbital has much lower contragradience [7]. Thus, for small distances, increased d character in the bond is favored. This trend is aided by the two π bonds. Thus the exchange interaction for one sσ bond and two 4dπ bonds is

$$E^{ex}(s\sigma, \pi_x, \pi_y) = -\frac{13}{2} K_{dd} - \frac{5}{2} K_{sd} ,$$

while for one dσ bond and two 4dπ bonds it is

$$E^{ex}(d\sigma, \pi_x, \pi_y) = -\frac{11}{2}K_{dd} - \frac{7}{2}K_{sd} \ ,$$

leading to

$$D(s\sigma, d\pi, d\pi) = D_{s\sigma} + 2D_{d\pi} - \frac{7}{2}K_{dd} - \frac{5}{2}K_{sd} = D_{s\sigma} + 2D_\pi - 2.655 \ eV$$

$$D(d_\sigma, d\pi, d\pi) = D_{d\sigma} + 2D_{d\pi} - \frac{9}{2}K_{dd} - \frac{3}{2}K_{sd} = D_{d\sigma} + 2D_\pi - 2.889 \ eV \ .$$

Thus, because of the π bonds, the loss in exchange stabilization due to a d σ bond is reduced, leading to increased d character in the bond. These factors explain the overall character of Figure 4.

III.A   Dipole Moment - ($^4\Sigma^-$) MoN

In Figure 5 we show the dipole moment (solid line) for $^4\Sigma^-$ MoN. At R_e the dipole moment is large (-3.123 Debye = -1.229 a.u.) and negative (corresponding to Mo^+N^-). In a point charge model this dipole moment would correspond to a charge transfer of 0.41 electrons from Mo to N. Noteworthy here is that the dipole moment does *not* change monotonically with R. Thus the dipole moment is a maximum (-5.982 Debye = -2.353 a.u.) at R = 2.60 Å, a distance 62% larger than R_e!

In order to examine the origin of this behavior, we have partitioned the *total dipole* into three parts: the contribution from the Mo nonbonded orbitals plus core orbitals; the contribution from the MoN σ bond; and finally, the contribution from the two π bonds. These results are listed in Table II and plotted in Figure 5. At R = 5.0 Å the various components of the dipole moment are all small. As R is decreased from 5.0 Å, the s character in the σ bond decreases and the d character increases so that by R = 2.50 Å an equal amount of s and d character is present (see Figure 4). This is the region in which the magnitude of the total MoN dipole moment

is the greatest, -2.353 a.u. (see Figure 5), with the polarity M^+N^-. As R is decreased further, the magnitude of the dipole decreases to -3.123 Debye (-1.2288 a.u.) at $R_e = 1.60$ Å, still with the polarity Mo^+N^-.

When the bond has Mo s character, there are two factors favoring a dipole moment with sign Mo^+N^-. First, the 5s orbital is easily polarized using the empty 5p orbital to obtain greater overlap with the N, whereas the 4d orbital is more costly to polarize (requiring a 4f-like orbital for maximal polarization). Secondly, the 5s IP (7.10 eV) [8] is much less than the 4d IP (8.56 eV) [8], allowing greater charge transfer. For example, at R = 2 Å, the strength of a purely ionic bond (ignoring overlap effects) would be

$$D_{s\,ion}\,(eV) \;=\; EA(N) \;+\; \frac{14.4}{R(A)} \;-\; IP(Mo\;5s) \;=\; 0.10\,eV$$

$$D_{d\,ion}\,(eV) \;=\; EA(N) \;+\; \frac{14.4}{R(A)} \;-\; IP(Mo\;4d) \;=\; -1.36\,eV \;,$$

for s and d bonds, respectively. This indicates that charge transfer will be important if the bond has Mo s character but not if it has Mo d character. As R decreases from ∞ to 2.6 Å, the charge transfer in the bond increases due to the greater favoring of ionic character (the 1/R term) despite the gradual increase in d character. As the bond becomes dominated by the d character for smaller R, there can be little charge transfer, leading to a dipole moment contribution at small R that is small (-0.64 D). The result then is a Morse-like dipole contribution from the σ bond, with a minimum of -5.98 D at 2.67 Å.

In addition to the above contributions from the σ bond, we find that for R < 1.8 Å the π system dominates. This is due to the charge transfer associated with the MoN covalent π bonds at smaller R. Note that for R >

2.6 Å the π system responds to the Mo^+N^- character in the σ system by donation of $N\pi$ character to the molybdenum (Figure 5).

B. Dipole Moment of MoN ($^4\Pi$)

Similar nonmonotonic behavior regarding the trend of the total dipole moment is also found for the $^4\Pi$ excited state. Just as there is a choice for MoN ($^4\Sigma^-$) between bonding an Mo 5s or Mo $4dz^2$ orbital to the N 2pz orbital, there is an analogous situation for the π system for MoN ($^4\Pi$). As Mo (^7P) and N (^4S) are brought together from their atomic limits, there is a choice between bonding an Mo 5py or Mo $4d_{yz}$ orbital to the N 2py orbital.

At large distances, the exchange terms favor bonding of the Mo 5py over Mo 4dyz and the IP (IP_{5p} = 3.89 eV versus IP_{4d} = 9.74eV) [8] is such that the charge transfer is even larger than for MoN ($^4\Sigma^-$). At smaller R, the *larger* covalent bond strength possible for Mo 4dyz leads to increased d character and eventually a decrease in the charge transfer. This results in a maximum in the dipole moment of μ(3.25 Å) = -4.542 a.u. = -11.545 D (see Figure 7) with polarity M^+N^- (corresponding to a transfer of 0.75 electrons from Mo to N). As R is decreased from 3.0 Å to R_e = 1.59 Å, the magnitude of the dipole decreases to -1.793 a.u. = -4.556 D, still with polarity M^+N^-. As R is decreased further and approaches 2.0 Å, the π bonding becomes more covalent, involving primarily the Mo 4dyz and N 2py orbitals. The overall effect is shown by a change in sign of the dipole derivative at R = 3.25 Å, which is where the N 2py orbital begins to donate charge *back* to the Mo 4dyz orbital.

IV. Spectroscopic Properties and the Excited State

The first excited state of MoN corresponds to excitation of the 5s-like nonbonding orbital into a 5p π-like orbital, leading to a $^4\Pi$ state. The

potential energy curves of these states are shown in Figure 8 and the spectroscopic properties tabulated in Table III. We find (see Table III) that removal of the nonbonding σ electron leads to a slightly longer R_e (by 0.005 Å) and a smaller vibrational frequency (by 200 cm^{-1}). The total excitation energy is calculated to be 2.13 eV = 17,166 cm^{-1}, which is in good agreement with the experimental value of 2.01 eV = 16,217 cm^{-1} [6].

V. Calculational Details

Electron correlation is extremely important for a system such as Mo≡N with multiple bonds. Thus, the Hartree-Fock (HF) description gives a bond distance too short by ~ 0.1 Å and shows MoN to be *unbound* by 0.35 eV (see Figure 9).

Wavefunctions

In order to adequately describe the bonding in MoN, we have carried out calculations using generalized valence bond (GVB) and GVB-RCI wavefunctions in which the three pairs of bonding orbitals (one σ and two π) have been correlated. In Figure 9 we show the results of a GVB-Perfect Pairing (GVB-PP) calculation leading to a bond dissociation energy D_e of 1.93 eV with respect to the appropriate atomic limits. Using the perfect-pairing restriction, the GVB wavefunction (denoted GVB-PP) dissociates properly to the atomic framents but not to the proper spin state [Mo(^{7}S) and N(^{4}S)]. The reason is that the three bond pairs remain singlet-coupled, prohibiting the high-spin coupling of the orbitals on each atom as dissociation occurs.

A common way to solve this problem is to use the *orbitals* from the GVB-PP wavefunction but to allow them to be combined so as to describe a general spin-coupling of the electrons. This is accomplished by a small configuration interaction (CI) calculation (referred to as GVB-RCI) in

which the two electrons of each singlet pair from GVB-PP are allowed any occupation of the two orbitals of that pair. In a CI description, the GVB-PP wavefunction of MoN ($^4\Sigma^-$) would have $2^3 = 8$ configurations, each with three open-shell (unpaired) electrons. In the GVB-RCI description, there are $3^3 = 27$ spatial configurations, some of which have up to nine open-shell (unpaired) electrons. The GVB-RCI leads to a bond energy of 4.03 eV, a significant improvement over the value of 1.93 eV for GVB-PP. [It is important to allow a total of nine open shells (three singly-occupied Mo orbitals plus six GVB orbitals involving three bond pairs); thus, if only five open shells are allowed, the calculated D_e is only 2.20 eV.]

Although the GVB-RCI gives a quantitatively good description for small R, it dissociates to a limit just slightly above that of the high-spin products. This is because the orbitals (obtained from GVB-PP) have incorrect shapes. The result is a small hump in the potential curve (0.36 eV at 3.00 Å). In order to obtain the optimum orbitals *while* including the optimum spin coupling, we use the GVB3 program [9] in which all orbitals are solved for self-consistently for the full 27 configurations of the RCI wavefunction (188 spin eigenfunctions). This corresponds closely to the *full GVB wavefunction* including spin-coupling optimization. As indicated in Figure 9, the GVB wavefunction dissociates monotonically to the Mo(^{7}S) and N(^{4}S) limit. At R_e the full GVB wavefunction leads to a bond energy of 4.075 eV, just slightly better than GVB-RCI (4.071 eV). Total energies, the equilibrium internuclear distance, and bond dissociation energies for the various wavefunctions are shown in Table IV.

As a final wavefunction, we allowed all single excitations from all occupied orbitals of the 27 GVB-RCI configurations to *all* the virtual orbitals (1199 configurations and 10,592 spin eigenfunctions). This is referred

to as GVB*S (for full GVB times singles). The result is a bond energy of 4.57 eV.

The spectroscopic properties in Table III were obtained from the full GVB wavefunction, while dipole moments (Table II and Figure 5) and orbital plots were derived from GVB-PP wavefunctions. Results from Table I and Figure 4 were obtained from the full GVB wavefunction.

The total energies of MoN ($^4\Sigma^-$) and MoN ($^4\Pi$) for the full GVB wavefunction at various internuclear distances are tabulated in Appendix II.

VI. Basis Set and Potential

We have replaced the Zn (Z = 30) core of Mo (Z = 42) by a relativistic effective potential (Hay [10]) thereby treating Mo as a $(4p)^6(4d)^5(5s)^1$ 12-electron system. The Mo basis consisted of a [3s,4p,2d] contraction basis of a (3s,5p,3d) set of primitive gaussians and is listed in Appendix I.A. For nitrogen, the Dunning [3s,2p] contraction of the Huzinaga (9s,5p) basis was used. We supplemented the nitrogen basis with polarization functions (α_d = 0.760) [11].

References

[1] (a) R. R. Schrock, J. Am. Chem. Soc. 96 (1974) 6796; ibid. 98 (1976) 5399; R. R. Schrock and P. R. Sharp, ibid. 100 (1978) 2389; (b) R. R. Schrock, S. Rocklage, J. Wengrovius, G. Rupprecht, and J. Fellmann, J. Mol. Catal. 8 (1980) 73.

[2] A. K. Rappe' and W. A. Goddard III, J. Am. Chem. Soc. 104 (1982) 448, 3287.

[3] E. L. Muetterties and E. Band, J. Am. Chem. Soc. 102 (1980) 6574.

[4] J. Chatt, J. R. Dilworth, and R. L. Richards, Chem. Rev. 78 (1978) 589.

[5] R. K. Grasselli and J. D. Burrington, Advances in catalysis (Academic Press, Inc., New York, 1981), p. 133.

[6] R. Carlson, Ph.D. Thesis, Michigan State University (1982).

[7] C. W. Wilson, Jr., and W. A. Goddard III, Chem. Phys. Letters 5 (1970) 45.

[8] C. E. Moore, Nat. Stand. Ref. Data Ser., Nat. Bur Stand. (U. S.), NSRDS-NBS 35, Vol. III (U. S. Government Printing Office, Washington D.C., 1971).

[9] (a) L. G. Yaffe and W. A. Goddard III, Phys. Rev. A 13 (1976) 1682; (b) M. M. Goodgame and W. A. Goddard III, to be published.

[10] P. J. Hay, private communication.

[11] R. A. Bair and W. A. Goddard III, J. Phys. Chem., submitted for publication.

TABLE I. Mulliken populations for the GVB orbitals of MoN ($^4\Sigma^-$).

a) The full GVB wavefunction (GVB-3)

σ - bond (two-electron total)				nonbonded σ orbital (one-electron total)		
R(Å)	Mo d	Mo sp	N spd	Mo d	Mo sp	N spd
1.60	0.76	0.04	1.20	0.10	0.87	0.03
2.00	0.60	0.12	1.28	0.22	0.77	0.01
2.50	0.44	0.34	1.22	0.47	0.53	0.00
3.00	0.34	0.56	1.10	0.64	0.36	0.00
5.00	0.04	0.96	1.00	0.94	0.06	0.00

b) The GVB-PP wavefunction

σ -bond (two-electron total)				nonbonded σ orbital (one-electron total)		
R(Å)	Mo d	Mo sp	N spd	Mo d	Mo sp	N spd
1.60	0.75	0.05	1.20	0.12	0.84	0.04
2.00	0.48	0.14	1.38	0.29	0.69	0.02
2.50	0.30	0.30	1.40	0.51	0.49	0.00
3.00	0.24	0.50	1.26	0.67	0.33	0.00
5.00	0.04	0.96	1.00	0.96	0.04	0.00

TABLE II. Contributions to the dipole moment (μ) of MoN ($^4\Sigma^-$) as a function of internuclear distance (R). Positive μ is for Mo^-N^+, based on GVB-PP wavefunctions.

R(Å)	Contributions (a. u.) [a]			Total Dipole (μ)	
	σ- bond	π-bonds (two)	nonbonding orbitals	a. u.	Debye
1.60	-0.2492	-1.2136	-0.2340	-1.2288	-3.1233
2.50	-2.1721	0.1224	-0.2860	-2.3357	-5.9368
5.00	-0.07544	0.004751	0.001436	-0.06925	-0.1760

[a] The dipole moment was partitioned into orbital contributions by calculating the orbital moment and adding the nuclear contribution due to an equal number of protons centered on appropriate centers (one proton on each nucleus for bond pairs).

TABLE III. Spectroscopic properties for MoN from the full GVB calculation (GVB-3).

| State | Total Energy (hartree)[e] | Bond Dissociation Energy D_e (eV) | Bond Distance (Å) | | Force Constant k (h/Å²)[f] | Harmonic Vibrational Frequency ω_e (cm⁻¹) | Excitation Energy T_0 (eV) | |
			Theory R_e	Expt.[c] R_0			Theory	Expt.
$^4\Sigma^-$	-102.773612	4.075[a]	1.603	1.633	2.0076	1100.4	0	0
$^4\Pi$	-102.695397	4.639[b]	1.608	1.654	1.3419	899.6	2.116	2.0107[d]

[a] For MoN ($^4\Sigma^-$), the D_e is with respect to (^{7}S) Mo and (^{4}S) N atomic limits.

[b] For MoN ($^4\Pi$), the D_e is with respect to (^{7}P) Mo and (^{4}S) N atomic limits.

[c] Calculated from rotational constant B_0 in Ref. 6.

[d] See Ref. 6.

[e] Calculations on the atoms yield E(Mo) = -48.229487 h and E(N) = -54.394390 h.

[f] To convert to dynes/cm, multiply by 4.359814×10^5.

-117-

TABLE IV. Total energies (h) for MoN ($^4\Sigma^-$) at selected distances.

	R = 1.60 Å	R = 5.0 Å	R = ∞	R_e	D_e
HF	-102.604386	-101.832822	-102.623877	1.531	-0.354
GVB-PP	-102.694597	-102.460020	-102.623877	1.586	+1.930
GVB-RCI	-102.371942	-102.617269	-102.623877	1.599	+4.029
GVB	-102.773604	-102.623951	-102.623877	1.602	+4.075
GVB*S	-102.791694	-102.623870	-102.623877	---	+4.566

APPENDIX I.

a) Molybdenum Basis (Hay, Ref. 10)

The [3s, 4p, 2d] contracted basis for Mo, $E = -48.229487$ h

s basis		p basis		d basis	
α_s	c_s	α_p	c_p	α_d	c_d
0.6748	1.0000	9.6460	-0.05404	2.3540	0.20492
0.07682	1.0000	1.2340	0.64149	0.7053	0.57382
0.02911	1.0000	0.4261	1.0000	0.1865	1.00000
		0.08874	1.0000		
		0.02660	1.0000		

APPENDIX I.

b)   Molybdenum relativistic effective potential (Hay, Ref. 10)

Zinc (Z = 30) core

Potential	n	Exponent	Coefficient
V(F)	-2.	1372.0024773	-0.0469492
	-1.	347.6884970	-22.4419712
	0.	109.3720055	-213.5085108
	0.	29.8704273	-81.4886889
	0.	9.9849325	-32.6181249
	0.	3.1672028	-4.6391726
	0.	1.1726745	-0.6331185
	0.	0.3500768	-0.0379478
V(S-F)	-2.	21.0238078	0.9759469
	-1.	337.7257282	30.4278849
	0.	84.1373438	389.5922948
	0.	24.3411662	82.1691652
	0.	6.1252823	45.6400558
	0.	2.0836763	20.9601999
	0.	0.7715966	6.4880764
	0.	0.2753636	0.7612272
V(P-F)	-2.	20.8605530	1.9683670
	-1.	707.9378987	106.2638639
	0.	116.6079108	659.3488281
	0.	27.8971504	254.1846899
	0.	7.7431203	69.6378928
	0.	2.2282950	8.5106535
	0.	0.5071089	-0.4207005
V(D-F)	-2.	13.0268827	2.9811493
	-1.	2588.2646370	296.0784376
	0.	507.9636789	2831.2924333
	0.	97.7322200	450.6802248
	0.	20.9699908	72.0312845
	0.	5.9597652	27.6522954
	0.	2.0768315	4.0536147
	0.	0.2284265	-0.0719758

APPENDIX II.

Total energies (a. u.) for MoN ($^4\Sigma^-$) and MoN ($^4\Pi$) as a function of inter-nuclear distance R(Å) for the full GVB wavefunction.

R(Å)	Energy (a. u.)	
	MoN ($^4\Sigma^-$)	MoN ($^4\Pi$)
1.30	-102.608924	-102.535795
1.50	-102.760771	-102.683865
1.55	-102.770538	-102.692835
1.60	-102.773604	-102.695356
1.65	-102.771565	-102.693954
1.70	-102.765753	-102.688178
1.80	-102.747031	-102.669822
1.90	-102.724136	-102.647518
2.00	-102.701492	-102.625385
2.50	-102.638433	-102.556650
3.00	-102.626591	-102.533309
4.00	-102.624228	-102.525966
5.00	-102.623951	-102.525112

GVB ORBITALS FOR THE SIGMA BOND OF MoN ($^4\Sigma^-$)

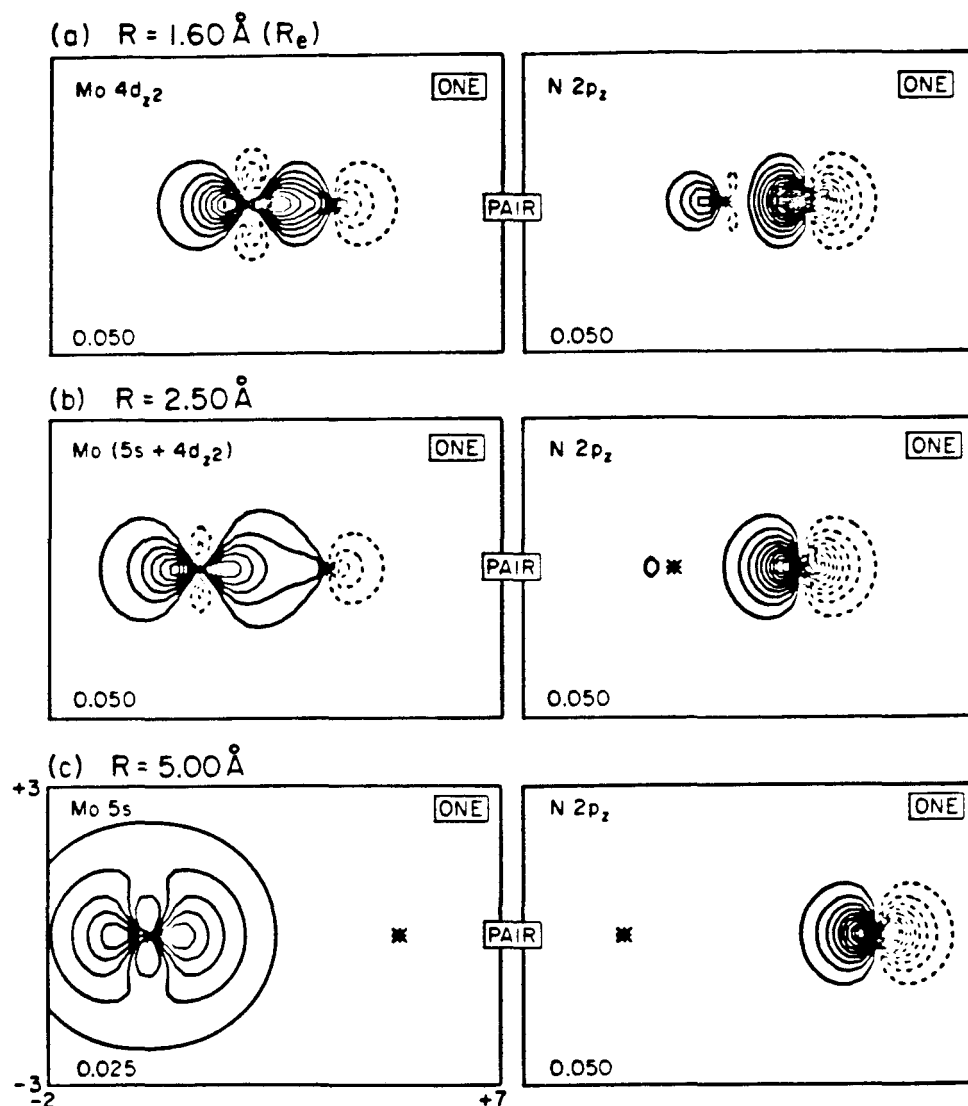(a) R = 1.60 Å (R_e)

(b) R = 2.50 Å

(c) R = 5.00 Å

Figure 1. GVB orbitals for the sigma bond of MoN ($^4\Sigma^-$) as a function of internuclear distance. Note the conversion of Mo 4dz²-like orbital at 1.60 Å (R_e) to an Mo 5s-like orbital at R = 5.00 Å. Contour increments (a.u.) noted in the lower left-hand corner. Solid lines indicate positive contours and dashed lines negative contours; the nodal lines are not shown.

GVB ORBITALS FOR THE PI BOND OF MoN($^4\Sigma^-$)
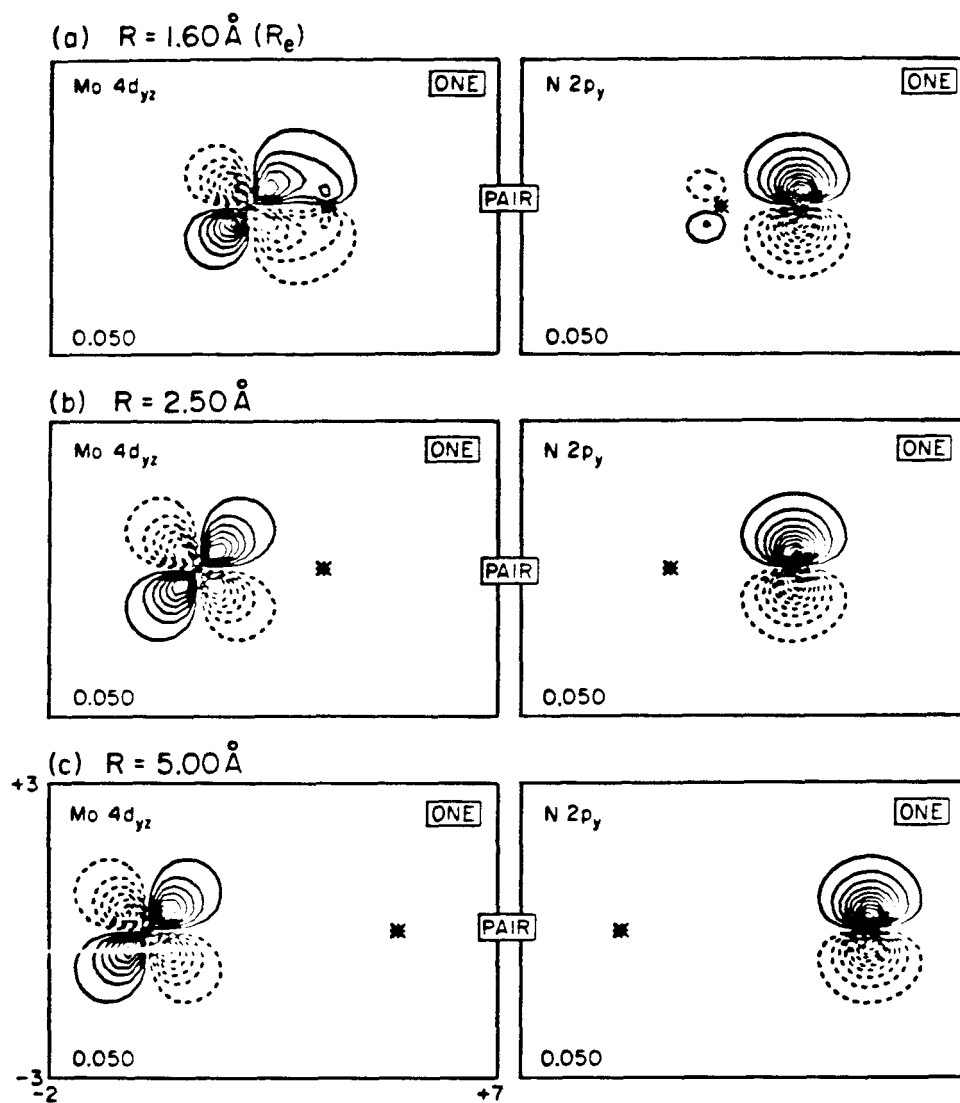
(a) R = 1.60 Å (R$_e$)

(b) R = 2.50 Å

(c) R = 5.00 Å

Figure 2. GVB orbitals for the π bond of MoN ($^4\Sigma^-$) as a function of inter-nuclear distance.

(a)

NONBONDED SIGMA ORBITAL
OF MoN ($^4\Sigma^-$)

R = 1.60Å (R_e)

Mo 5s   ONE

0.025

R = 2.50Å

Mo (5s + 4d$_{z^2}$)   ONE

0.050

R = 5.00Å

+3

Mo 4d$_{z^2}$ ONE

0.050

-3
-2

(b)

NONBONDED PI ORBITAL
OF MoN ($^4\Pi$)
EXCITED STATE

R = 1.60Å

Mo (5p$_y$ + 4d$_{yz}$)   ONE

0.050

R = 2.50Å

Mo (5p$_y$ + 4d$_{yz}$)   ONE

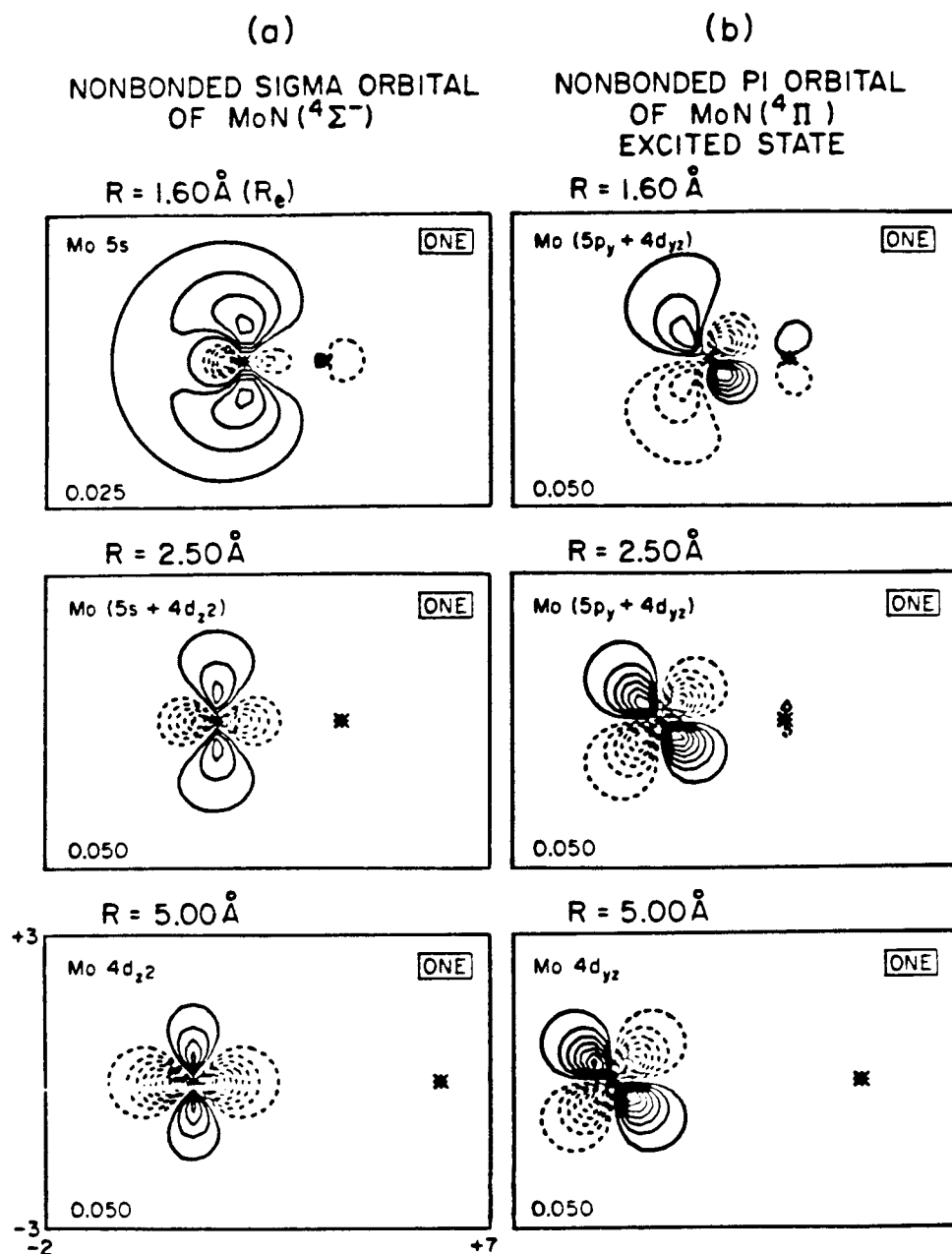0.050

R = 5.00Å

Mo 4d$_{yz}$ ONE

0.050

+7

Figure 3. (a) Singly-occupied sigma nonbonded orbital of MoN ($^4\Sigma^-$) as a function of internuclear distance. Note the conversion of the diffuse Mo 5s-like orbital at R = 1.60 Å (R_e) to an Mo 4dz^2-like orbital at R = 5.00 Å. (b) Singly-occupied MoN ($^4\Pi$) pi nonbonded orbital as a function of internuclear distance. Note the increasing Mo 4dyz character as R is increased.
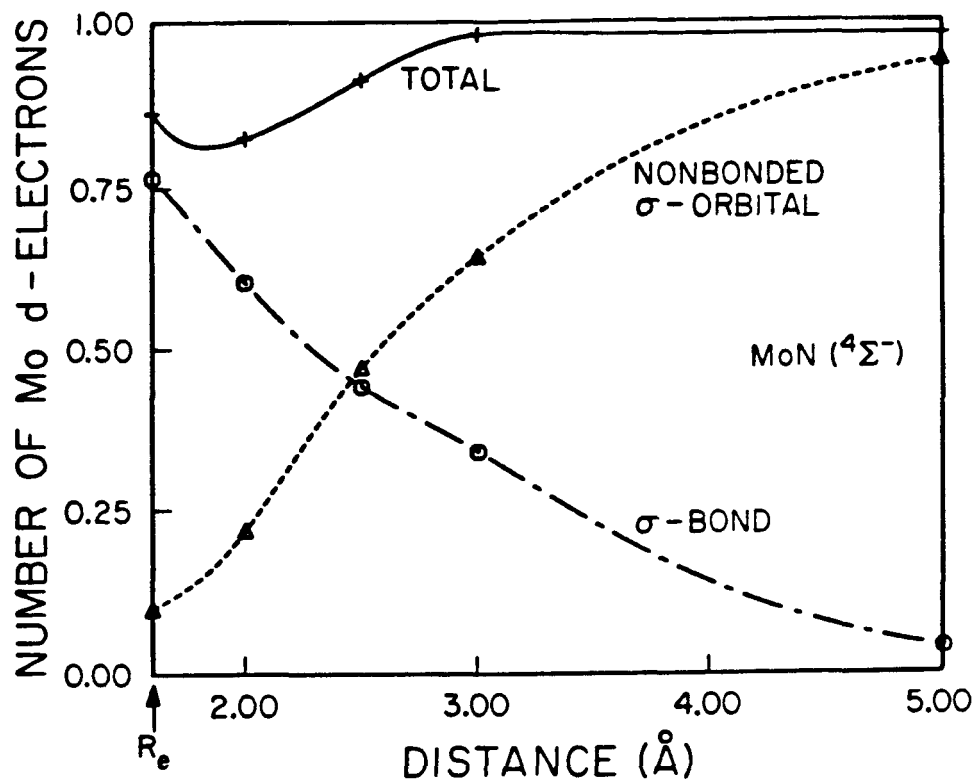
Figure 4. Number of Mo d electrons for the Mo σ nonbonded orbital and the MoN σ bond.

Figure 5. Dipole moment of MoN ($^4\Sigma^-$) as a function of internuclear distance. The four curves represent the π-bond contribution, the σ-bond contribution, the nonbonded contribution, and the overall total dipole moment.
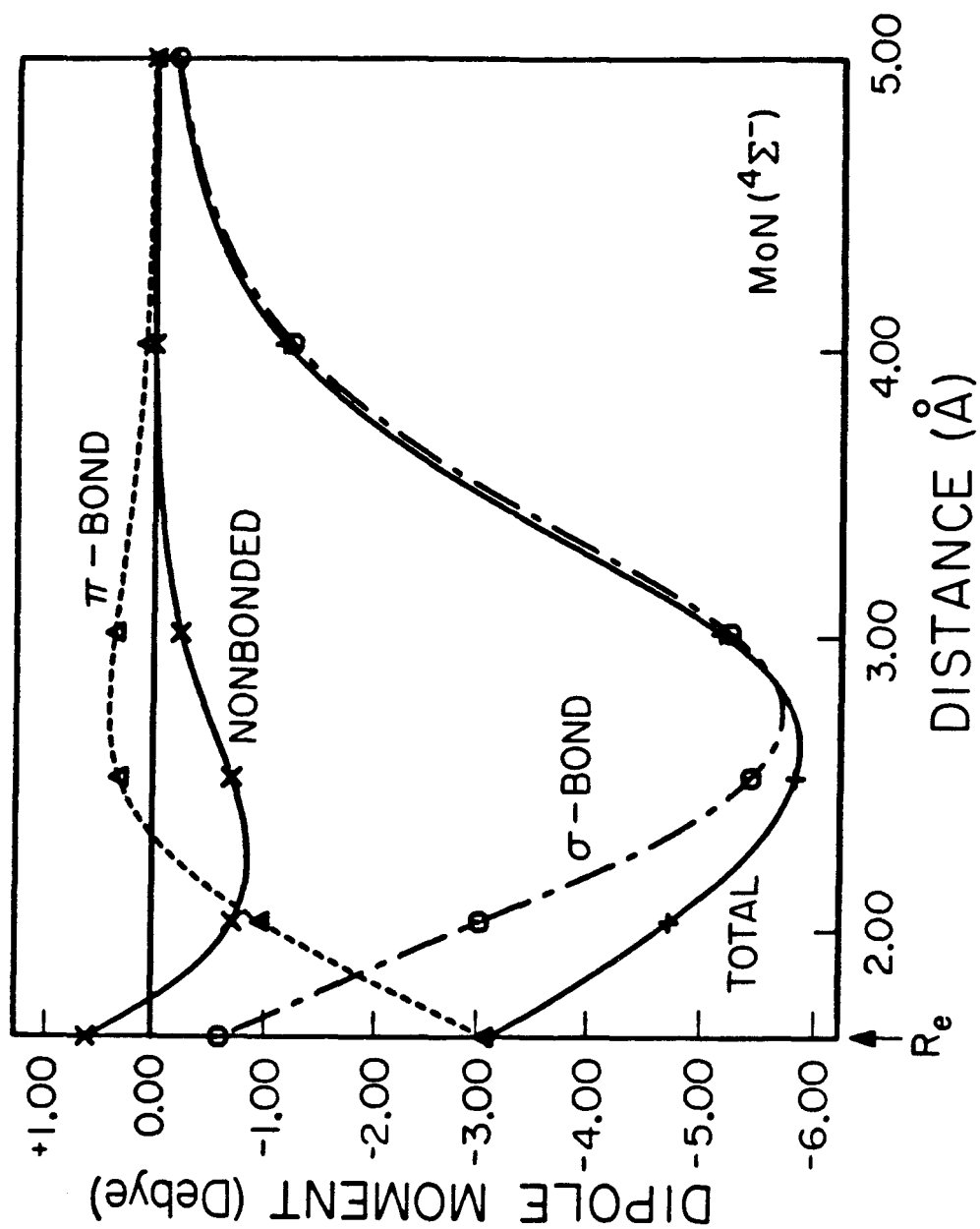
Figure 5.

GVB ORBITALS FOR PI BOND OF MoN ($^4\Pi$) EXCITED STATE

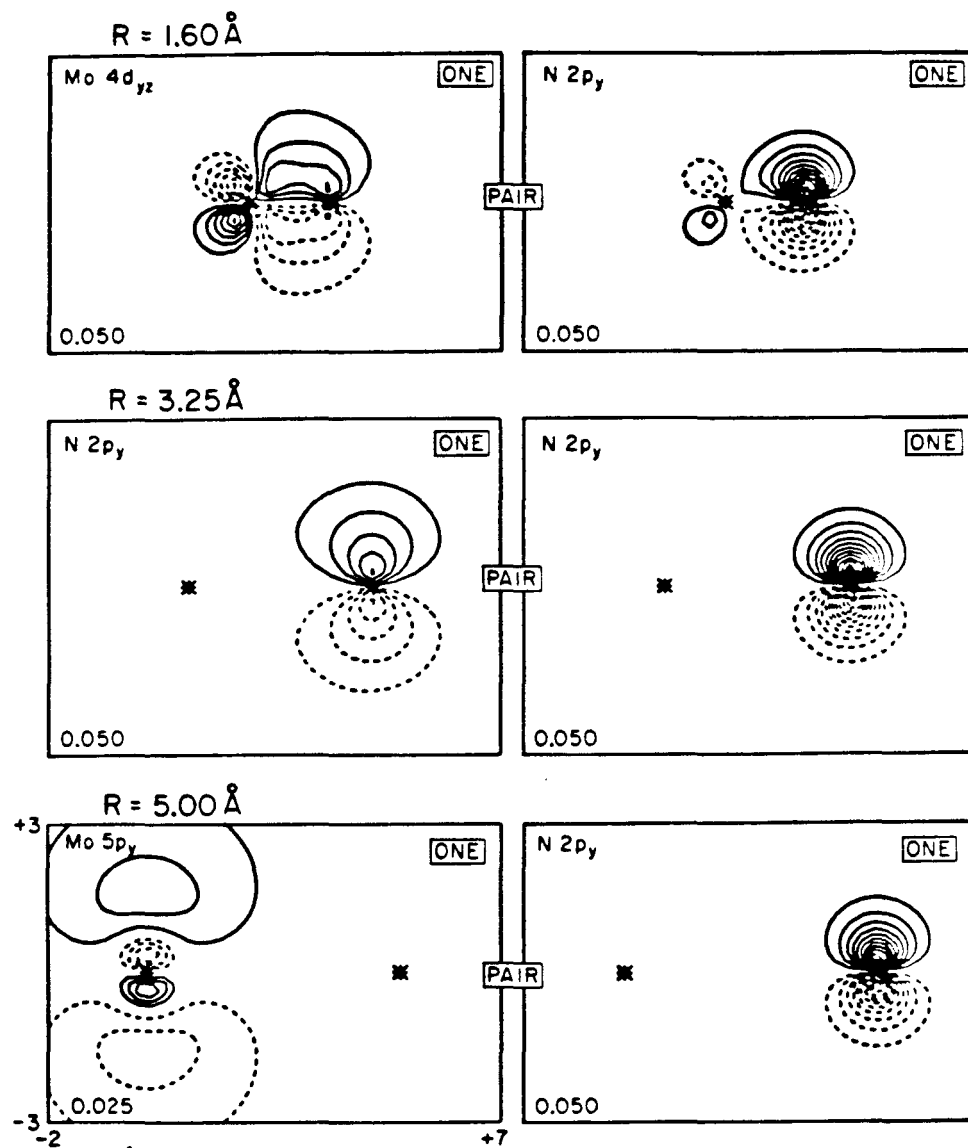**Figure 6.** GVB orbitals for the π bond of MoN ($^4\Pi$) as a function of internu-clear distance.
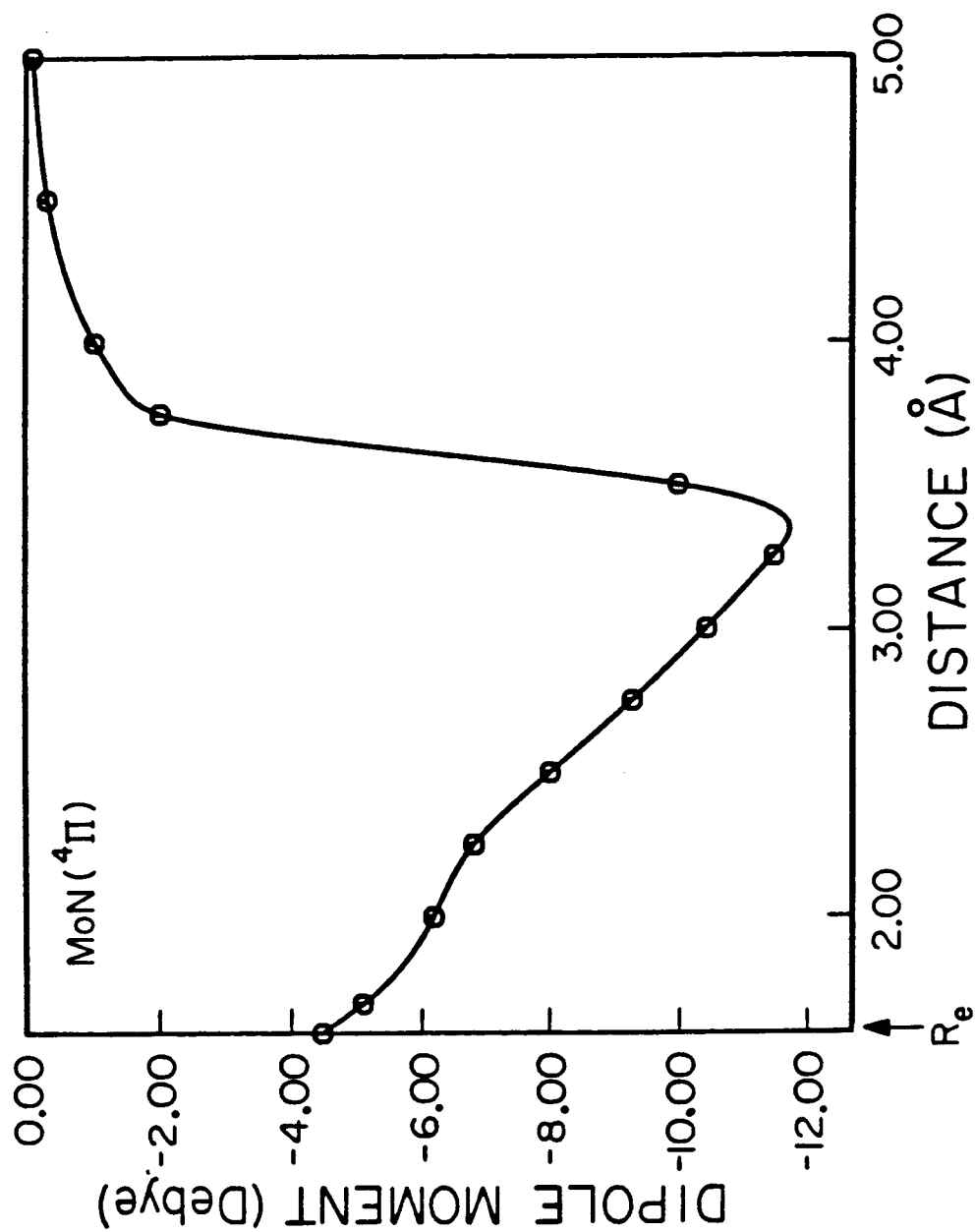
Figure 7. Total dipole moment of MoN ($^4\Pi$) as a function of internuclear distance.
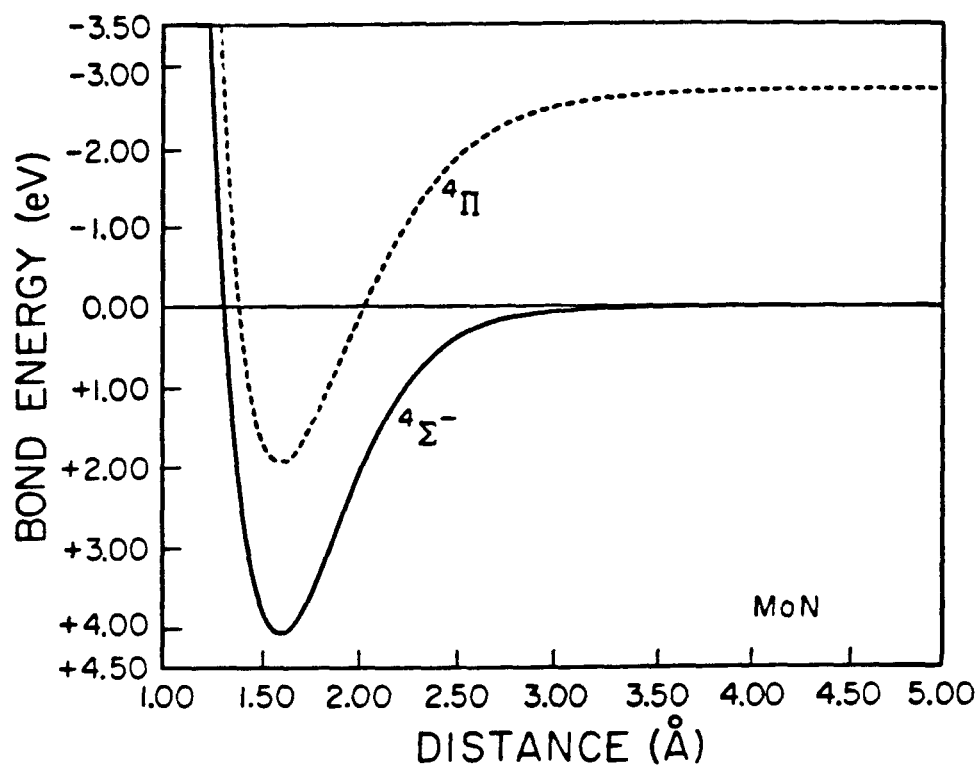
Figure 8. Potential curves for the ($^4\Sigma^-$) ground state and ($^4\Pi$) excited state of MoN using the full GVB wavefunction. The energy (eV) is relative to Mo (^{7}S) and N (^{4}S) HF atomic limits.
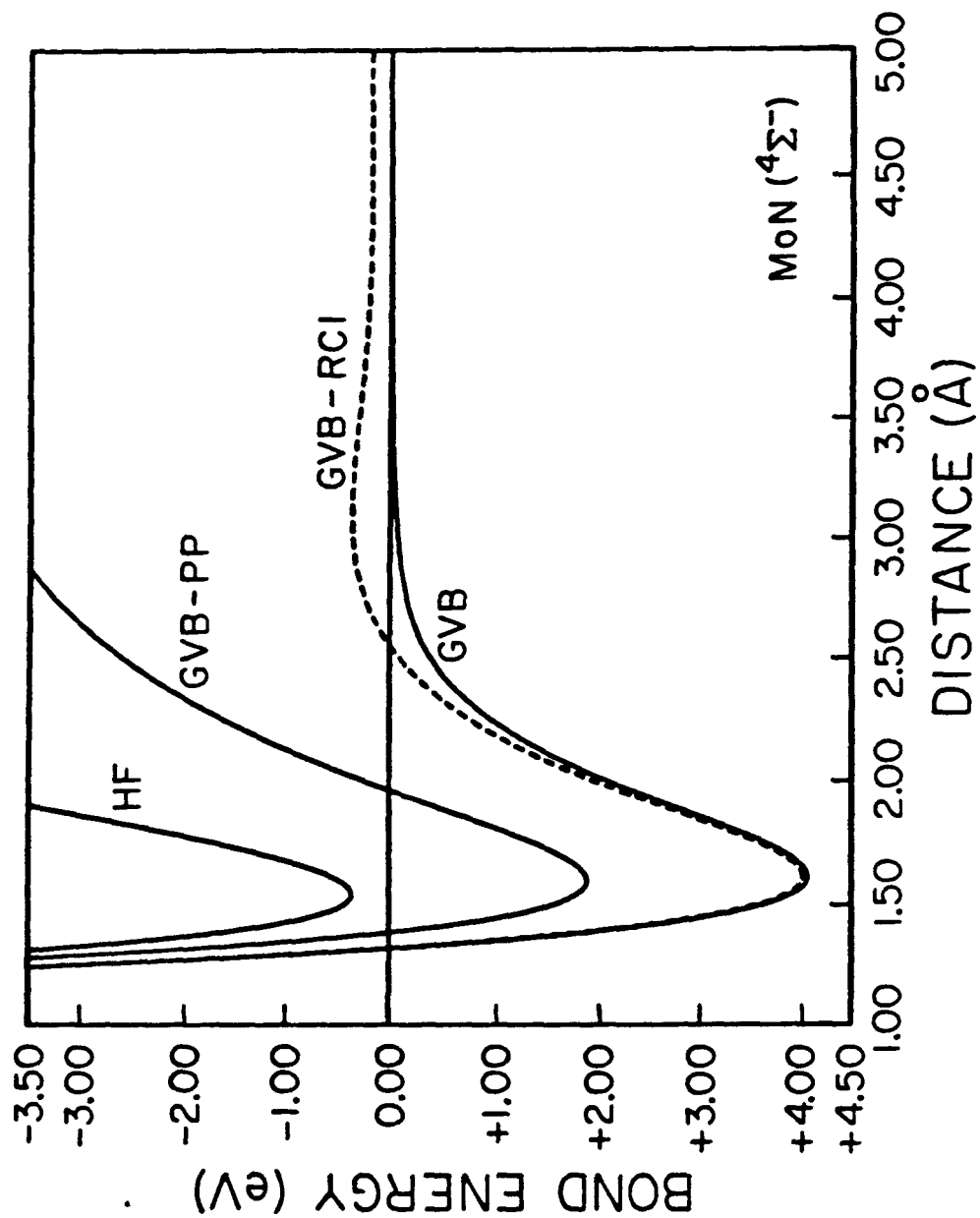
Figure 9. Potential curves for MoN ($^4\Sigma^-$) using HF, GVB-PP, GVB-RCI, and GVB wavefunctions.

APPENDIX I

CALCULATIONAL DETAILS

Calculational Details

Electron correlation is essential in order to properly desribe multiply-bonded ligands to transition metals. That the Hartree-Fock (HF) description for bond energies of multiply-bonded ligands to molybdenum is inadequate is shown in Table VII, where we see that in general the HF bond energy is ~1/2 that of the Generalized Valence Bond Perfect Pairing (GVB-PP) description, and only ~1/3 that of the GVB configuration interaction calculation (referred to as GVB-RCI). In the GVB calculations reported here, we have correlated all metal-ligand bond pairs of N, NH, and O as well as the N2s and O2s orbitals. (The metal-Cl bond pairs are not correlated.) For example, in the $(Cl)_4Mo \equiv O$ complex, the sigma bond and the two pi bonds between Mo and O have been correlated as well as the O2s orbital. This leads to an overall GVB(4/8) description. In an analogous way, when there are two oxygens bound to molybdenum as in $(Cl)_2Mo=(O)_2$, this leads to an overall GVB(8/16) description. In the GVB-RCI calculations, two electrons of each singlet pair from GVB-PP are allowed any occupation of the two orbitals of that pair. For $(Cl)_2Mo=(O)_2$, this leads to 1277 configurations in the GVB-RCI calculation, which allows for sextuple excitations from the GVB-PP wavefunction with a maximum of six singly-occupied orbitals.

It is believed that this high level of correlation is necessary in order to remove bias when describing bond pairs in the calculations. Since the maximum bond order of individual ligands bound to molybdenum in Table VII is three, a minimum level calculation of GVB(3/6) might be expected to suffice, ($1\sigma + 2\pi$) correlated bonds. However, because the N2s orbital does play a role in dative bonding in the imido complexes, we feel that both molybdenum-nitrogen and molybdenum-oxygen systems should be

Table VII. Vertical "snap" Bond Energies (kcal).

Molecule	HF	GVB-PP	GVB-RCI
$(Cl)_4Mo{\equiv}O$	40	90	138[a]
$(Cl)_4Mo{=}NH$	34	83	118[a]
$(Cl)_2(O)Mo{=}O$	42	88	109[b]
$(Cl)_2(NH)Mo{=}O$	60	104	135[b]
$(Cl)_2(O)Mo{=}NH$	31	71	89[b]
$(Cl)_2(NH)Mo{=}NH$	43	83	104[b]

[a] GVB(4/8) calculation. Bond energy is with respect to C_{4v} $MoCl_4$ (σ, δ, triplet).

[b] GVB(8/16) calculation.

.

described by GVB(4/8) calculations, (1σ + 2π + N2s/O2s) correlated bonds.

The following scheme has been used in determining energetics for chemical processes on molybdate surfaces. Total energies for surface species are calculated for the possible surface sites which are derived from bulk molybdate structures. The bridging oxygens have been replaced by chlorines to provide ionic ligands which truncate the model of the surface. Specific bond energies are calculated by taking the total energy of a surface species *before* a selected bond is broken and comparing this to the sum of the energies of the remaining molecular fragment and the isolated ligand *after* the bond has been broken. It is this energy difference which represents the calculated bond energy. Due to geometric constraints imposed by the surface, vertical "snap" bond energies (frozen fragment geometries) appropriately describe the surface reactions. Adiabatic "relaxed" bond energies would not give as good a description because the energy of surface reconstruction is negligible when compared with the relaxation energy for *individual* molecules. For example, in breaking the Mo=O bond in a C_{4v} symmetry molecule such as $MoCl_4O$, which is then converted to a T_d symmetry product $MoCl_4$, we find the calculated relaxation energy is 2.2 eV. In contrast, the fixed geometry held by the surface strictly limits relaxation possibilities of surface molybdate intermediates. The overall contribution to zero point energy ($\frac{1}{2}\omega_e$) is minimal; therefore it has not been included in our calculations, i.e., for a typical Mo=O double bond the vibrational frequency is ~ 1000 cm^{-1} which converts to a zero point correction on the order of only a kcal. Using $MoCl_4O$ as an example, we note that in breaking the Mo=O bond for the reaction $MoCl_4O \rightarrow MoCl_4 + O$ we are left with a polyatomic

product plus an oxygen atom. Using the ideal gas approximation and assuming a temperature of 500°K, it is estimated that the rotational and translational contribution to heat capacity is 2.5 kcal ($\frac{5}{2}$R + 4R - 4R). In an analogous manner, it is estimated that the vibrational contribution to heat capacity is small up to 500°K as kT for that temperature is 350 cm^{-1}, which is ~ 1 kcal. Therefore, these corrections have not been included in our calculations. However, the change in entropy (ΔS) is significant as the temperature (T) and the mole change (Δn) in the reaction is varied. For example, using Benson-type thermochemistry, we estimate that the (TΔS) contribution in converting ΔH → ΔG, using ΔG = ΔH - TΔS at 1 atmosphere with Δn = -1, is ~11 kcal at 25°C; ~18 kcal at 200°C; ~23 kcal at 400°C; and ~31 kcal at 600°C. These (TΔS) corrections were obtained by averaging representative organic reactions wherein experimental data are readily obtainable with well-defined accuracies and have been applied to the calculated bond energies.

Basis Sets and Potentials

We have replaced the Zn (Z = 30) core of Mo (Z = 42) by a relativistic effective potential; consequently, Mo is treated as a $(4p)^6(4d)^5(5s)^1$ 12-electron system. Complete details regarding the effective potential and Mo basis have been reported elsewhere.[1] The basis sets for N, O, and H were of the valence double zeta type. For nitrogen and oxygen, we used the Dunning [3s,2p] contraction of the Huzinaga (9s,5p) basis sets, supplemented with polarization functions (α_D(N) = 0.76; (α_D(O) = 0.95).[2] A double zeta contraction of Huzinaga's (4s) basis scaled 1.2 was used for H. The Cl atoms were described using the SHC effective potential to replace the core electrons, and the basis set was contracted to minimal basis.[3]

References

1) J. N. Allison and W. A. Goddard III, *Chem. Phys.*, **81,** 263-271 (1983).

2) T. H. Dunning, Jr., and P. J. Hay, in *Methods of Electronic Structure Theory*, H. F. Schaefer III, Ed. (Plenum Press, New York, 1977), Chap. 1.

3) A. K. Rappé, T. A. Smedley, and W. A. Goddard III, *J. Phys. Chem.*, **85,** 1662-1666 (1981).